FINAL REPORT

DESIGN HURRICANE STORM SURGE PILOT STUDY

FDOT CONTRACT NO.: BD 545 #42
UF CONTRACT NO.: 000 52102

SUBMITTED TO:

FLORIDA DEPARTMENT OF TRANSPORTATION
RESEARCH OFFICE
TALLAHASSEE, FL
605 SUWANNEE STREET
TALLAHASSEE, FLORIDA 32399-0450

SUBMITTED BY:

D. MAX SHEPPARD
DON SLINN
SCOTT HAGEN
CIVIL AND COASTAL ENGINEERING DEPARTMENT
UNIVERSITY OF FLORIDA
GAINESVILLE, FL 32611

DECEMBER 2006

Rick Renna, P.E., Project Manager
December, 2006
Disclaimer

The opinions, findings, and conclusions expressed in this publication are those of the author and not necessarily those of the State of Florida Department of Transportation.

SI (MODERN METRIC) CONVERSION FACTORS (from FHWA)

APPROXIMATE CONVERSIONS TO SI UNITS

SYMBOL	WHEN YOU KNOW	MULTIPLY BY	TO FIND	SYMBOL
LENGTH				
in	inches	25.4	millimeters	mm
ft	feet	0.305	meters	m
yd	yards	0.914	meters	m
mi	miles	1.61	kilometers	km
SYMBOL	WHEN YOU KNOW	MULTIPLY BY	TO FIND	SYMBOL
AREA				
in^2	squareinches	645.2	square millimeters	mm^2
ft^2	squarefeet	0.093	square meters	m^2
yd^2	square yard	0.836	square meters	m^2
ac	acres	0.405	hectares	ha
mi^2	square miles	2.59	square kilometers	km^2
SYMBOL	WHEN YOU KNOW	MULTIPLY BY	TO FIND	SYMBOL
VOLUME				
fl oz	fluid ounces	29.57	milliliters	mL
gal	gallons	3.785	liters	L
ft^3	cubic feet	0.028	cubic meters	m^3
yd^3	cubic yards	0.765	cubic meters	m^3
NOTE: volumes greater than 1000 L shall be shown in m^3				
SYMBOL	WHEN YOU KNOW	MULTIPLY BY	TO FIND	SYMBOL
MASS				
oz	ounces	28.35	grams	g
lb	pounds	0.454	kilograms	kg
T	short tons (2000 lb)	0.907	megagrams (or "metric ton")	Mg (or "t")
SYMBOL	WHEN YOU KNOW	MULTIPLY BY	TO FIND	SYMBOL
TEMPERATURE (exact degrees)				
^oF	Fahrenheit	5 (F-32)/9 or (F-32)/1.8	Celsius	^oC
SYMBOL	WHEN YOU KNOW	MULTIPLY BY	TO FIND	SYMBOL
ILLUMINATION				
fc	foot-candles	10.76	lux	lx
fl	foot-Lamberts	3.426	candela/m^2	cd/m^2
SYMBOL	WHEN YOU KNOW	MULTIPLY BY	TO FIND	SYMBOL
FORCE and PRESSURE or STRESS				
lbf	poundforce	4.45	newtons	N
lbf/in^2	poundforce per square inch	6.89	kilopascals	kPa

APPROXIMATE CONVERSIONS TO ENGLISH UNITS

SYMBOL	WHEN YOU KNOW	MULTIPLY BY	TO FIND	SYMBOL
LENGTH				
mm	millimeters	0.039	inches	in
m	meters	3.28	feet	ft
m	meters	1.09	yards	yd
km	kilometers	0.621	miles	mi
SYMBOL	WHEN YOU KNOW	MULTIPLY BY	TO FIND	SYMBOL
AREA				
mm^2	square millimeters	0.0016	square inches	in^2
m^2	square meters	10.764	square feet	ft^2
m^2	square meters	1.195	square yards	yd^2
ha	hectares	2.47	acres	ac
km^2	square kilometers	0.386	square miles	mi^2
SYMBOL	WHEN YOU KNOW	MULTIPLY BY	TO FIND	SYMBOL
VOLUME				
mL	milliliters	0.034	fluid ounces	fl oz
L	liters	0.264	gallons	gal
m^3	cubic meters	35.314	cubic feet	ft^3
m^3	cubic meters	1.307	cubic yards	yd^3
SYMBOL	WHEN YOU KNOW	MULTIPLY BY	TO FIND	SYMBOL
MASS				
g	grams	0.035	ounces	oz
kg	kilograms	2.202	pounds	lb
Mg (or "t")	megagrams (or "metric ton")	1.103	short tons (2000 lb)	T
SYMBOL	WHEN YOU KNOW	MULTIPLY BY	TO FIND	SYMBOL
TEMPERATURE (exact degrees)				
^oC	Celsius	1.8C+32	Fahrenheit	^oF
SYMBOL	WHEN YOU KNOW	MULTIPLY BY	TO FIND	SYMBOL
ILLUMINATION				
lx	lux	0.0929	foot-candles	fc
cd/m^2	$candela/m^2$	0.2919	foot-Lamberts	fl
SYMBOL	WHEN YOU KNOW	MULTIPLY BY	TO FIND	SYMBOL
FORCE and PRESSURE or STRESS				
N	newtons	0.225	poundforce	lbf
kPa	kilopascals	0.145	poundforce per square inch	lbf/in^2

*SI is the symbol for the International System of Units. Appropriate rounding should be made to comply with Section 4 of ASTM E380.(Revised March 2003)

Technical Report Documentation Page

<table>
<tr><td>1. Report No.</td><td>2. Government Accession No.</td><td colspan="2">3. Recipient's Catalog No.</td></tr>
<tr><td colspan="2">4. Title and Subtitle
Design Hurricane Storm Surge Pilot Study
BD-545, RPWO 42

UF CONTRACT NO.: 000 52102</td><td colspan="2">5. Report Date
December 2006

6. Performing Organization Code</td></tr>
<tr><td colspan="2">7. Author(s)
D. Max Sheppard, Don Slinn, Scott Hagen</td><td colspan="2">8. Performing Organization
University of Florida
University of Central Florida</td></tr>
<tr><td colspan="2" rowspan="2">9. Performing Organization Name and Address
Department of Civil and Coastal Engineering
365 Weil Hall
University of Florida
Gainesville, Florida 32611</td><td colspan="2">10. Work Unit No. (TRAIS)</td></tr>
<tr><td colspan="2">11. Contract or Grant No.
BC-545 RPWO-42</td></tr>
<tr><td colspan="2" rowspan="2">12. Sponsoring Agency Name and Address
Florida Department of Transportation
605 Suwannee Street, MS 30
Tallahassee, FL 32399</td><td colspan="2">13. Type of Report and Period Covered
Final Report
11/22/2004 – 12/31/2006</td></tr>
<tr><td colspan="2">14. Sponsoring Agency Code</td></tr>
<tr><td colspan="4">15. Supplementary Notes</td></tr>
<tr><td colspan="4">16. Abstract
Several aspects of storm surge and wave hindcasting were investigated in this study including one- and two-way coupling between storm surge and wave models and the impact of tidal and the adjoining bays on water elevations in the ocean/gulf in the vicinity of the inlet during a hurricane. A number of useful conclusions regarding these issues are presented.</td></tr>
<tr><td colspan="2">17. Key Word
hurricane, hindcast, surge-wave models</td><td colspan="2">18. Distribution Statement
No restrictions.</td></tr>
<tr><td>19. Security Classif. (of this report)
Unclassified.</td><td>20. Security Classif. (of this page)
Unclassified.</td><td>21. No. of Pages
149</td><td>22. Price</td></tr>
</table>

Executive Summary

This study investigated two problem areas related to hurricane storm surge hindcasting. The first problems addressed are associated with the need for coupling between hydraulics (storm surge) and wind wave models. The second problem is associated with the impact of tidal inlets and bay systems on open coast storm surge elevations. The report is divided into two parts; one covering the first issues and the second covering the inlet-bay impact. Numerous numerical experiments were performed with an idealized ocean, inlet and bay system and the results verified with a hindcast of an actual storm making landfall on the Louisiana Coast. The parameters investigated include steady and unsteady wind fields, different bed slopes, and a range of coupling intervals.

It was found that one-way coupling (i.e. periodically inputting wave model output into the storm surge model) has a significant effect on storm surge elevations over running the surge model with no wave input. It was also found that two-way coupling (wave model output to surge model and surge model output to wave model) over one-way coupling has little impact on storm surge elevations. It was also found that including periodic storm surge model output to the wave model has a significant effect on the wave parameters in water depths less than about one-half the wave lengths. For the conditions considered in this study coupling intervals less than about 3 hours produce only minor changes in both storm surge elevations and wave heights and periods.

An extensive investigation of the effect of tidal inlets and the adjoining bay systems on water levels in the ocean/gulf in the vicinity of the inlet resulted in a quantification of this effect. From a practical application point of view the impact of bay storage on open coast storm surge hydrographs was found to be only important for large inlet-bay systems.

Introduction:

The purpose of this study was to examine several aspects of the processes by which storm surges are predicted including 1) the importance of two-way coupling between storm surge and wave models, and 2) under what conditions do tidal inlets impact water elevations on open coast storm surge hydrographs in the vicinity of the inlet during hurricanes.

Shallow water wave (computer) models, such as SWAN, output wave induced radiation stresses that can be input to depth-averaged hydraulics models, such as ADCIRC, to produce a more accurate estimation of the water elevation. The time dependent water elevations from ADCIRC can then be input to SWAN to produce more accurate wave predictions. In this report, one-way coupling refers to periodically inputting the radiation stresses from the wave model to the hydraulics model. Two-way coupling refers to the procedure of periodically inputting radiation stresses from the wave model to the hydraulics model and periodically inputting water elevations from the hydraulics model to the wave model. The time interval for the information exchange need not be the same; in fact the frequency of water elevation exchange can be lower than the wave radiation stress exchange. Most storm surge predictions/hindcasts to date that include waves have only used one-way coupling (radiation stress from wave model input to hydraulics model). Two of the questions addressed in this study were "How does two-way (over one-way) coupling impact 1) storm surge elevations and 2) wave parameters during a hurricane hindcast?".

Most storm surge analyses for coastal bays, estuaries, etc. only extend the seaward extent of their mesh a short distance into the ocean/gulf (on the order of a mile). The desired probability storm surge (return interval) hydrograph for the open coast at that location is applied to the open coast boundary. The question is; "Under what conditions (size of inlet, etc.) is the hydrograph significantly affected by the inlet?" This study addressed both the coupling and the inlet/bay issues.

The work on this study was divided into two parts. Drs. Sheppard and Slinn (and their postdoctoral and graduate students) at the University of Florida were responsible for the

one and two-way coupling issues and Dr. Hagen (and his graduate students) at the University of Central Florida were responsible for the inlet impact issues. This report is also divided into two separate parts with Part I covering the model coupling issues and Part II covering the tidal inlet aspects of the problem.

PART 1 TABLE OF CONTENTS

PART 1 LIST OF FIGURES

Part I STORM SURGE & WAVE MODEL COUPLING

Objectives:

The objectives of this part of the study were as follows:

- Develop one- and two-way coupling code and procedures for coupling the hydraulics model, ADCIRC, and the wave model, SWAN utilizing.
- One- and two-way coupling code perform numerical experiments with idealized and real geometries with steady, uniform and unsteady, hurricane wind fields.
- Different bed slopes
- Different frequencies of information exchange between models
- Analyze the results of the numerical experiments to determine the differences in water elevations and wave parameters for the one- and two-way coupling.

Procedure Summary:

Algorithms were developed for one- and two-way coupling between ADCIRC2DDI (depth averaged flow and storm surge model) and SWAN (shallow water wave model). The initial numerical experiments were conducted with idealized coastlines and bed slopes (continental shelf slopes). Both storm surge (ADCIRC) and wave (SWAN) meshes were developed for these idealized situations. Numerical experiments were conducted for a range of bed slopes and wind conditions with both one- and two-way coupling between the models and the results analyzed and compared. The frequency of information exchange between the models was also varied to see the effect on both water elevation and wave parameters. Once the tests with idealized geometries were completed the models were configured for a real geometry (coastline, bathymetry and topography) and tests performed with a hindcasted wind field generated by the authors for Hurricane Katrina. The next phase of this part of the study was to test the one- and two-way coupling codes for an actual hurricane and coastline. The results from this test were analyzed and compared with those from the previous tests with idealized coastlines and wind fields.

Test Configurations:

In order to examine the effects of bed slope on the results of one- and two- way coupling an idealized coastline with uniform continental shelf slopes were created and analyzed. Figure 1 shows the two slopes considered. Figure 2 shows elevation and plan views of the model. The two slopes considered are 0.00072 and 0.0021 which cover a common range of slopes found in Florida. All idealized model meshes contained an inlet and bay system.

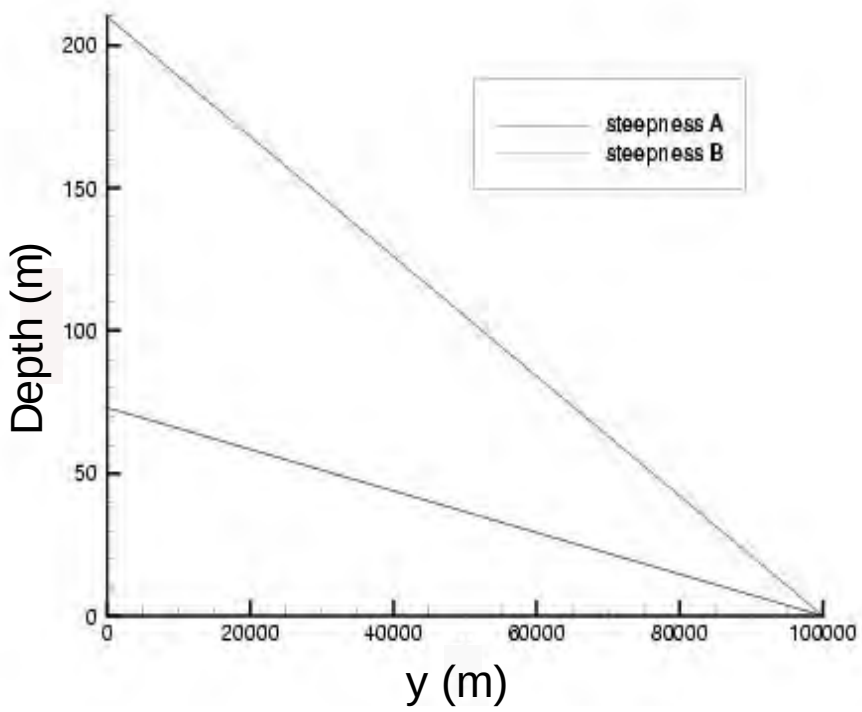

Figure 1 The two idealized bed slopes used in the analyses. The origin for the y coordinate is located 100,000 m offshore and the positive direction is toward the shore.

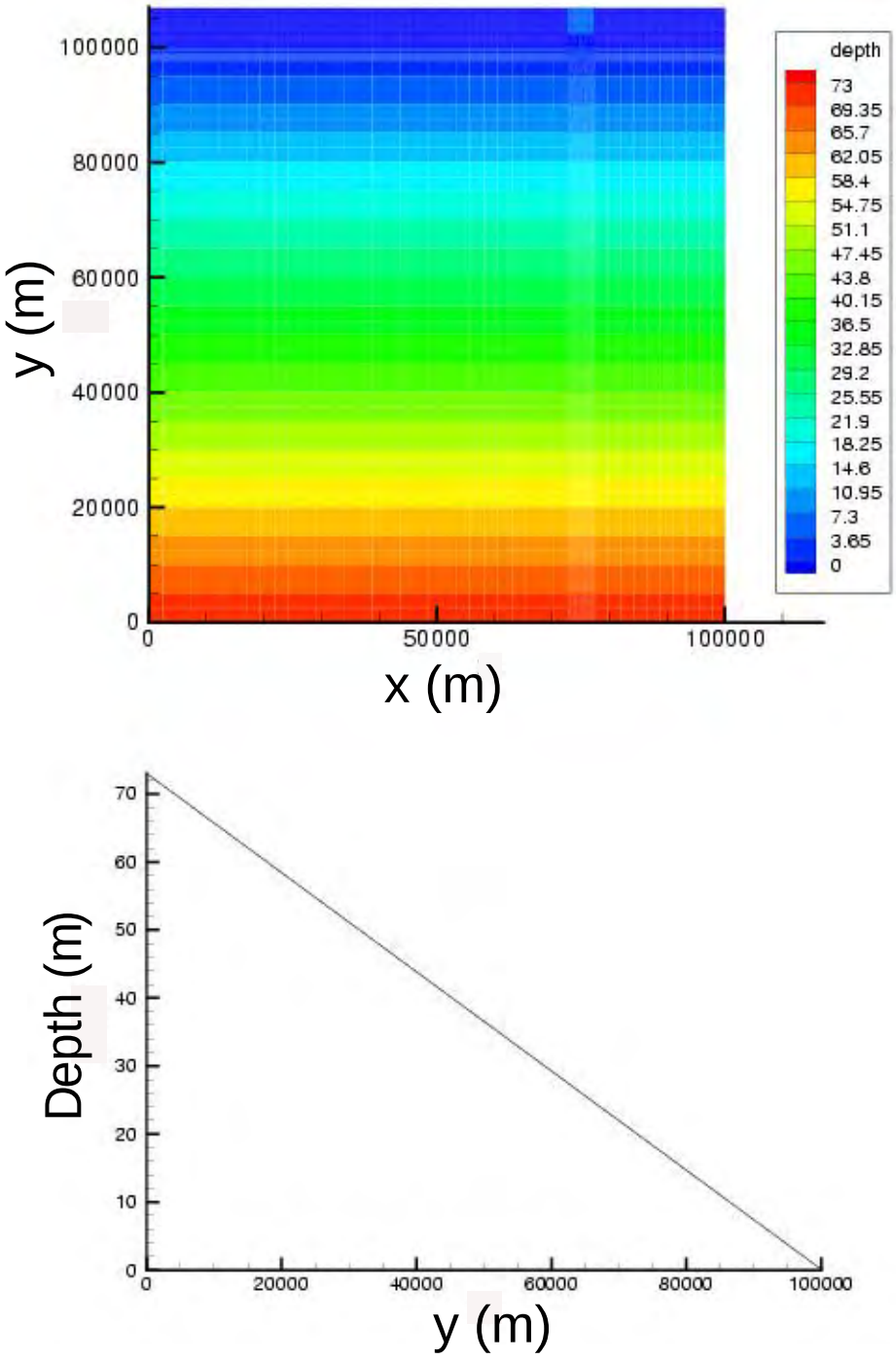

Figure 2 Elevation and plan views of the idealized model geometry for one of the bed slopes.

Two basically different wind fields were used in these tests. One was a uniform and steady wind field directed toward and normal to the shore (Figure 3). The second wind field was that of an idealized hurricane whose path was normal to the shore (Figure 4).

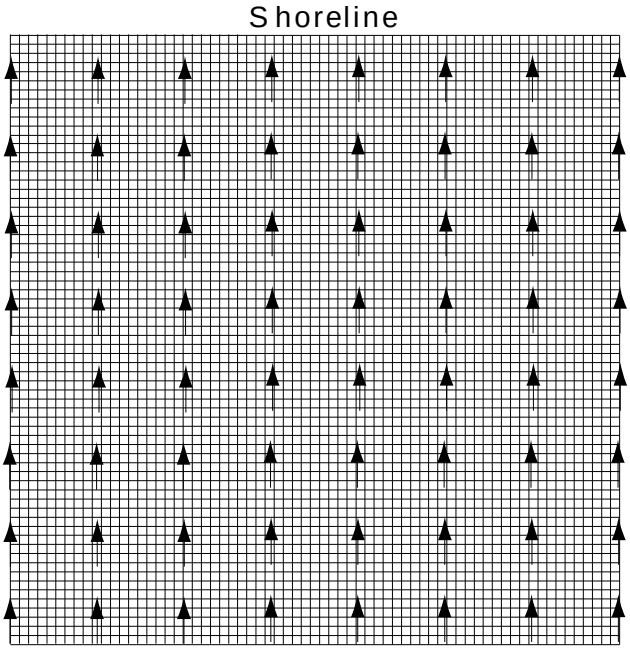

Figure 3 Wave model mesh showing steady, uniform wind field.

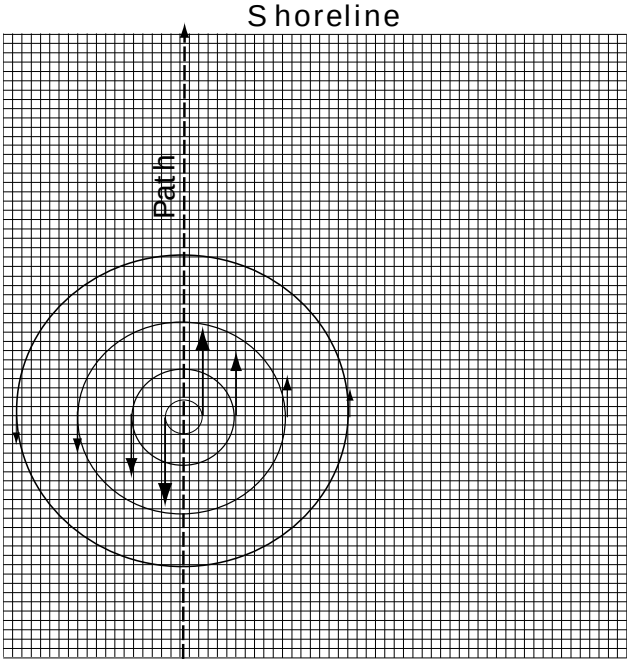

Figure 4 Wave model mesh with idealized hurricane wind field.

The tests with a real geometry (shoreline, bathymetry and topography) were conducted with Hurricane Katrina that made landfall on the Louisiana Coast in the summer of 2005 (Figure 5). The Katrina wind field for this study was generated using a wind model developed by the authors of this report. The ADCIRC (hydraulics model) mesh for these tests is shown in Figure 6. There was considerable damage to the infrastructure in Louisiana, Mississippi, and Alabama.

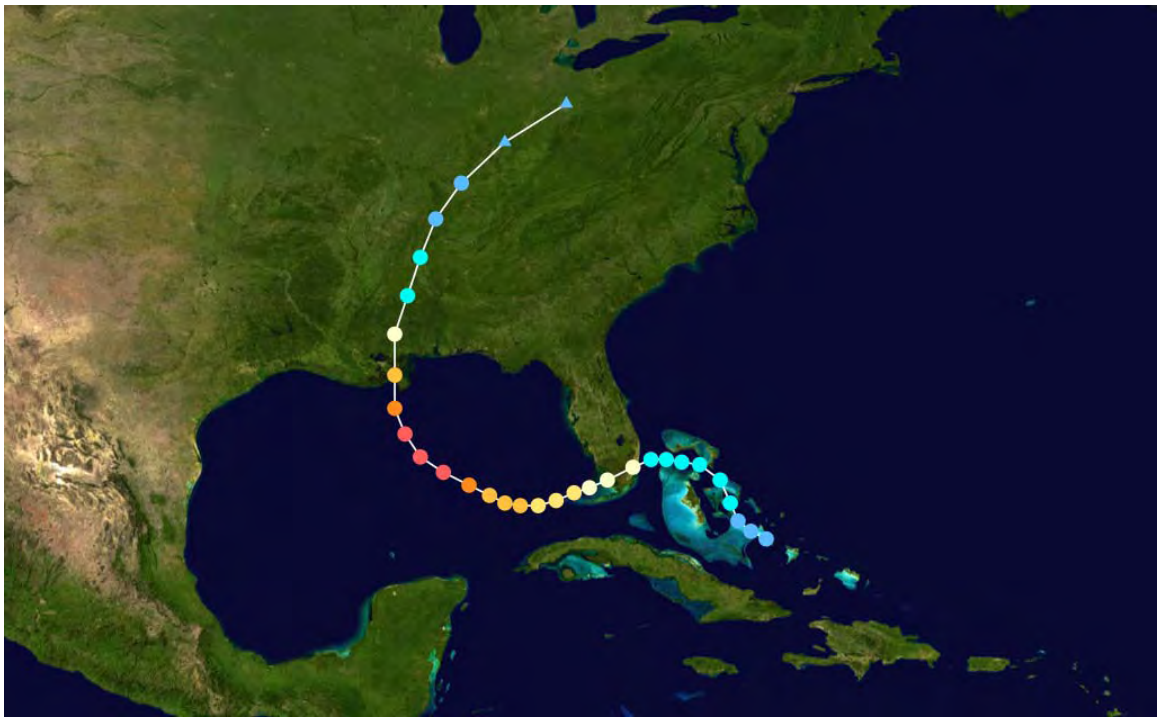

Figure 5 Hurricane Katrina's path.

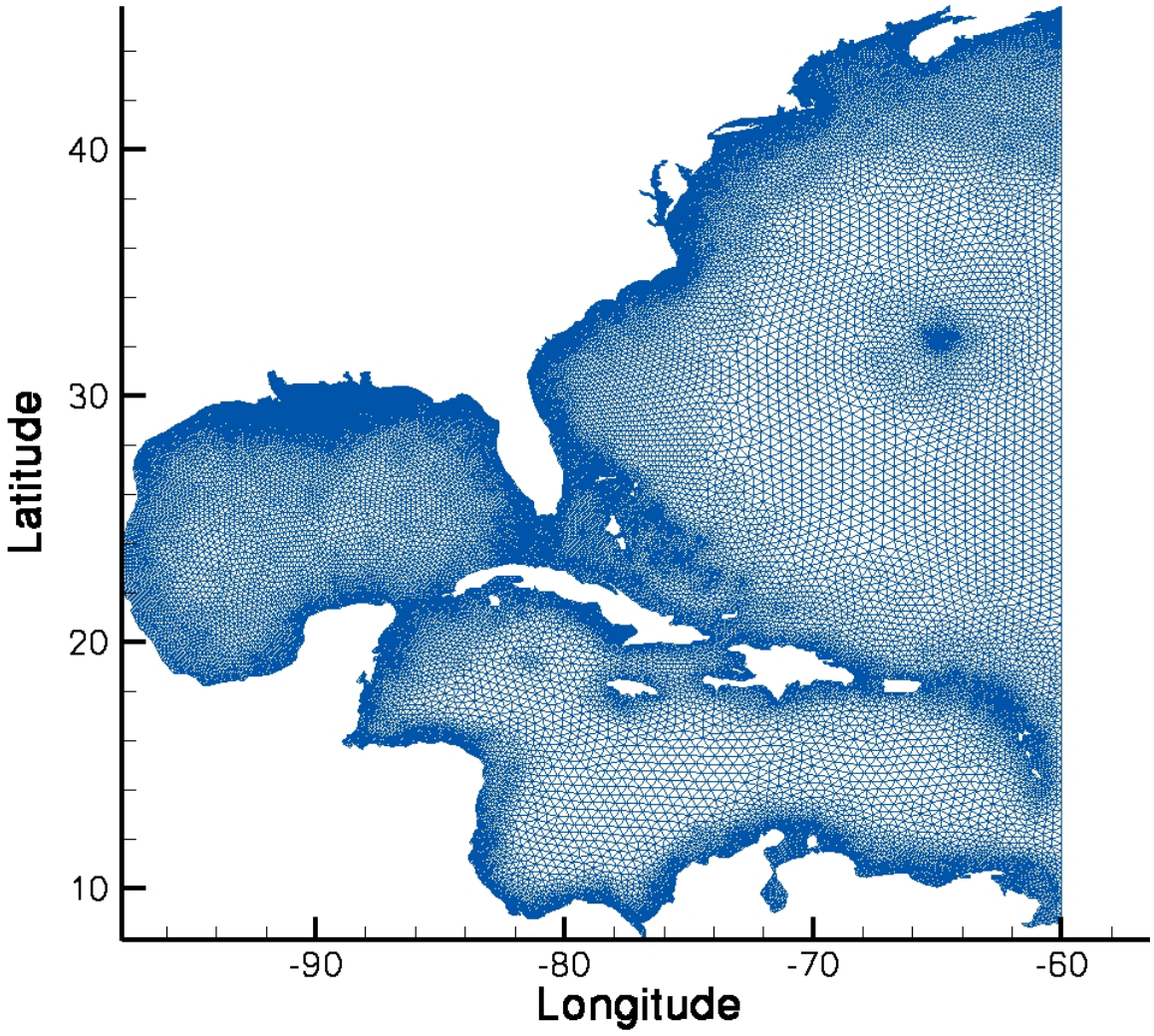

Figure 6 ADCIRC Model Mesh Used in Hurricane Katrina Hindcast.

Ideal Configuration Runs:

The ADCIRC and SWAN meshes for the idealized coastline and bay system are shown in Figure 7 and Figure 8, respectively.

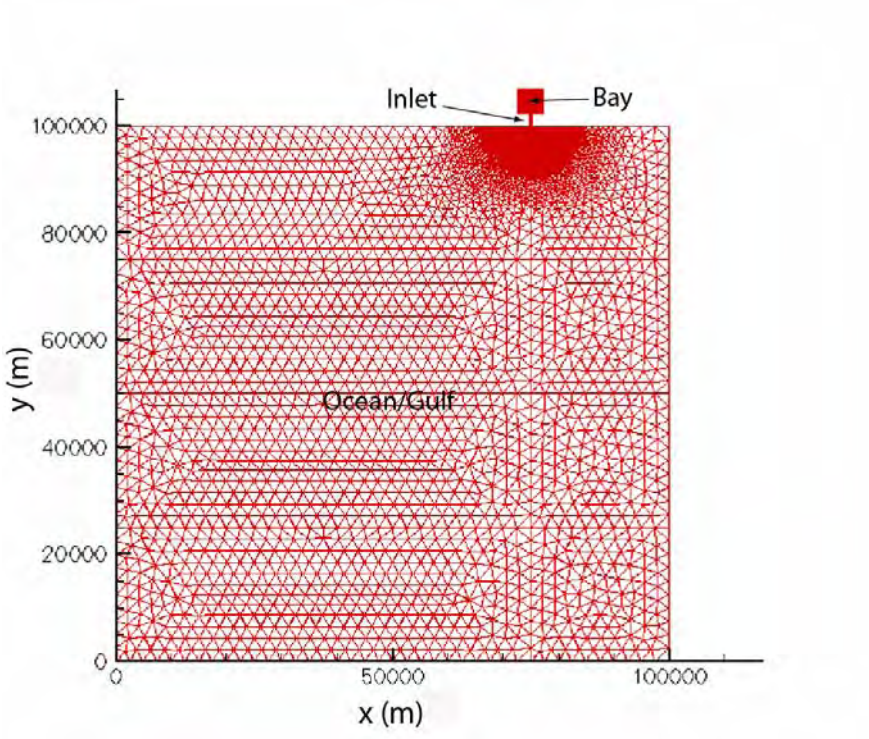

Figure 7 ADCIRC model mesh for idealized coastline and bay system.

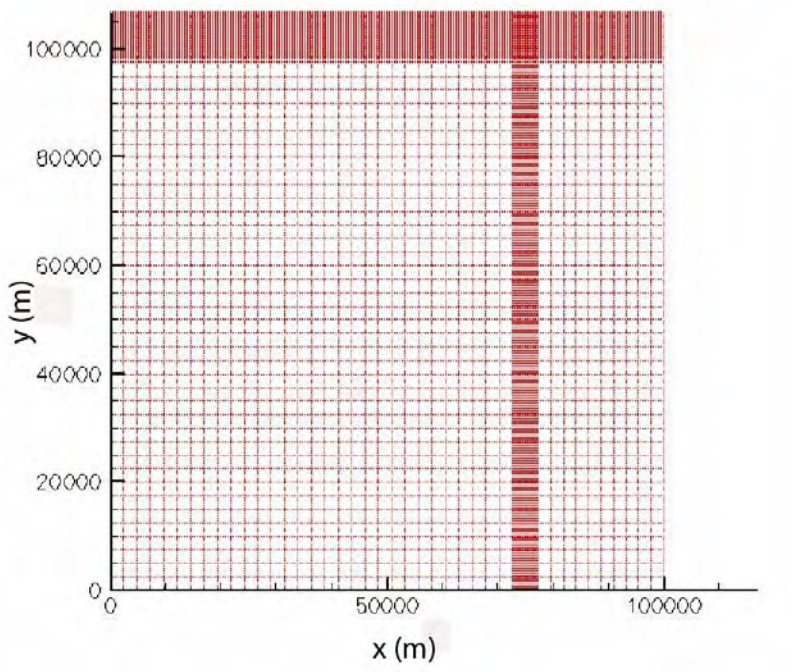

Figure 8 SWAN model mesh for the idealized coastline and bay system.

The element size for the rectilinear SWAN mesh is dictated by the size of the inlet. The depth of the inlet was held at 3.7 m and the widths varied. Note that the reason for inclusion of the inlet bay system in Part 1 of this study was to provide a means to verify the results from the Part 2 investigation.

Numerous tests were performed with the idealized coastline, inlet-bay system. The conditions for each of the test sequences are outlined below along with the results from each run. Output from the model runs at several offshore and bay locations are presented. The locations are identified by numbers in the definition sketches shown in Figure 9 and Figure 10.

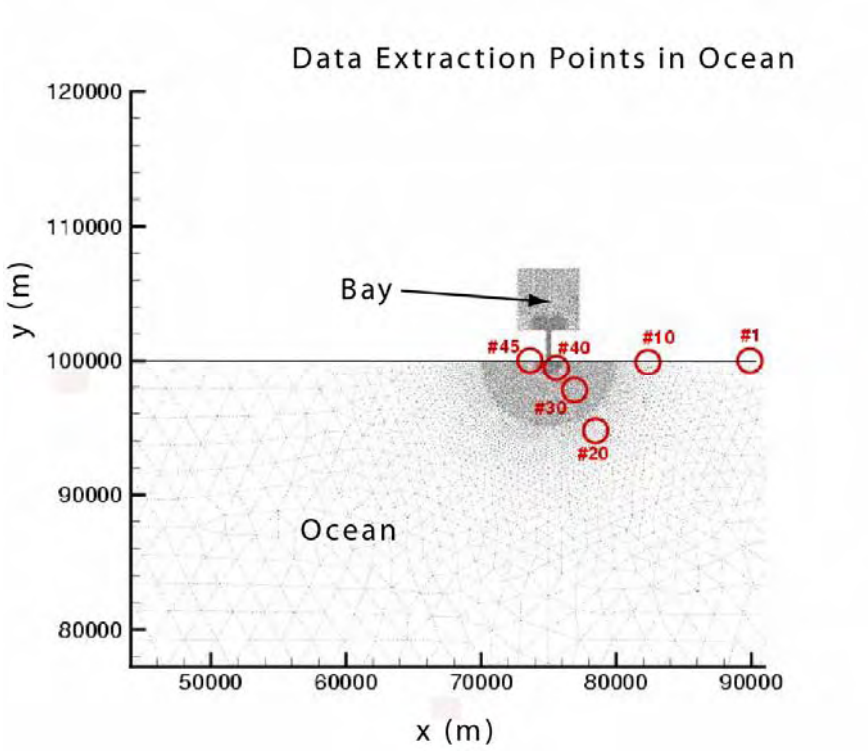

Figure 9 Definition drawing showing locations where data was extracted.

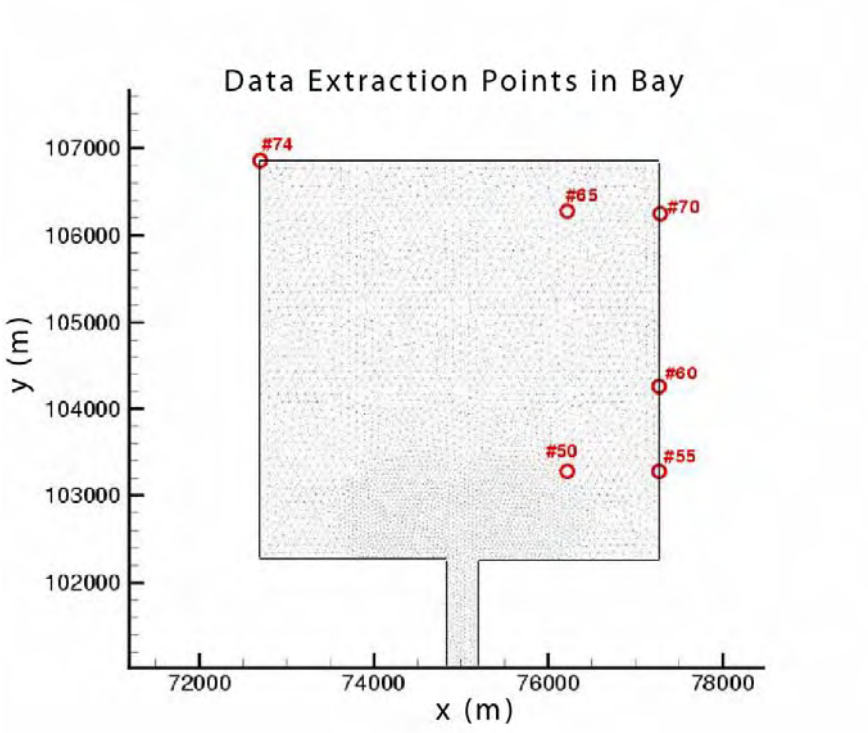

Figure 10 Definition drawing showing locations where data was extracted.

Test Sequence 1

A series of tests were performed with an idealized coast and inlet-bay system and steady, uniform wind speeds and an idealized hurricane wind field with parameters similar to that of Hurricane Ivan. Four computer model scenarios were run 1) ADCIRC with wind only (no wave input), denoted by "ele_wind" in the figures, 2) ADCIRC and SWAN with one-way (SWAN to ADCIRC) coupling (SWAN run with initial water elevations and input into ADCIRC; denoted by "ele_one-way" in the figures, 3) ADCIRC and SWAN with two-way (SWAN to ADCIRC and ADCIRC to SWAN every 3 hours) coupling, ADCIRC started with "hotstarts" at each information exchange; denoted by "ele_3" in the figures, 4) ADCIRC and SWAN with two-way coupling every 3 hours, "pausing" ADCIRC at each information exchange; denoted by 'ele_paused" in the figures. Scenarios 3 and 4 are just two different ways of executing the information exchange in the two-way coupling between ADCIRC and SWAN. These tests were carried out for three different steady and uniform wind speeds, 30, 50 and 70 m/s (67, 111 and 157 mi/hr) and for an unsteady idealized hurricane wind field. The results at a number of points in the ocean and bay system were monitored and are presented in Figures. Note

that the model boundaries are rigid (no flow normal to the boundary). The wave heights increase with fetch length until wave steepness limitations take over (wave length shortens as the waves shoal). The setup patterns are impacted by return flow along the side boundaries.

Wind speed of 30 m/s

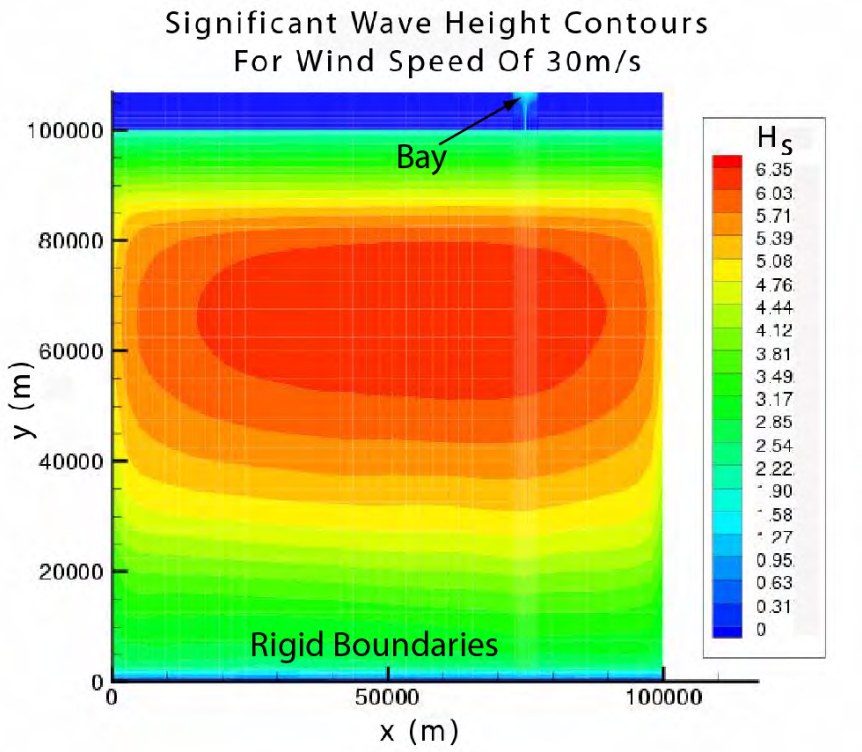

Figure 11 Significant wave heights for steady, uniform 30 m/s onshore wind.

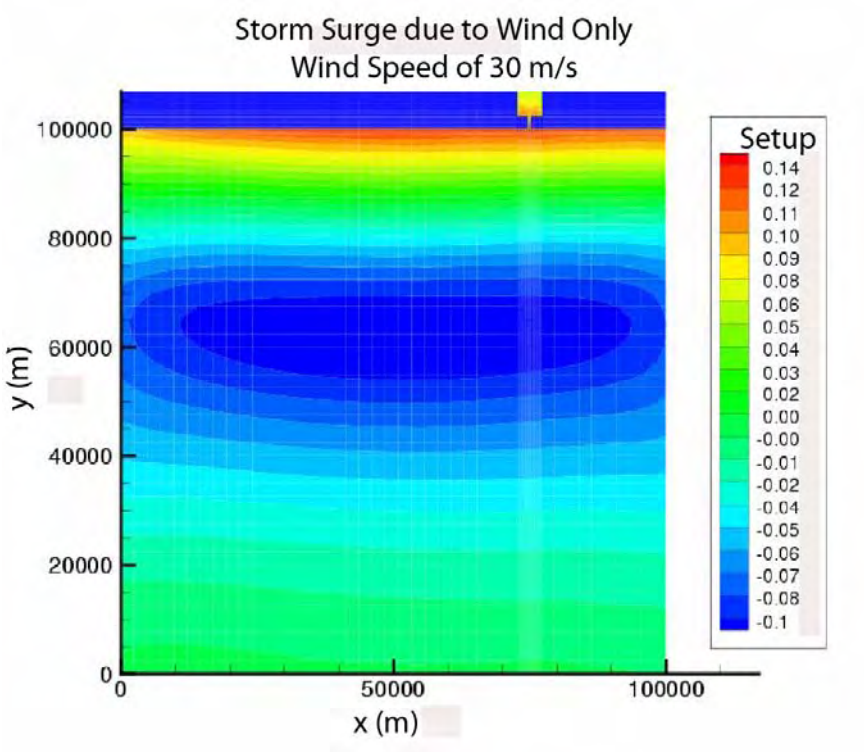

Figure 12 Wind setup for a 30 m/s onshore wind speed.

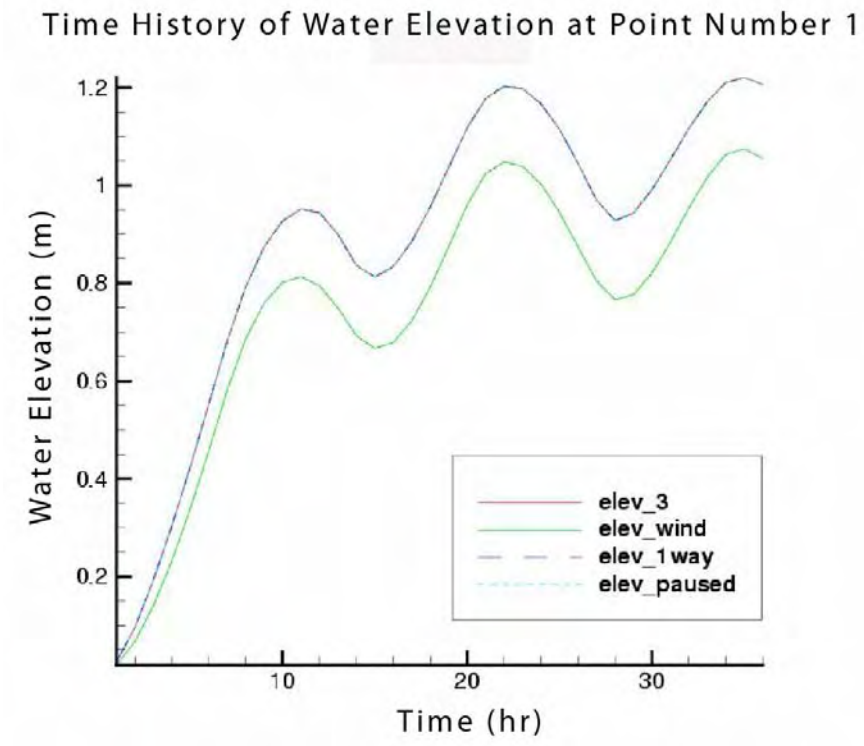

Figure 13 Time history of water elevation at Point 1 on the open coast (see Figure 9), Wind Speed = 30 m/s.

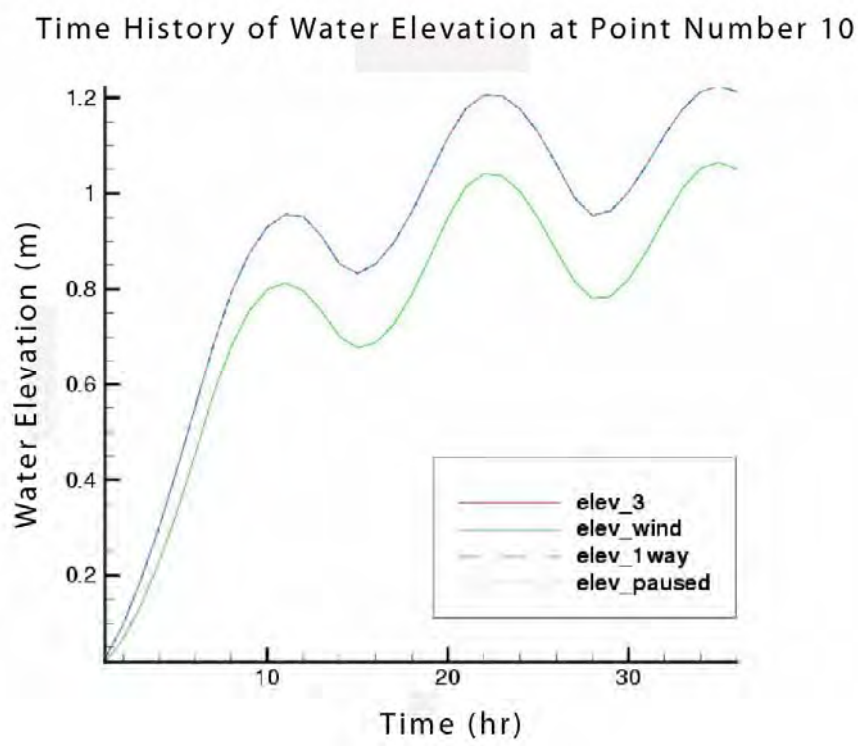

Figure 14 Time history of water elevation at Point 10 on the open coast (see Figure 9), Wind Speed = 30 m/s.

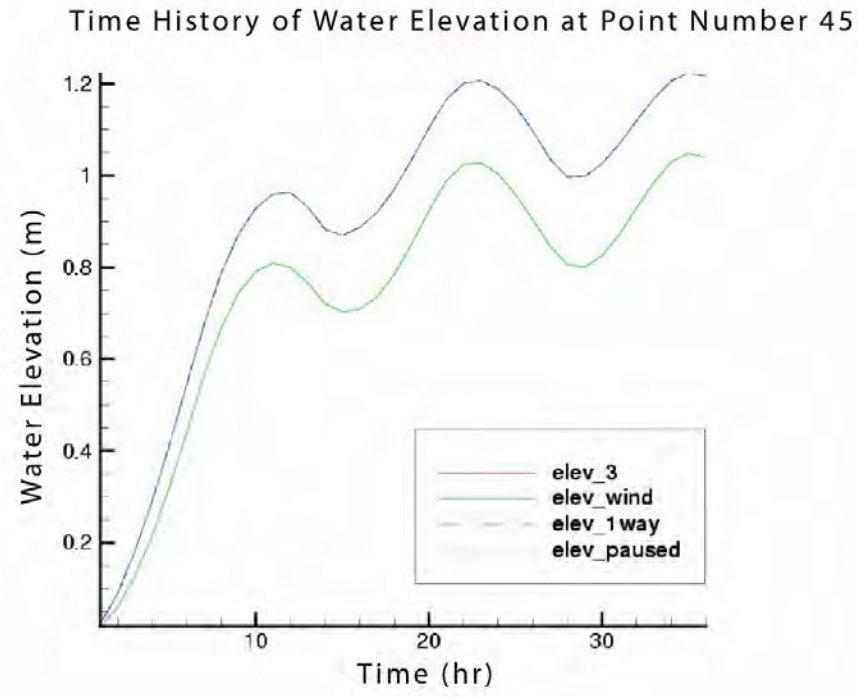

Figure 15 Time history of water elevation at Point 45 near the inlet (see Figure 9), Wind Speed = 30 m/s.

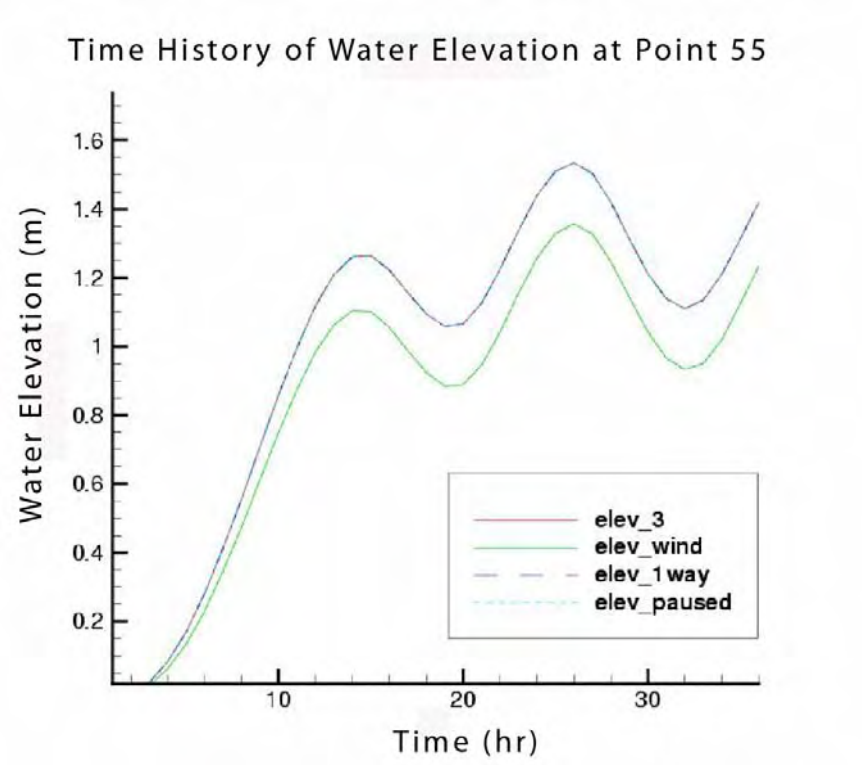

Figure 16 Time history of water elevation at Point 55 inside the bay (see Figure 10), Wind Speed = 30 m/s.

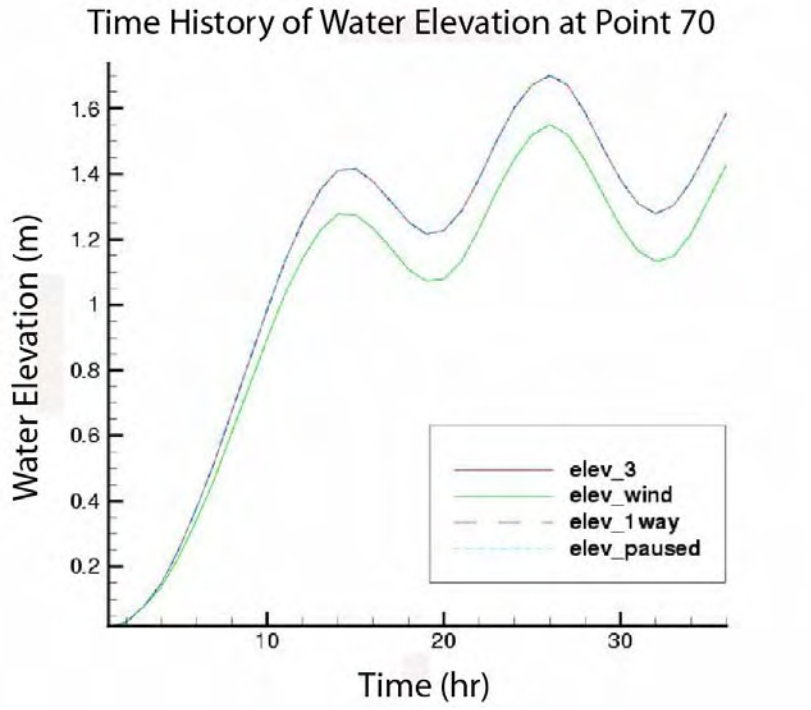

Figure 17 Time history of water elevation at Point 70 inside the bay (see Figure 10), Wind Speed = 30 m/s.

Wind speed of 50 m/s

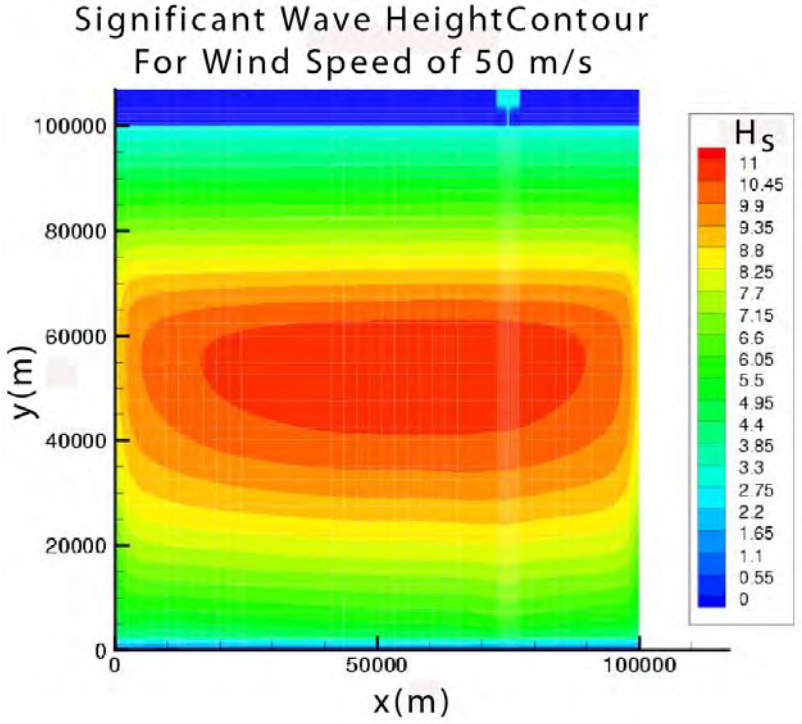

Figure 18 Significant wave heights for steady, uniform 50 m/s onshore wind.

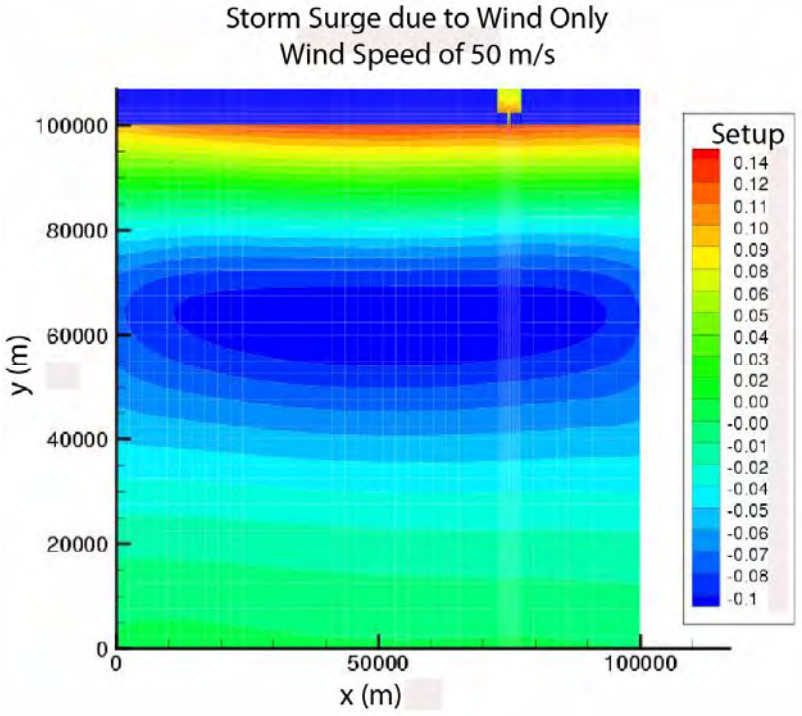

Figure 19 Storm Surge due to 50 m/s Wind Only (No Wave Input), Wind Speed = 50 m/s.

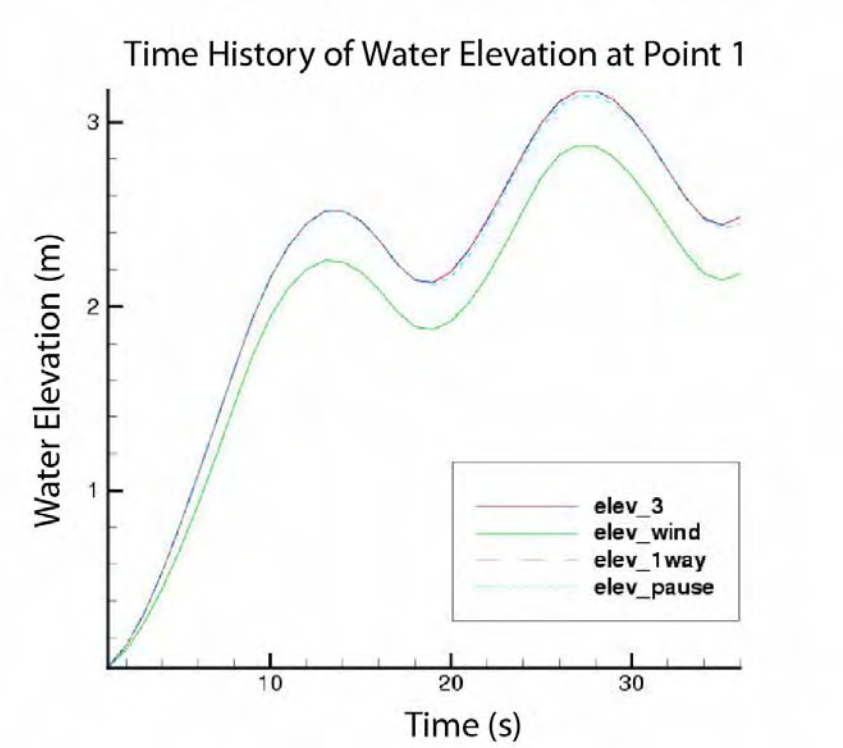

Figure 20 Time history of water elevation at Point 1 on the open coast (see Figure 9), Wind Speed = 50 m/s.

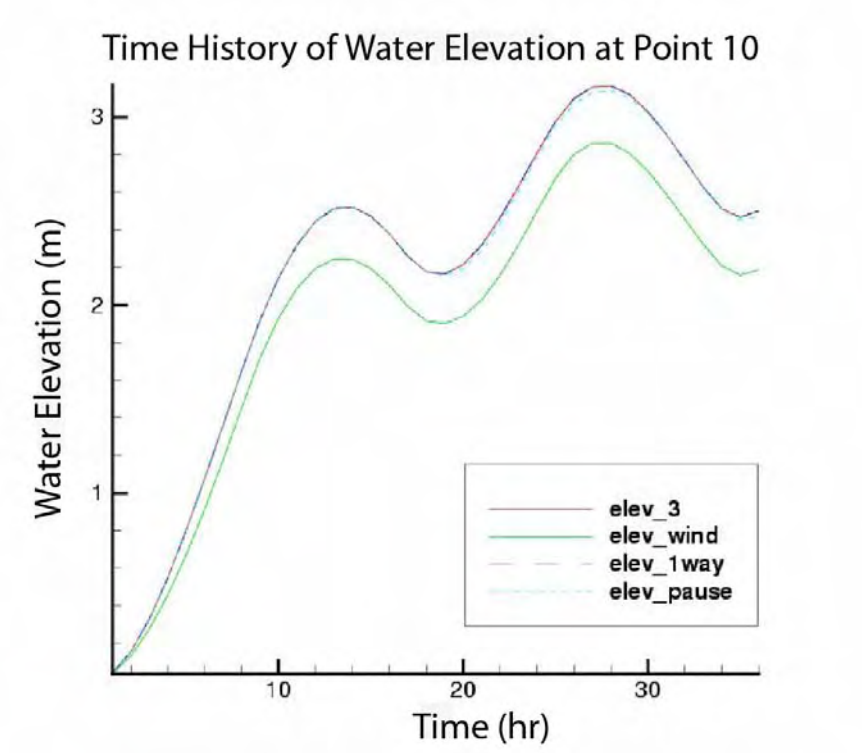

Figure 21 Time history of water elevation at Point 10 on the open coast (see Figure 9), Wind Speed = 50 m/s.

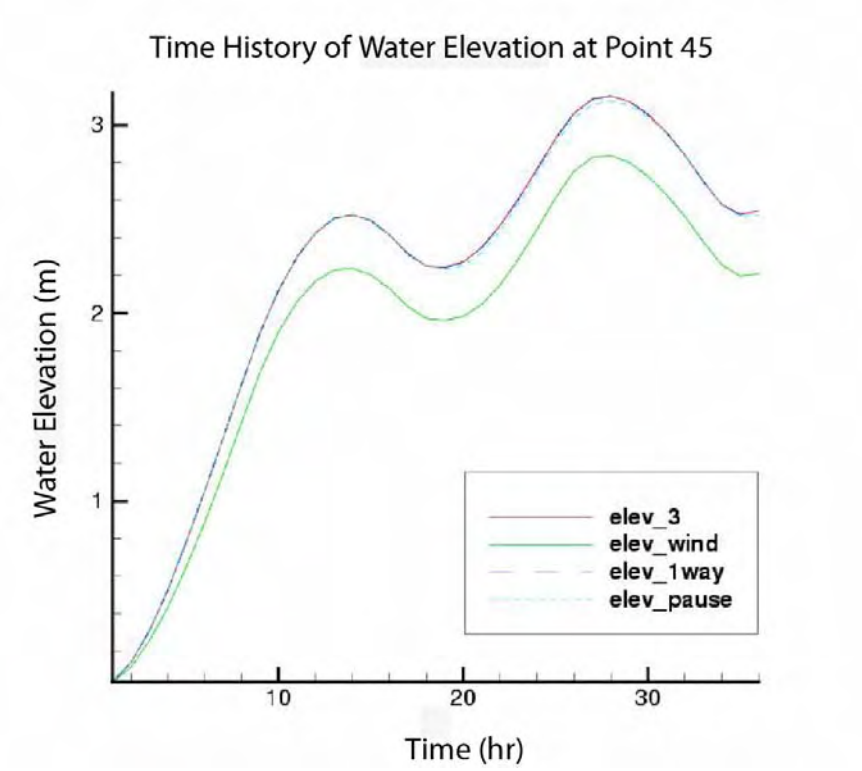

Figure 22 Time history of water elevation at Point 45 near the inlet (see Figure 9), Wind Speed = 50 m/s.

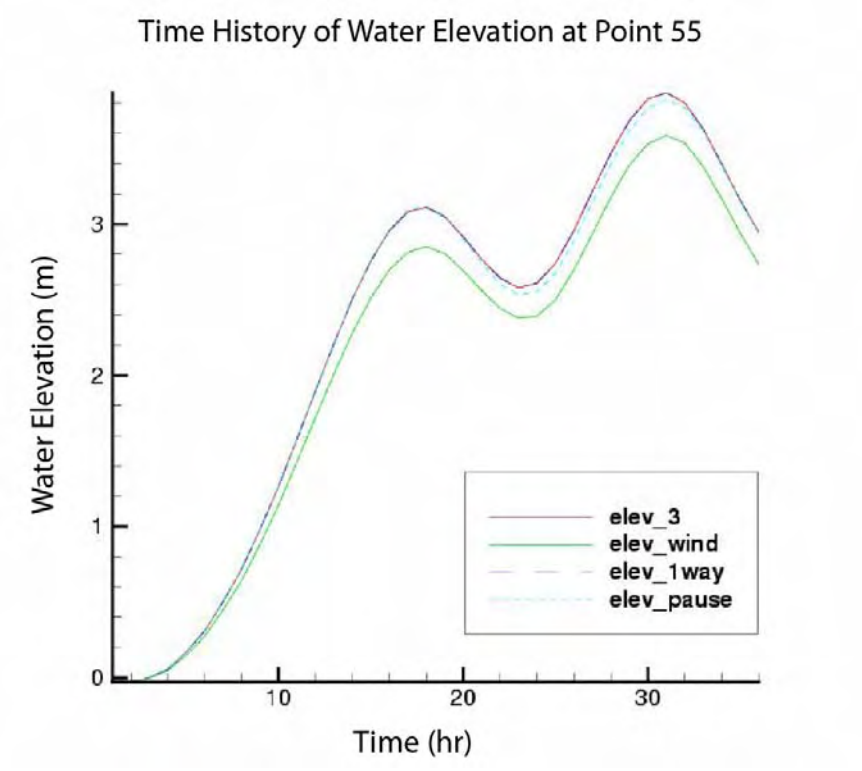

Figure 23 Time history of water elevation at Point 55 near the inlet (see Figure 10), Wind Speed = 50 m/s.

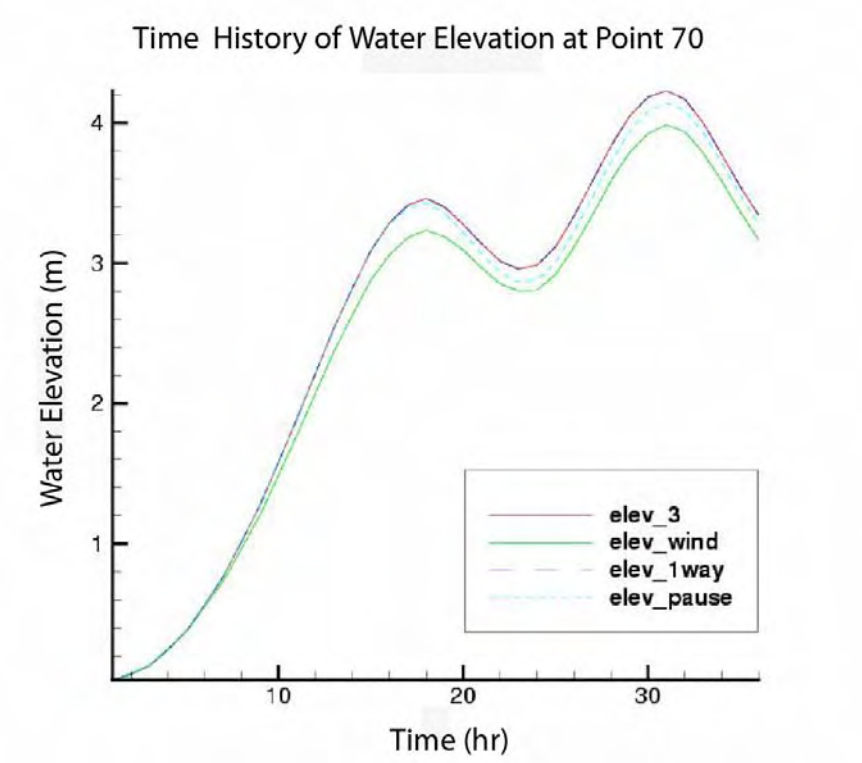

Figure 24 Time history of water elevation at Point 70 near the inlet (see Figure 10), Wind Speed = 50 m/s.

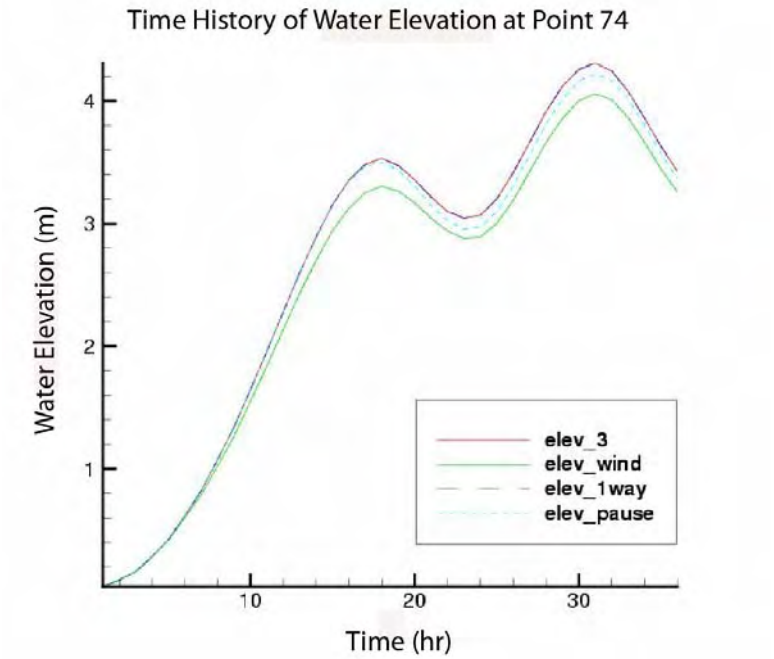

Figure 25 Time history of water elevation at Point 74 near the inlet (see Figure 10), Wind Speed = 50 m/s.

Wind speed of 70 m/s

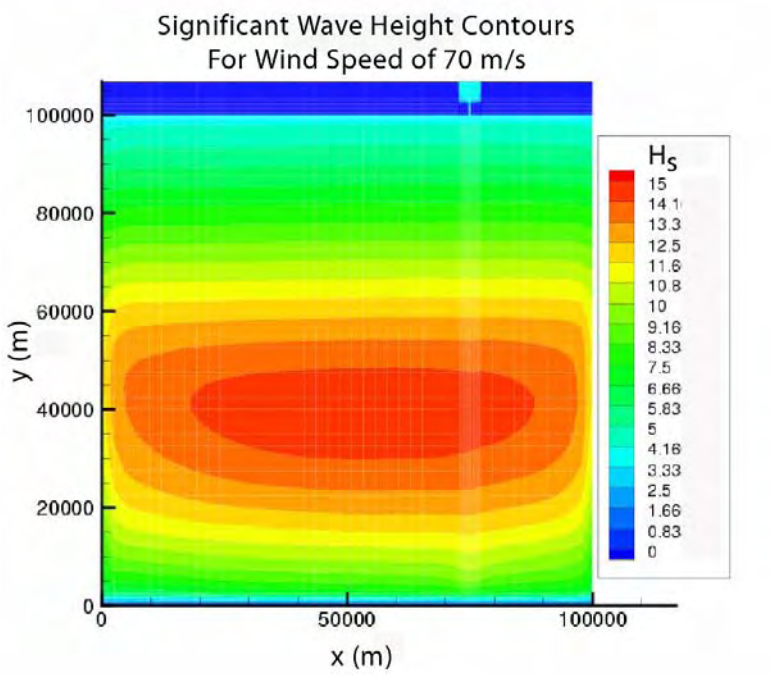

Figure 26 Significant wave heights for steady, uniform 70 m/s onshore wind.

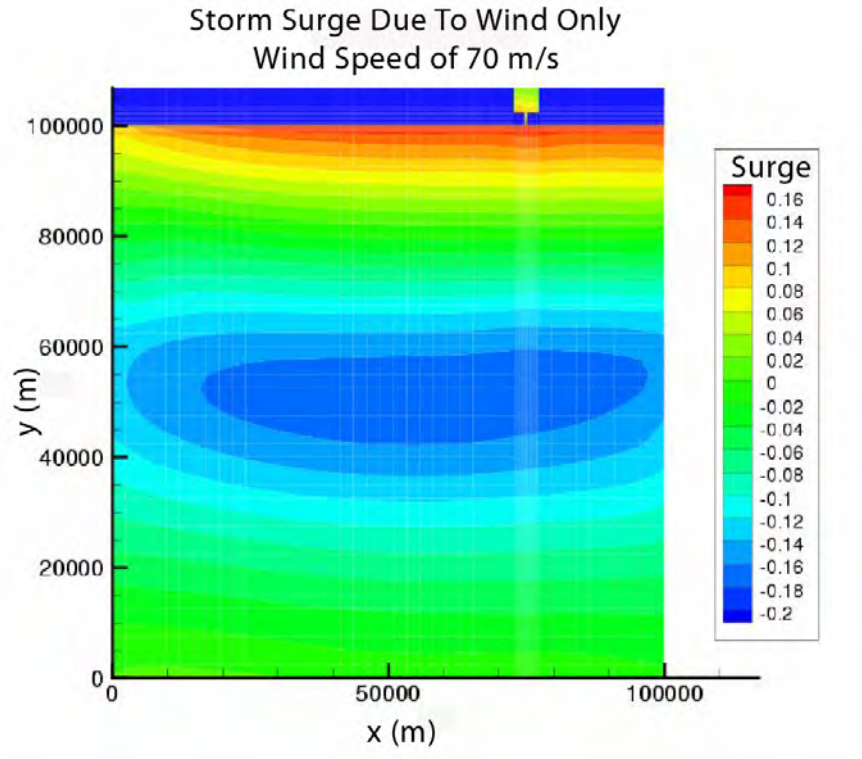

Figure 27 Storm Surge due to 70 m/s Wind Only (No Wave Input).

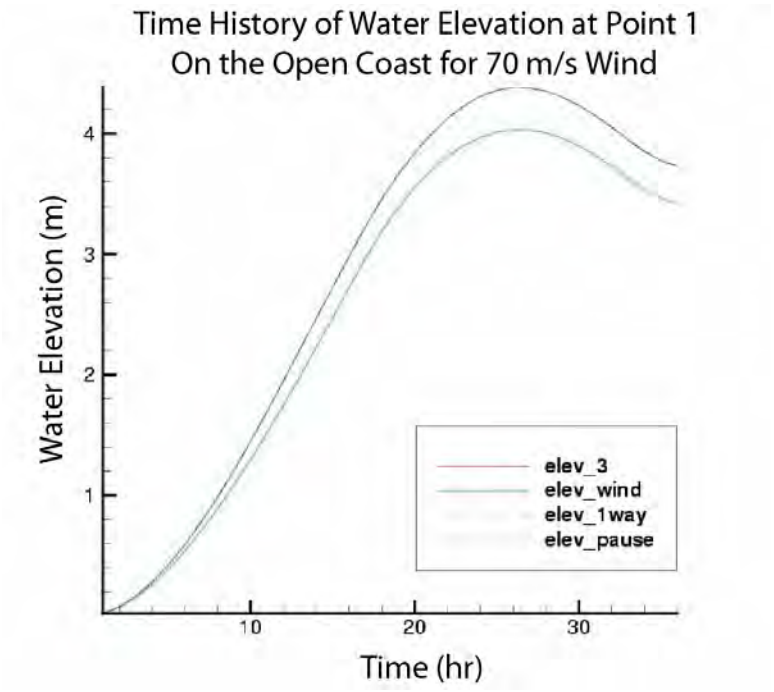

Figure 28 Time history of water elevation at Point 1 on the open coast (see Figure 9), Wind Speed = 70 m/s.

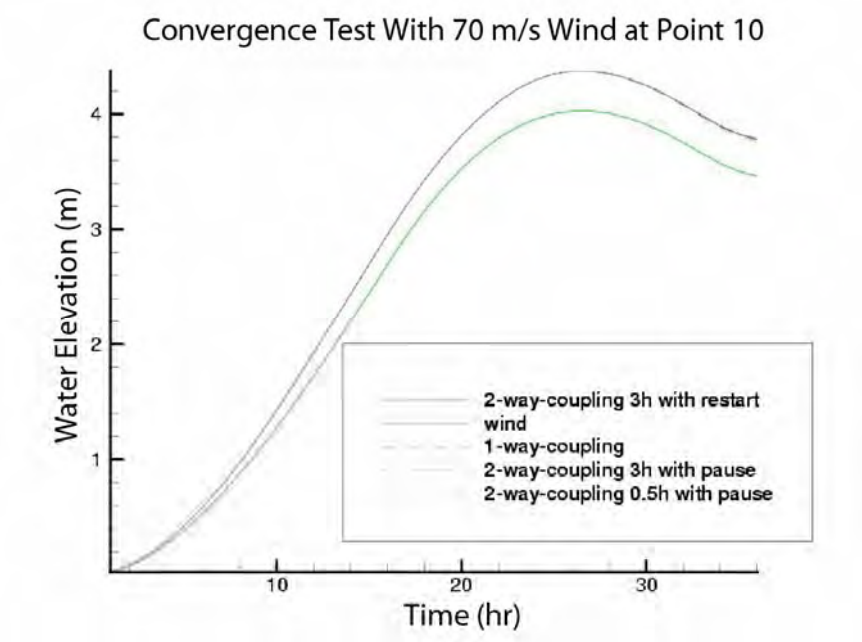

Figure 29 Time history of water elevation at Point 10 on the open coast (see Figure 9), Wind Speed = 70 m/s.

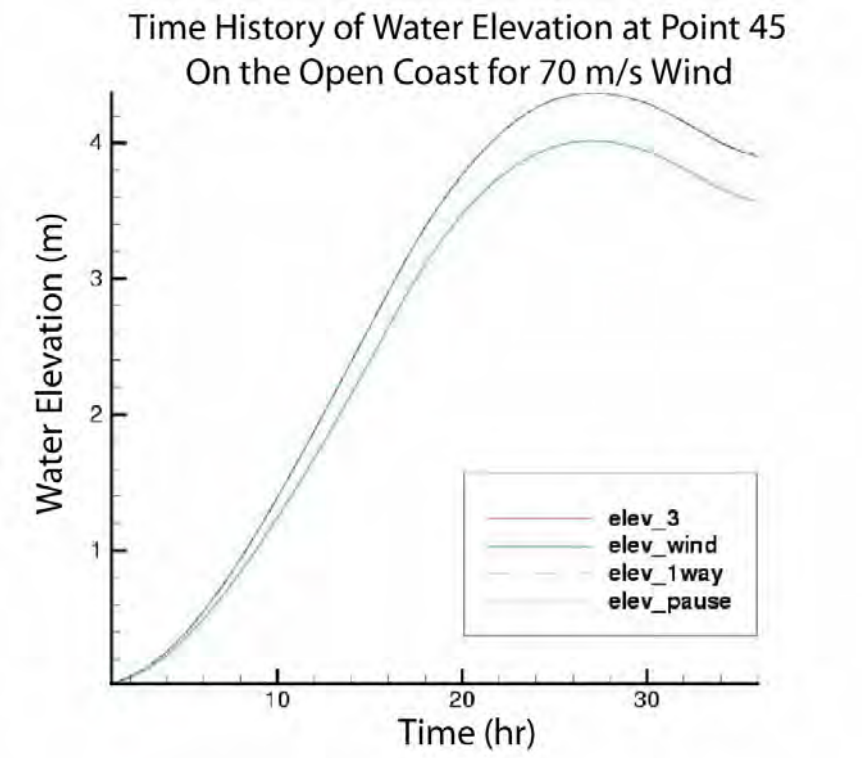

Figure 30 Time history of water elevation at Point 45 near the inlet (see Figure 9), Wind Speed = 70 m/s.

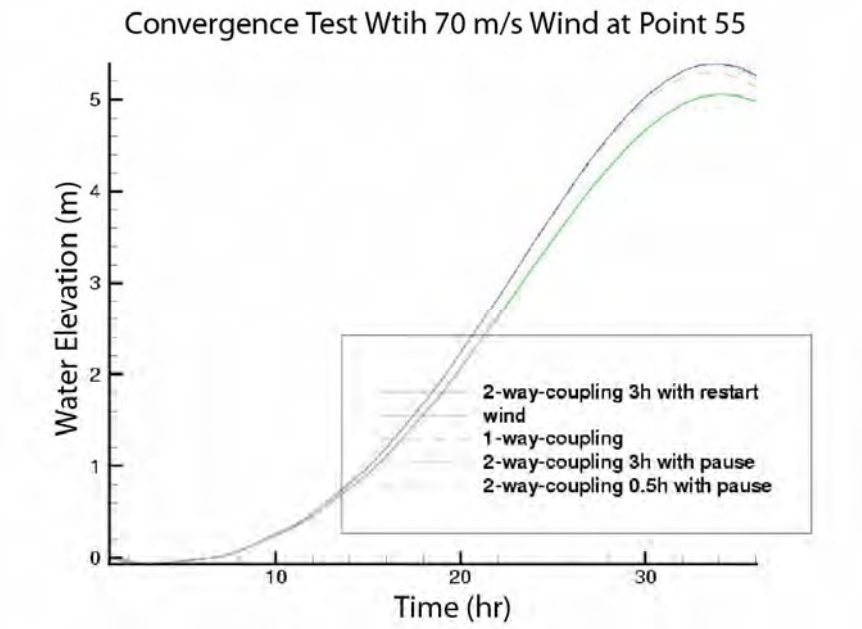

Figure 31 Time history of water elevation at Point 55 inside the Bay (see Figure 10), Wind Speed = 70 m/s.

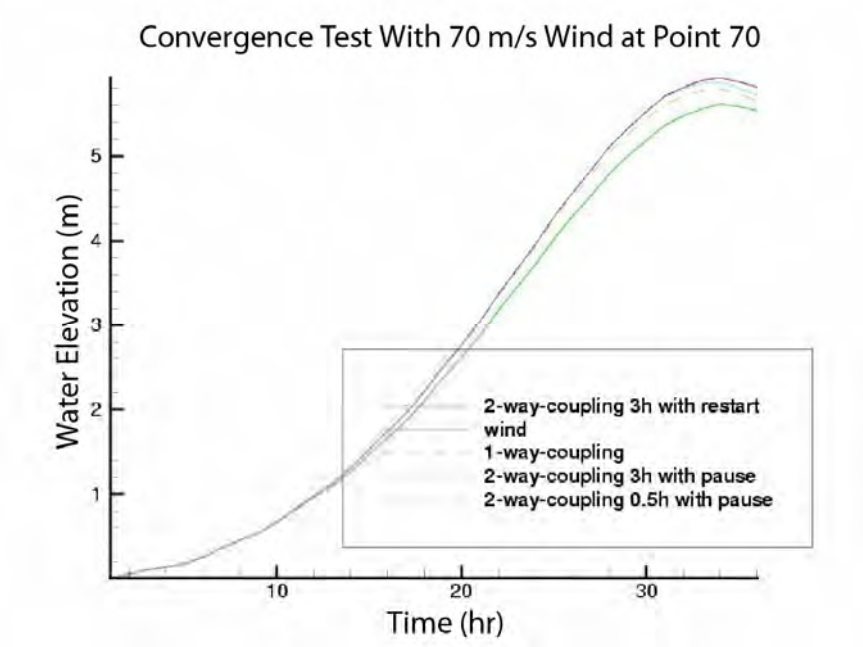

Figure 32 Time history of water elevation at Point 70 inside the Bay (see Figure 10), Wind Speed = 70 m/s.

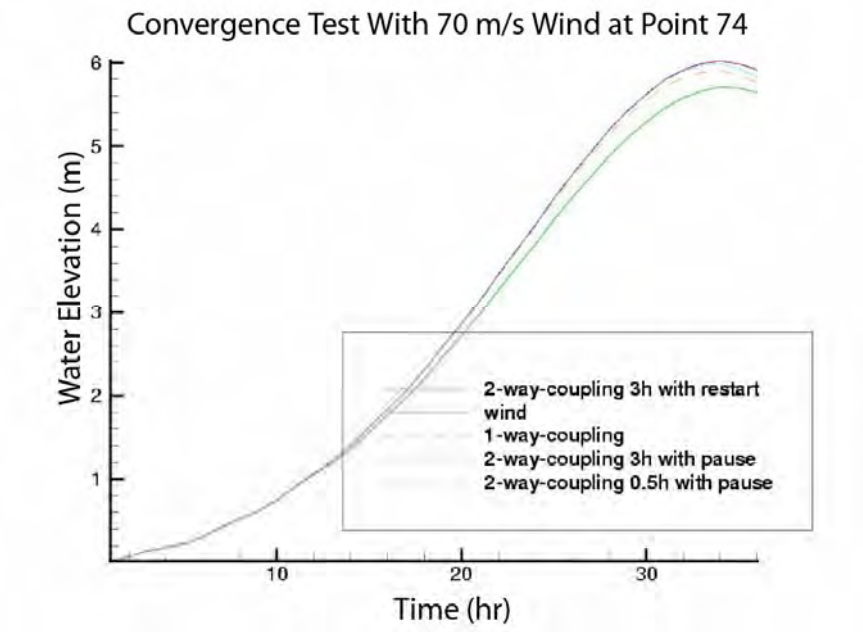

Figure 33 Time history of water elevation at Point 74 inside the Bay (see Figure 10), Wind Speed = 70 m/s.

Test Sequence 2

In this sequence tests with the idealized coastline, inlet-bay system were performed with a hurricane wind field. The wind field was generated with a wind model developed by the authors of this report and the hurricane parameters (maximum wind speeds and radius

to maximum winds) were similar to that of Hurricane Ivan. The path of the hurricane was normal to the shoreline and made landfall to the left of the inlet-bay system. Atmospheric pressure contours for the hurricane as it makes landfall are shown in the 3 hour sequence of plots shown in Figure 34.

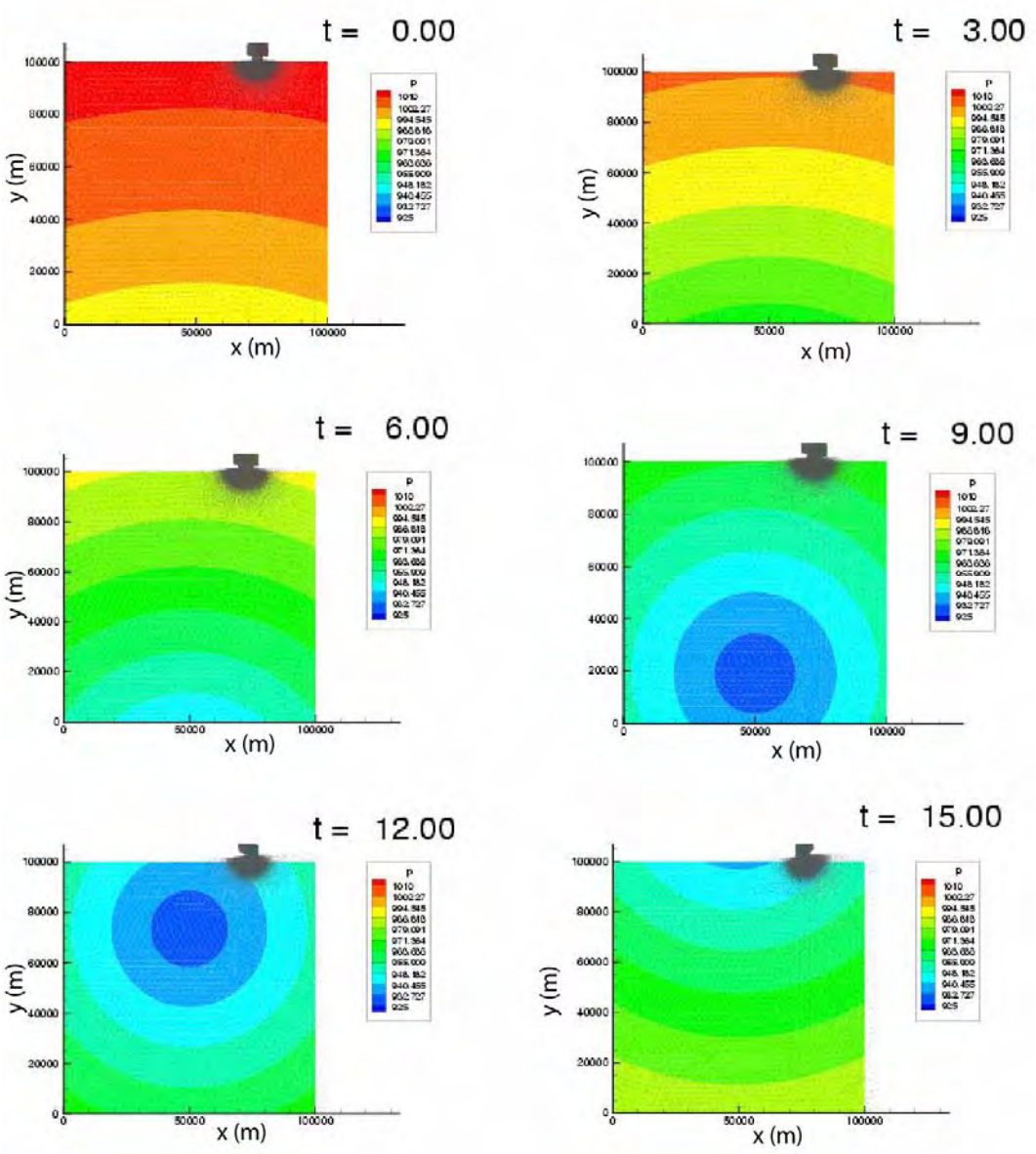

Figure 34 Hurricane Pressure Fields at 3 hour Intervals as the Hurricane Makes Landfall.

Significant wave heights within the model domain as the eye of the hurricane progresses along its path are shown in Figures 35-41. Surface elevations are shown in Figures 42-47. It should be noted that the sides of the model are treated as solid boundaries.

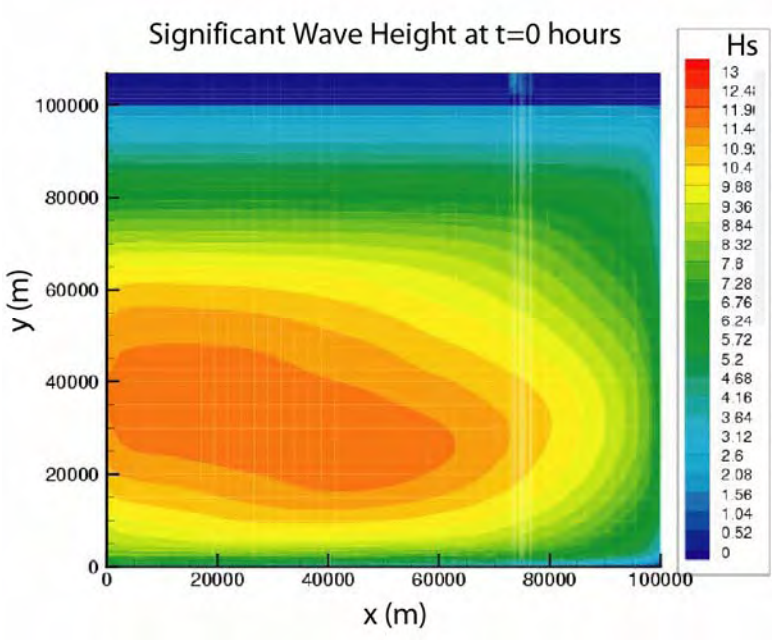

Figure 35 Significant Wave Heights at Time = 0 hours.

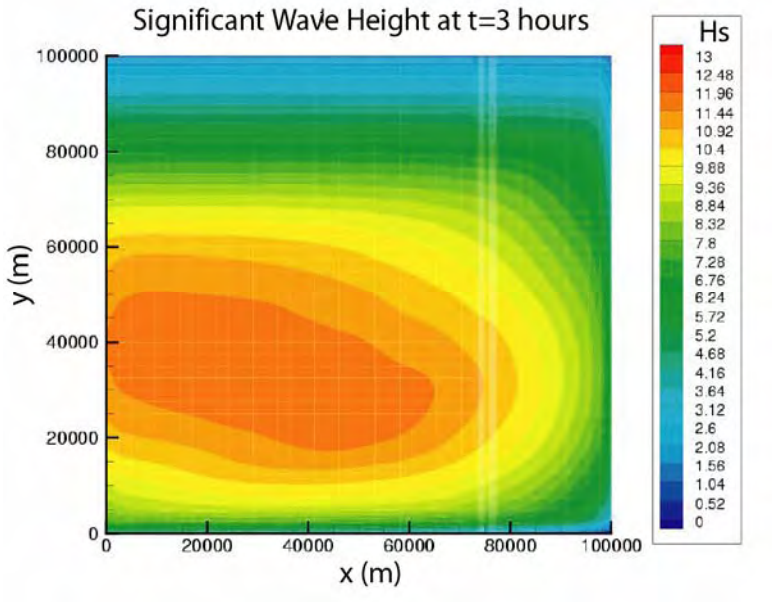

Figure 36 Significant Wave Heights at Time = 3 hours.

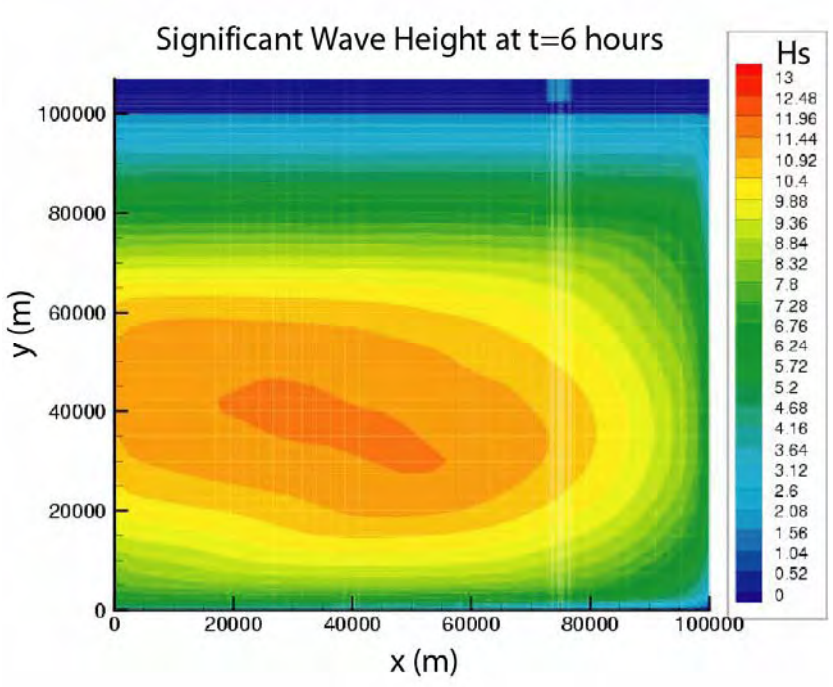

Figure 37 Significant Wave Heights at Time = 6 hours.

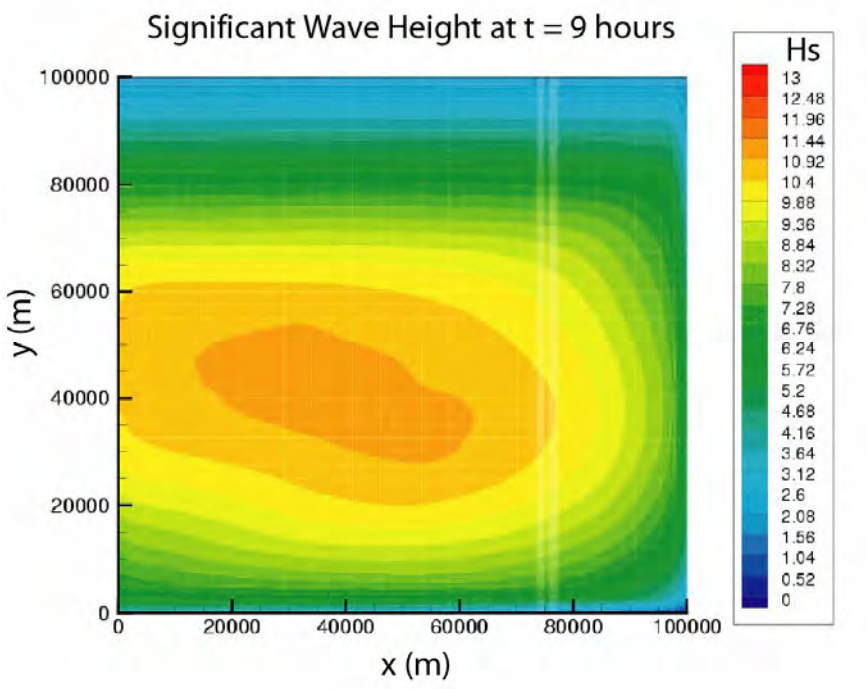

Figure 38 Significant Wave Heights at Time = 9 hours.

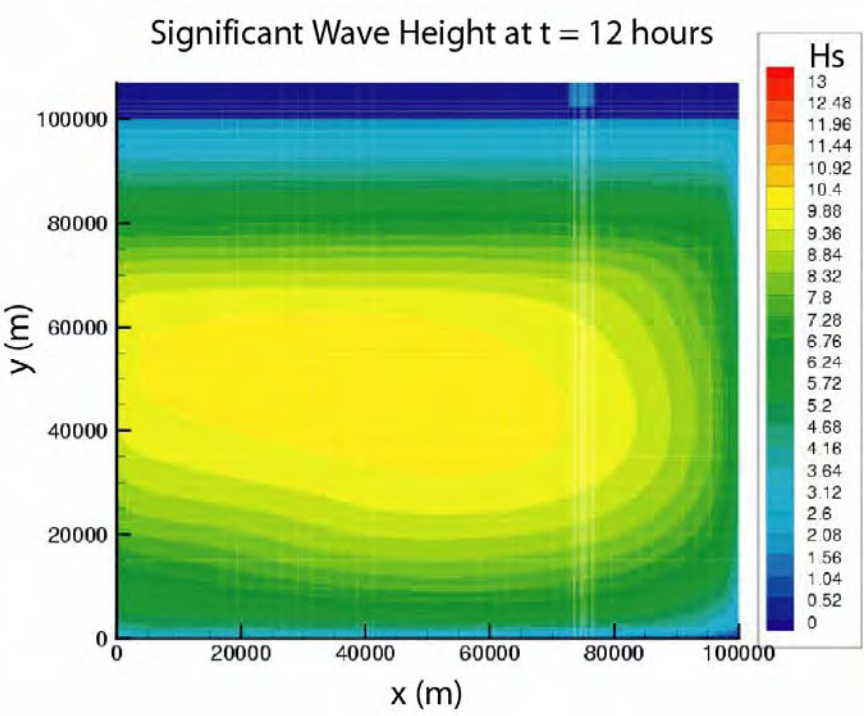

Figure 39 Significant Wave Heights at Time = 12 hours.

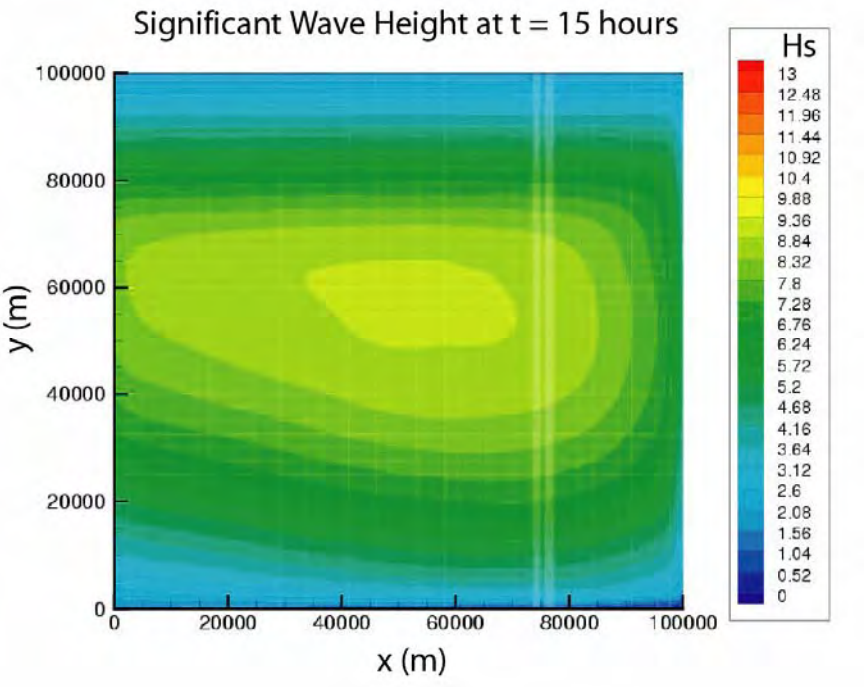

Figure 40 Significant Wave Heights at Time = 15 hours.

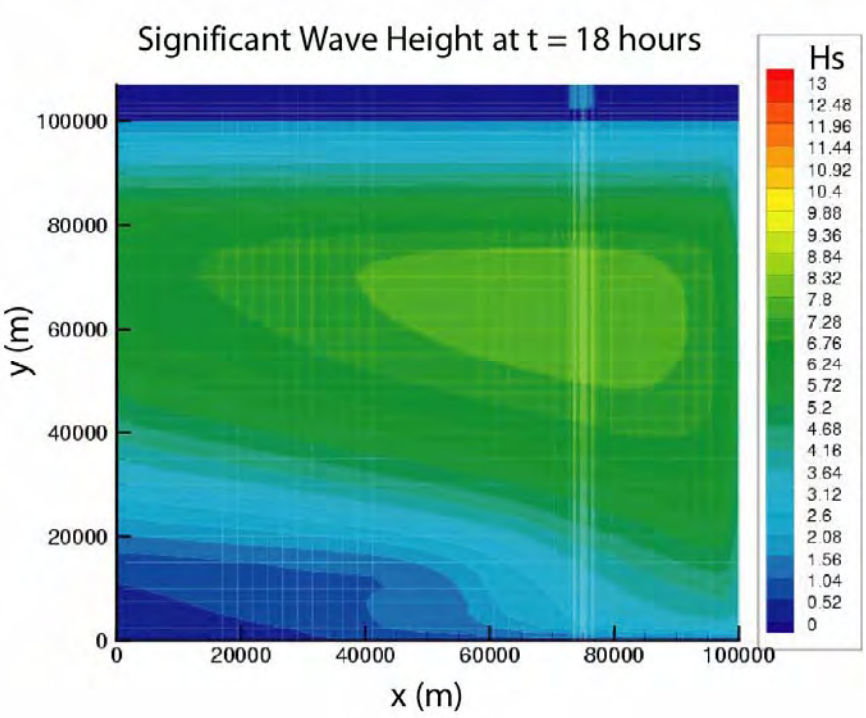

Figure 41 Significant Wave Heights at Time = 18 hours.

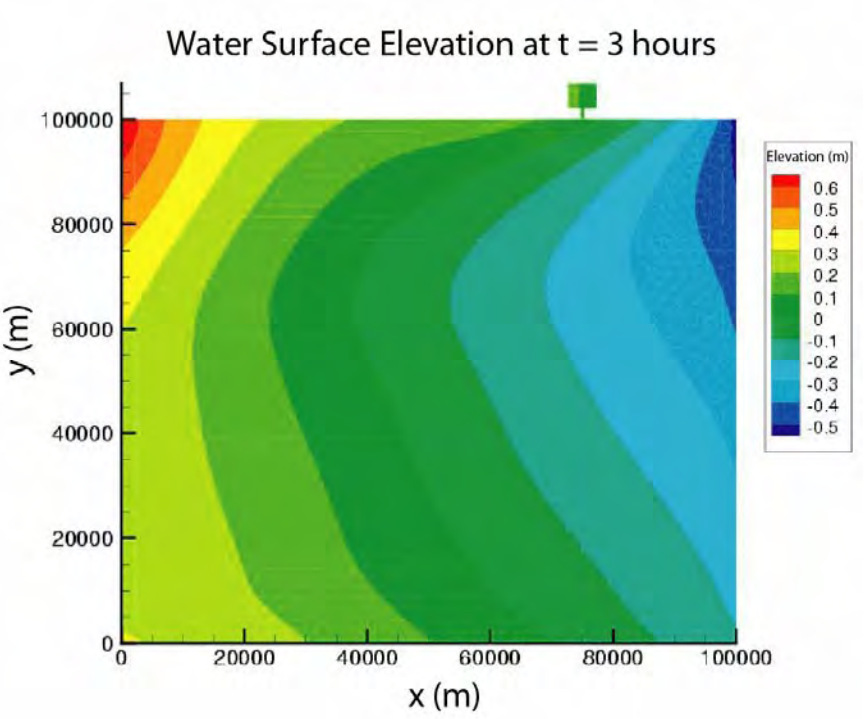

Figure 42 Water Surface Elevation at Time = 3 hours.

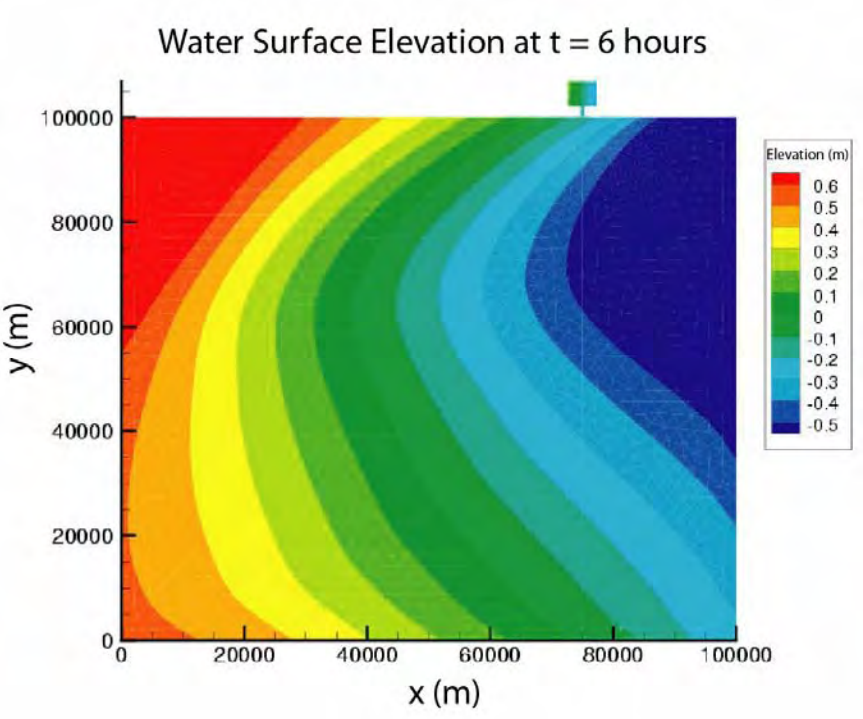

Figure 43 Water Surface Elevation at Time = 6 hours.

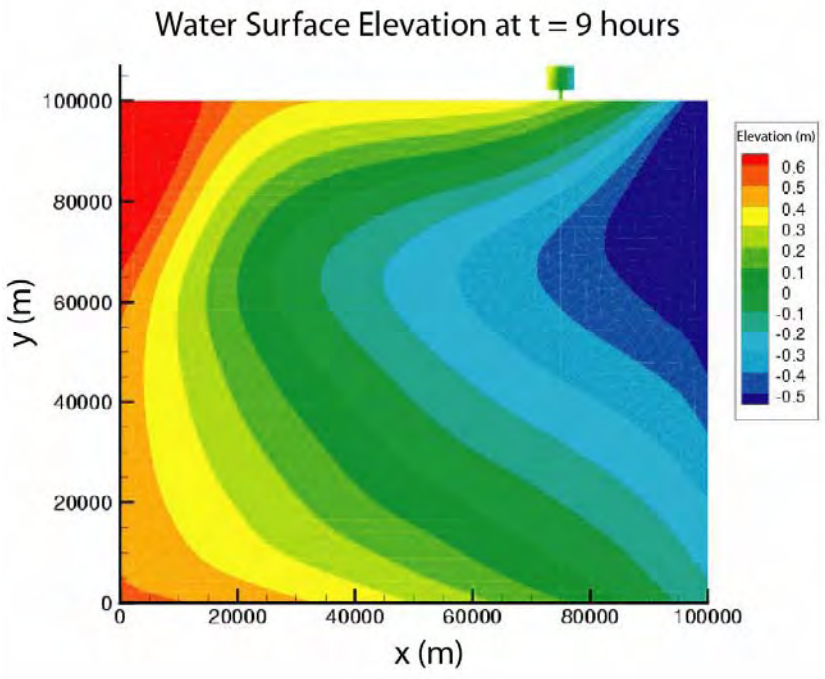

Figure 44 Water Surface Elevation at Time = 9 hours.

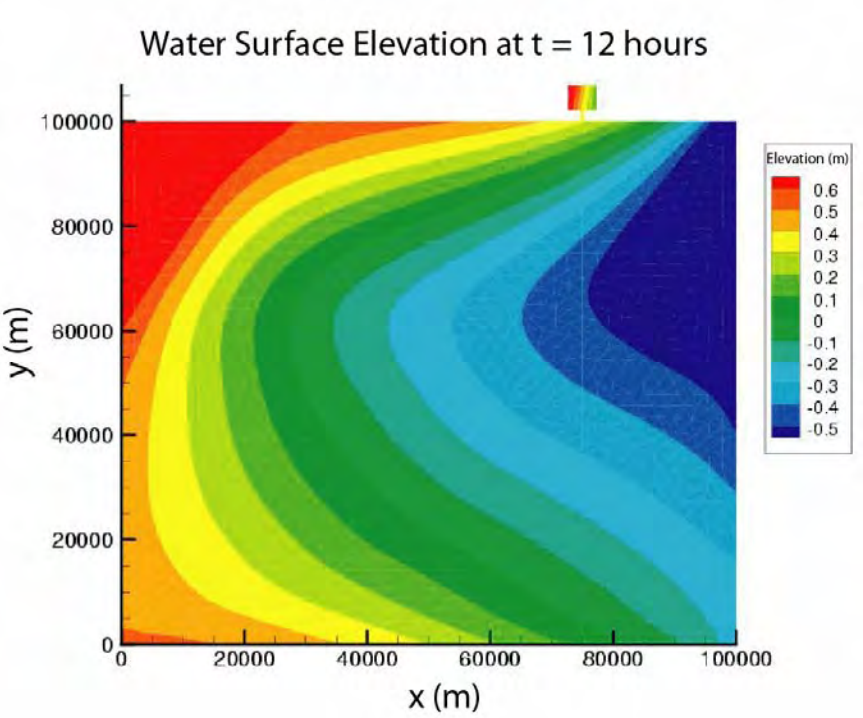

Figure 45 Water Surface Elevation at Time = 12 hours.

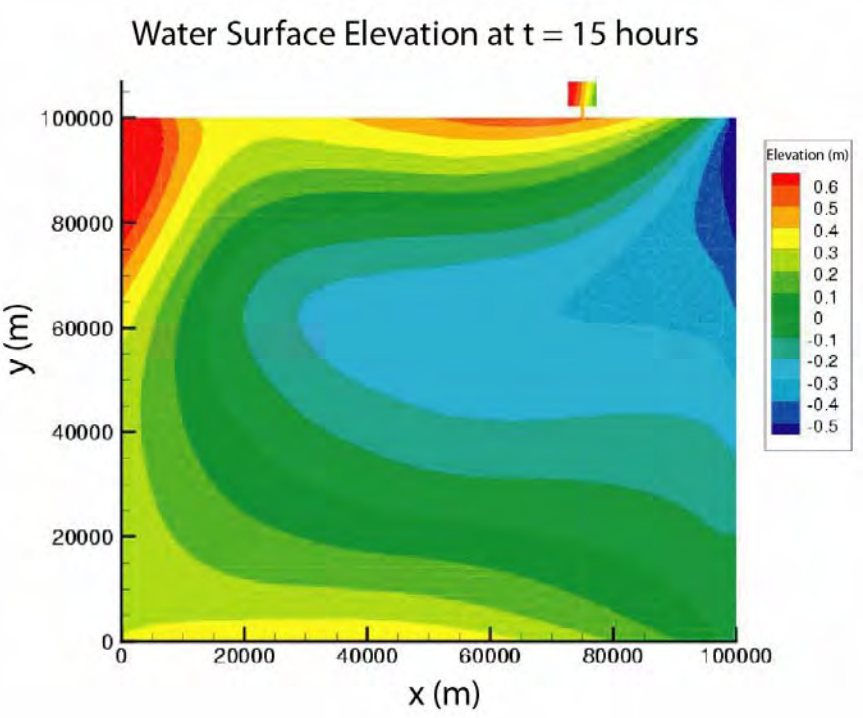

Figure 46 Water Surface Elevation at Time = 15 hours.

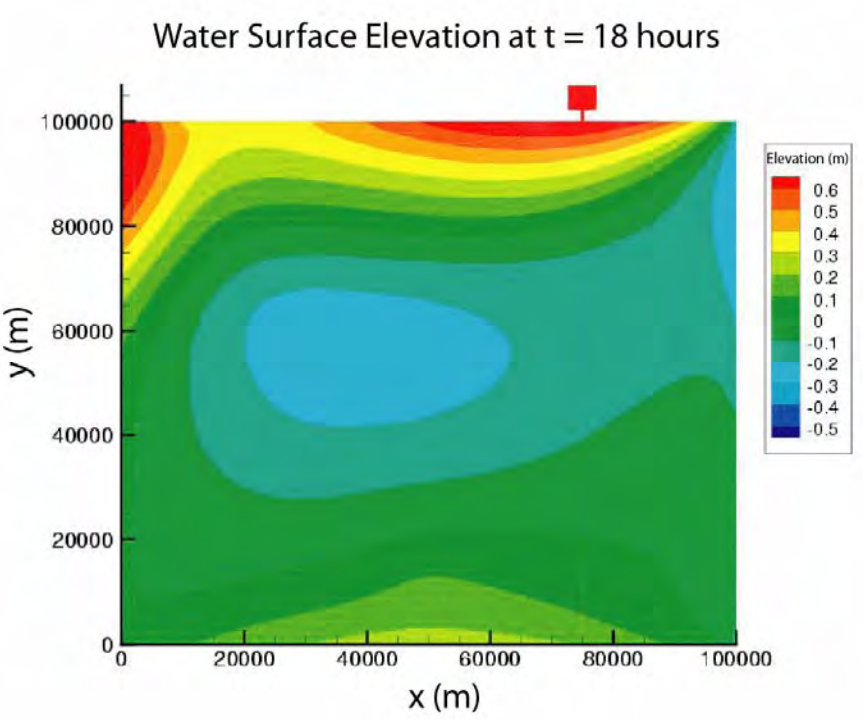

Figure 47 Water Surface Elevation at Time = 18 hours.

The storm surge and wave models were run with two-way coupling for a range of information exchange (coupling) frequencies and the water elevations observed at several observation points. The observation point numbers are shown in Figures 9 and 10. The results of these analyses are presented in the following Figures.

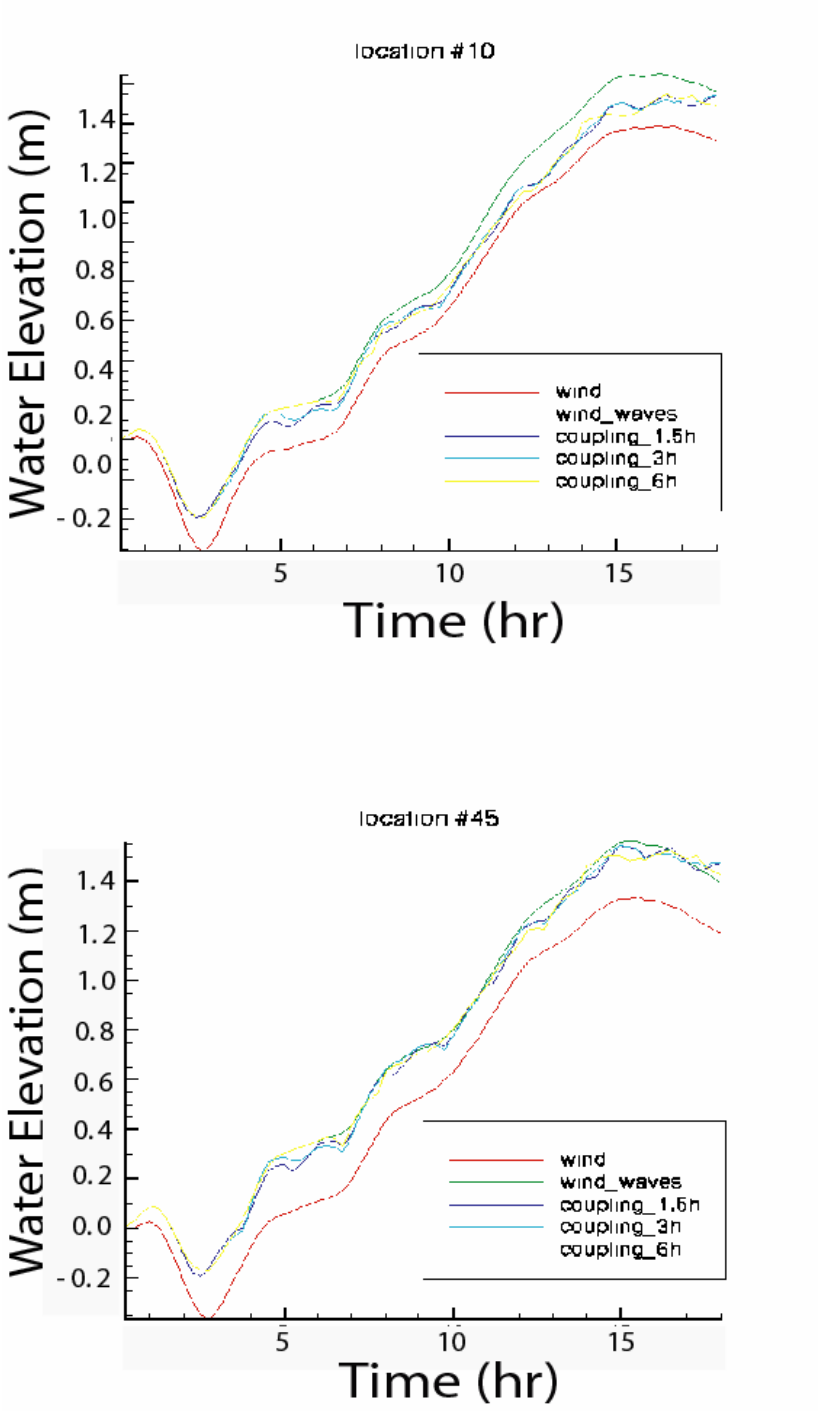

Figure 48 Convergence Tests at Points 10 and 45.

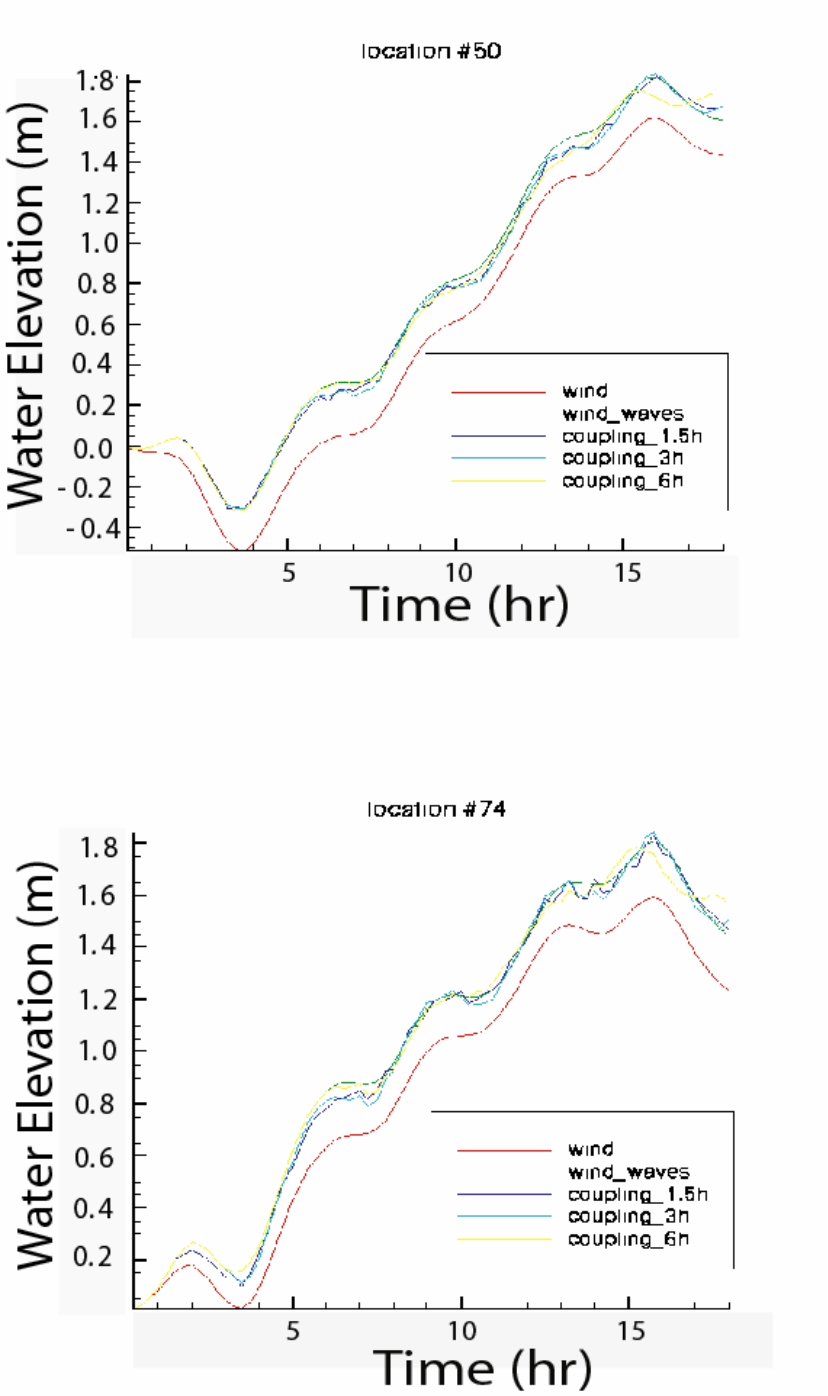

Figure 49 Convergence Tests at Points 50 and 74.

Next the effect of bed slope on hydraulics and wave model coupling was examined. Two different slopes were considered as shown in Figures 1. The milder slope is referred to as Slope A and the steeper slope as Slope B. Slope B is 3 times Slope A. The ADCIRC

model was run with the hurricane wind field and the water elevations computed with and without wave input. The results from these tests are shown in the following Figures.

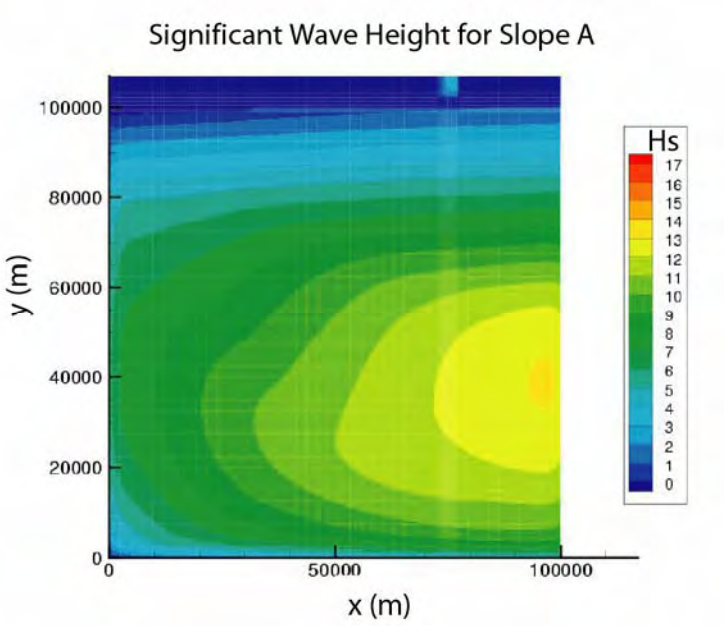

Figure 50 Significant Wave Height Contours for Slope A (same time as Figure 51).

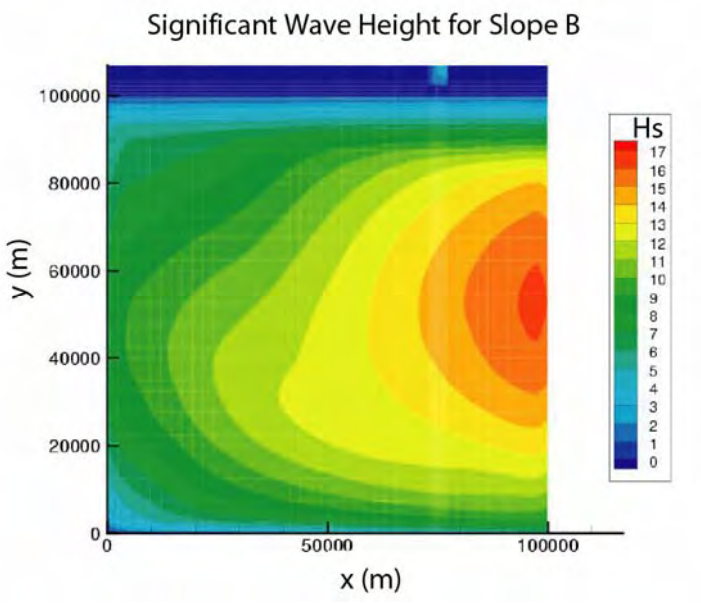

Figure 51 Significant Wave Height Contours for Slope B (same time as Figure 50).

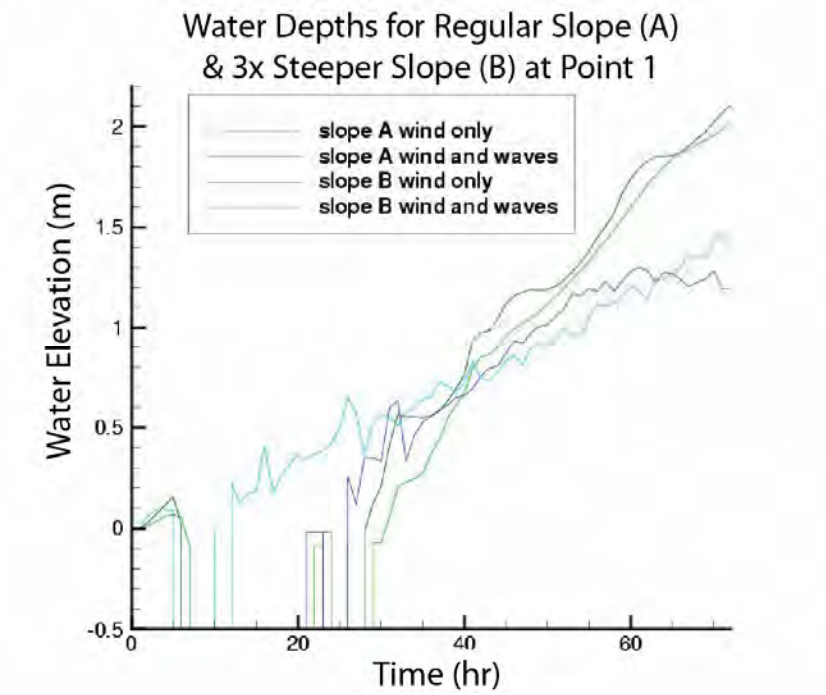

Figure 52 Water depths at point 1 over two slopes with wind forcing and with wind plus wave forcing applied (see Figure 9).

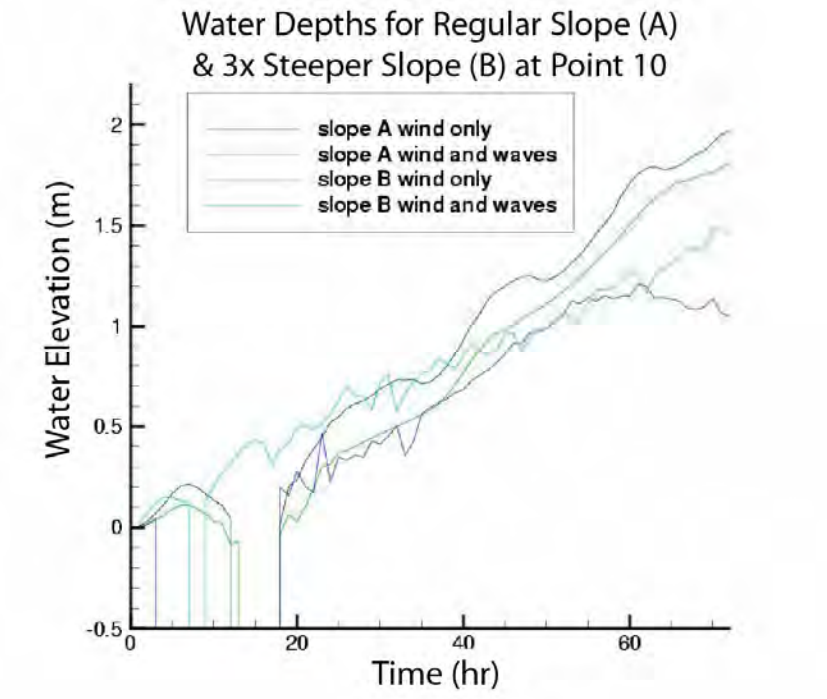

Figure 53 Water depths at point 10 over two slopes driven by wind forcing and by wind plus wave forcing (see Figure 9).

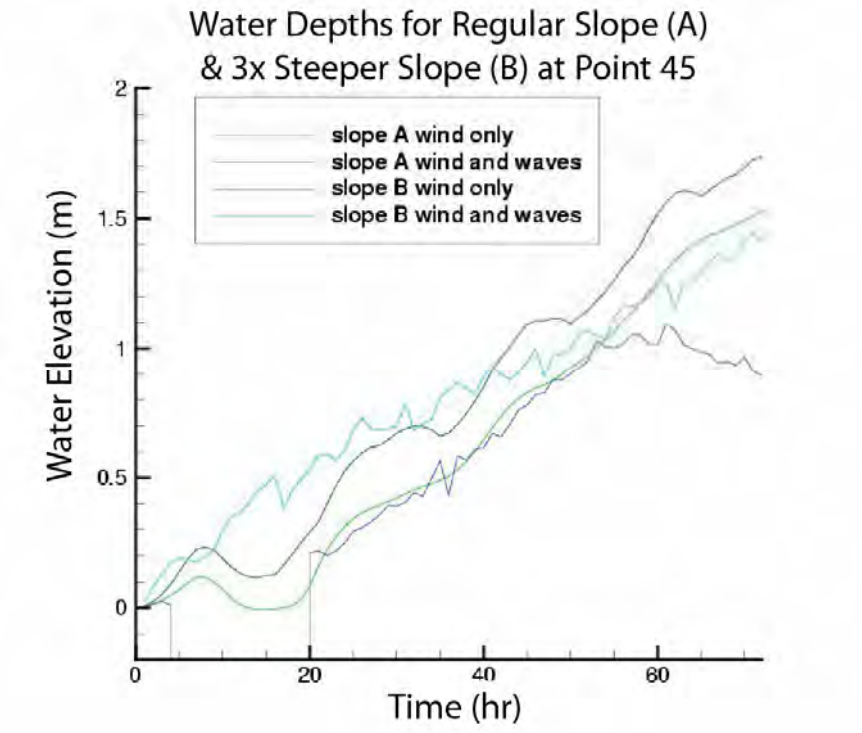

Figure 54 Water depths at point 45 over two slopes driven by wind forcing and by wind plus wave forcing (see Figure 9).

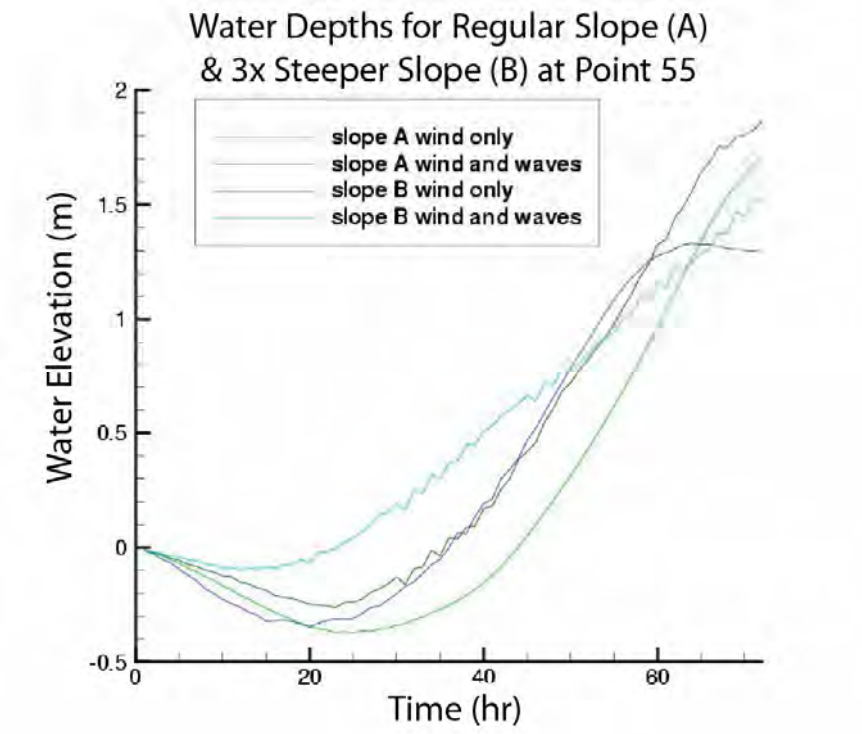

Figure 55 Water depths at point 55 over two slopes driven by wind forcing and by wind plus wave forcing (see Figure 10).

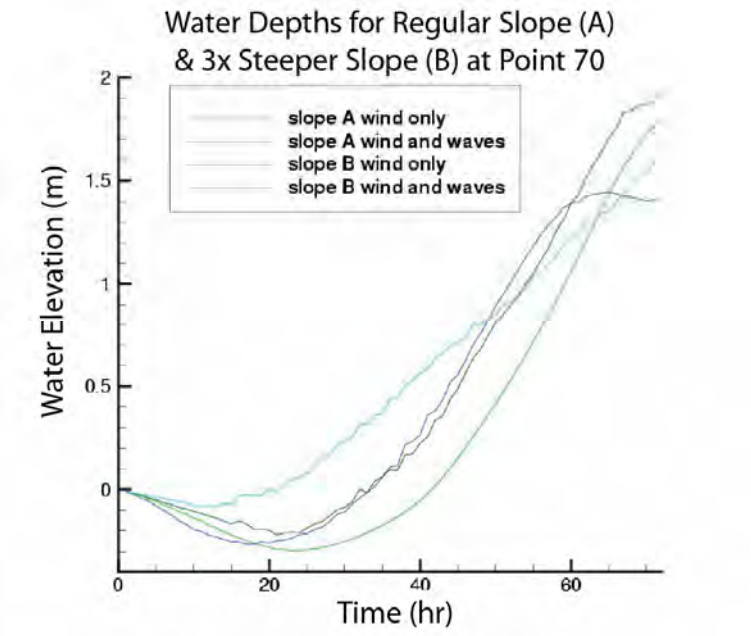

Figure 56 Figure 57 Water depths at point 70 over two slopes driven by wind forcing and by wind plus wave forcing (see Figure 10).

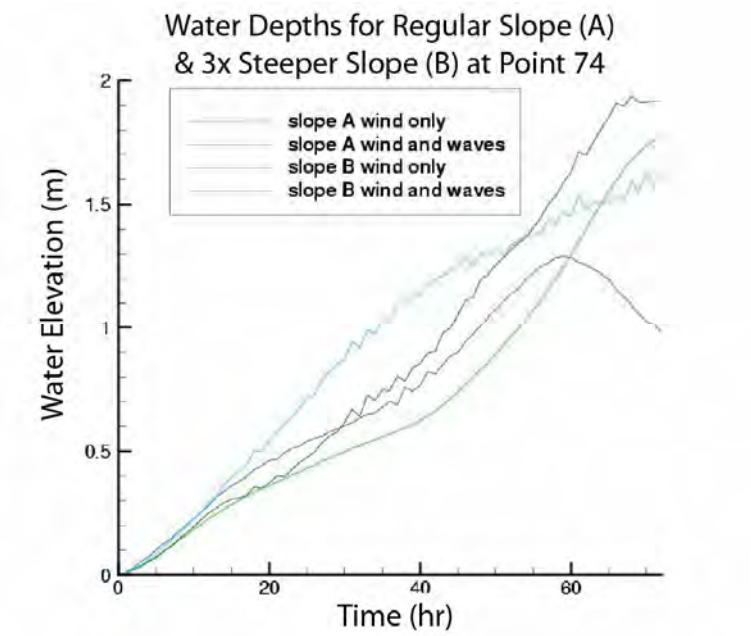

Figure 58 Water depths at point 70 over two slopes driven by wind forcing and by wind plus wave forcing (see Figure 10).

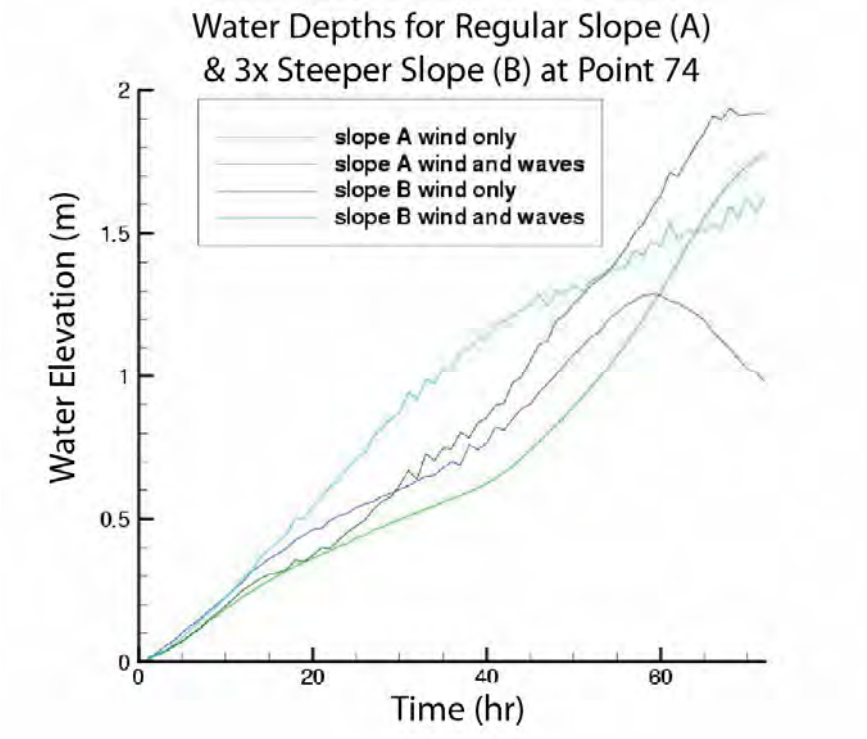

Figure 59 Water depths at point 74 over two slopes driven by wind forcing and by wind plus wave forcing (see Figure 10).

Real Coastline, Bathymetry, Bay and Hurricane Wind Field:

For this sequence an actual coastline, inlet and bay system and historical hurricane was investigated. The hurricane used was Hurricane Katrina that made landfall in Louisiana during the summer of 2005. The results from this study were basically no different from that for the idealized coast, inlet-bay system. That is, one-way coupling produced higher water elevations over no wave (radiation stress) input and two-way coupling had little or no effect over one-way coupling values. The effect of no wave and one-way coupling can be seen in Figure 59.

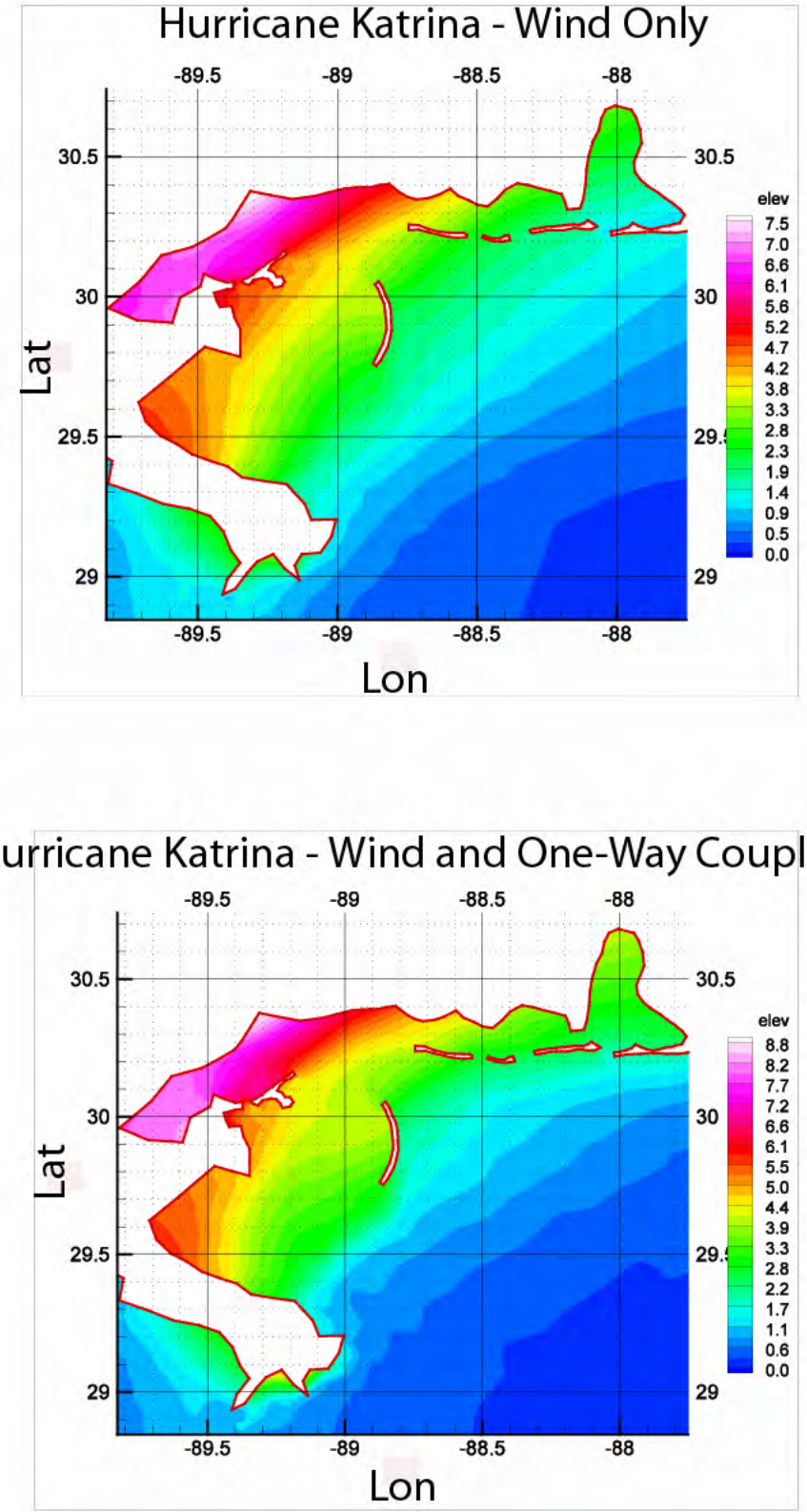

Figure 60 Water Elevations during Hurricane Katrina Without Waves and With One-Way Coupling.

The effects of storm surge on waves were tested in the following way. SWAN was run with the hindcasted wind field and ambient water levels and the radiation stresses extracted at each time step. The ADCIRC model was then run with the radiation stresses from SWAN and the hindcasted wind field. SWAN was run once again, this time with the spatial and time varying water elevations produced by the ADCIRC run. The wave heights are significantly different between the two runs as might be expected since the maximum height of waves are governed by water depths and wave steepness (height/length). Wave heights without and with storm surge input at several locations are presented in the following Figures.

The wave heights for the two cases are shown in Figure 61 - 64.

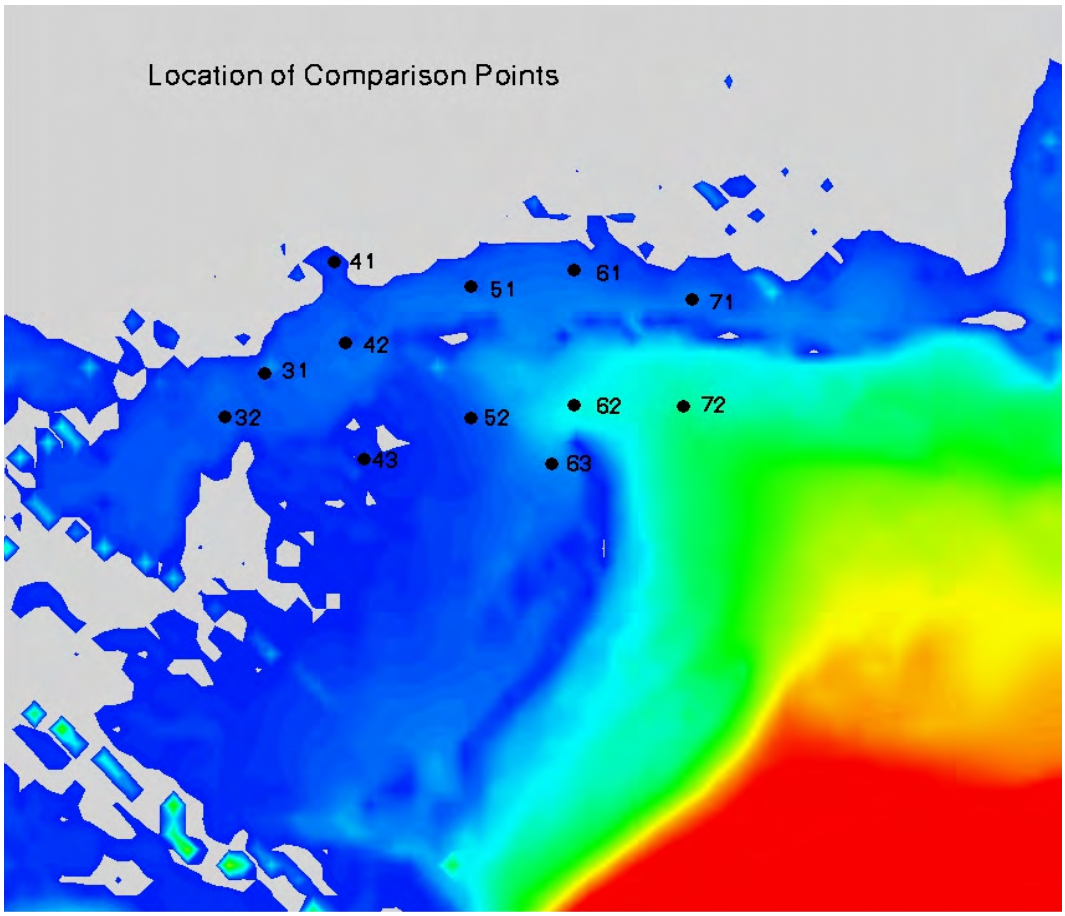

Figure 61 Diagram Showing Observation Point Locations.

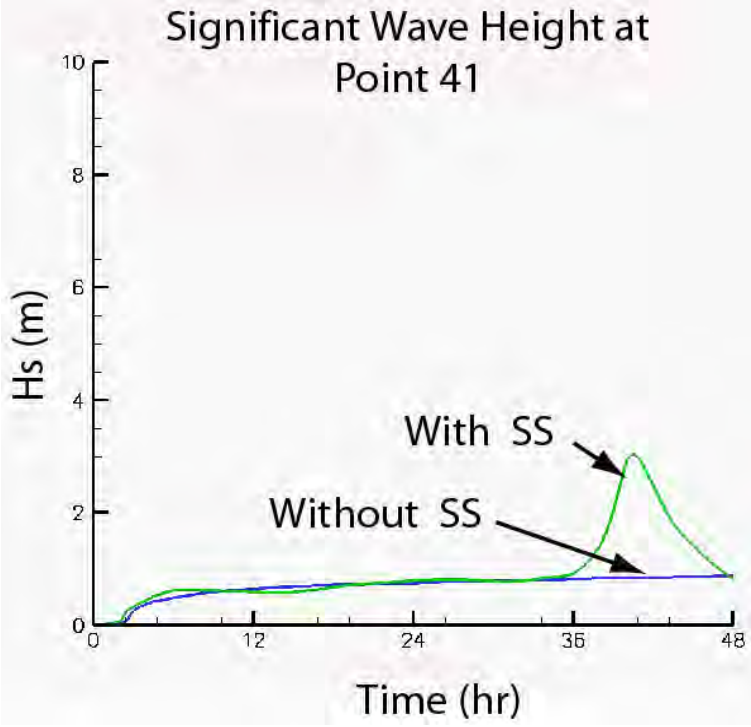

Figure 62 Significant Wave Height at Point 41 (see Figure 60) Without and With Storm Surge (SS) Input.

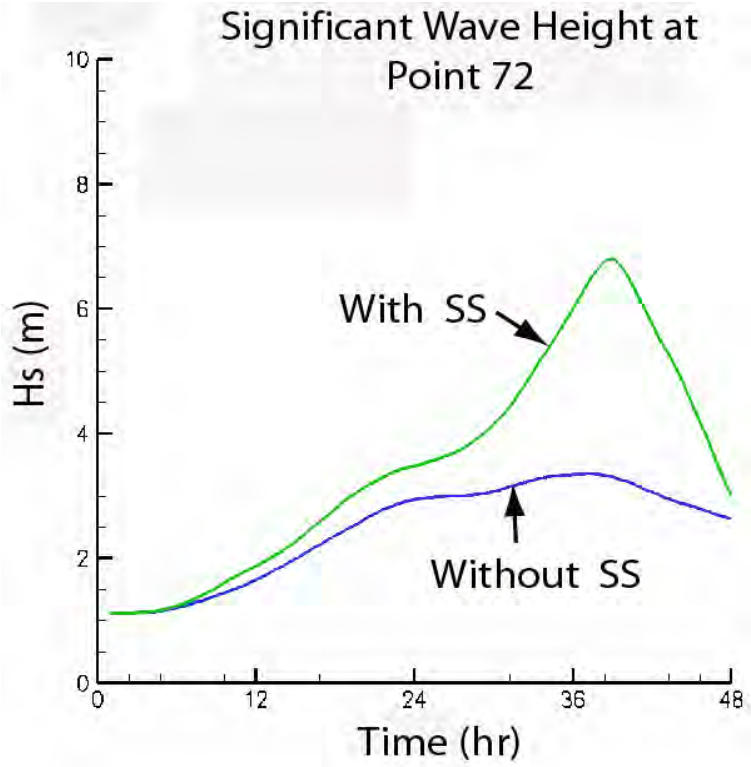

Figure 63 Significant Wave Height at Point 72 (see Figure 60) Without and With Storm Surge (SS) Input.

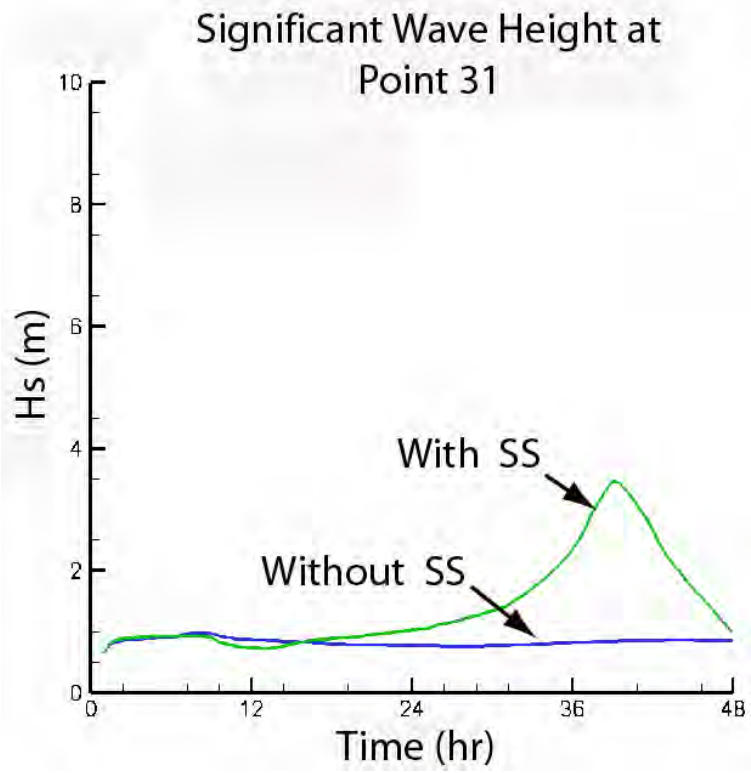

Figure 64 Significant Wave Height at Point 31 (see Figure 60) Without and With Storm Surge (SS) Input.

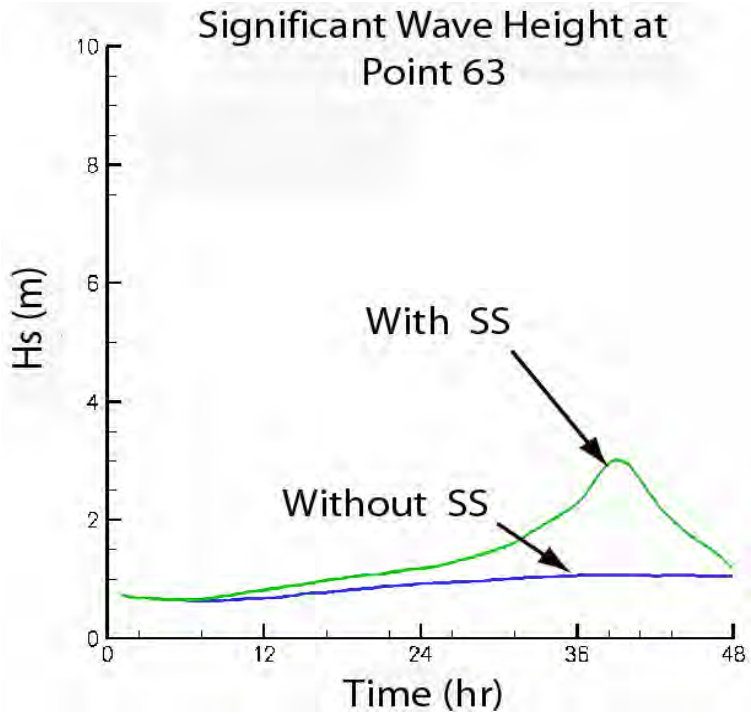

Figure 65 Significant Wave Height at Point 63 (see Figure 60) Without and With Storm Surge (SS) Input.

Discussion of Results and Conclusions:

This study produced a number of interesting and useful results. In nature waves contribute to the increased water elevation continuously during a hurricane. Likewise an increasing water level constantly impacts the wave parameters. At present storm surge and waves are commonly computed with separate computer models. Both phenomena are complex and thus the models used to solve their governing equations are complex and in most cases require a significant amount of time to solve. Coupling the models can increase run time significantly. For the coastal/ocean engineer/scientist confronted with the need to provide environmental design parameters (water levels, wave heights and wave periods, etc.) for coastal projects and construction important questions arise:

- How does one-way coupling (wave information periodically passed to storm surge model) impact predicted storm surge levels?
- If one-way coupling is important, at what time interval should the coupling occur?
- How does two-way coupling (wave information periodically passed to storm surge model, storm surge information periodically passed to the wave model) impact predicted storm surge elevations?
- How does one-way coupling (storm surge information periodically passed to the wave model) impact predicted wave parameters?
- Do the answers to the above questions depend on the location within a coastal system?
- Do the answers to the above questions depend on the slope of the ocean bed (continental shelf)?

If the impact is small and within the accuracy of the prediction then the increased time and cost may not be justified. If, however, the change is large then it must be accounted for directly or indirectly. This study addressed these questions for two commonly used models, ADCIRC and SWAN.

The results from tests with the idealized ocean bay system indicate that there is a significant increase in storm surge levels between no wave input and one-way coupling between the wave and surge models. The effect of two-way coupling (over one-way coupling) on storm surge elevations is, however, very small and is, for the situations and locations considered in this study, negligible.

The effect of periodically inputting storm surge information into the wave model does change the wave parameters at relatively shallow water locations. That is, at locations where the water depth is less than about one-half of the wave length.

Regarding the effect of bed slope, (refer to Figures 52 – 58) waves make a larger relative contribution to the total storm surge over the steeper slope. One way coupling is sufficient to account for the contribution of wave forces on the water elevation. Two way coupling does not significantly increase the contribution of wave setup to the total surge. Two-way coupling does, however, contribute to the accuracy of the spatial distribution of wave heights. The physical explanation is that the total amount of momentum that the waves have to contribute to the total setup at the shoreline is a function of the deep water wave height. Since the deep water wave heights are not changed by storm surge, the same amount of wave momentum is transferred to the water column independent of the storm surge. The cross shore location at which this occurs is altered, and larger waves propagate closer to shore when the water levels increase due to coastal flooding. This changes the wave heights at particular locations, but it does not change the total contribution to the flooding due to the waves.

Storm surge elevation does not appear to be very sensitive to the frequency at which coupling occurs. The runs presented in Figures 11-33 show some variation with information exchange frequency, but exchange intervals less than about 3 hours do not affect the results at most locations.

In summary, for most storm surge applications one-way coupling at intervals of approximately 3 hours appears to be adequate. If approximate wave conditions are needed then the procedure described above should be used. That is, run the wave model with ambient water levels and save the radiation stresses at each time step. Input the radiation stresses and wind field to the surge model and obtain water levels throughout the domain at each time step. Using the storm surge generated water elevations recompute the waves throughout the model domain at each time step. If more accurate results are required then two-way coupling may be required. For two-way coupling, wave to surge and surge to wave the information exchange interval should be approximately 3 hours or less

Part II IMPACT OF TIDAL INLETS AND BAYS ON OPEN COAST STORM SURGE ELEVATIONS

PART 2 TABLE OF CONTENTS

PART 2 LIST OF FIGURES

PART 2 LIST OF TABLES

PART 2 LIST OF SYMBOLS

t = time

x, y = horizontal coordinates, aligned in the East and North directions respectively

ζ = free surface elevation, relative to the geoid

U = depth-averaged horizontal velocity, x direction

V = depth-averaged horizontal velocity, y direction

H = total water column depth, $h + \zeta$

h = bathymetric depth relative to the geoid

$f = 2\Omega \sin\phi$ = Coriolis parameter

Ω = angular speed of the earth

ϕ = degrees latitude

p_S = atmospheric pressure at the free surface

g = acceleration due to gravity

η = Newtonian equilibrium tide potential

α = earth elasticity factor

ρ_0 = reference density of water

τ_{SX} = applied free surface stress, x direction

τ_{SY} = applied free surface stress, y direction

$\tau_* = C_f \dfrac{\sqrt{U^2 + V^2}}{H}$ = bottom stress

C_f = bottom friction coefficient

$M_X = E_{h_2}\left[\dfrac{\partial^2 UH}{\partial x^2} + \dfrac{\partial^2 UH}{\partial y^2}\right]$ = depth-integrated momentum dispersion, x direction

$M_Y = E_{h_2}\left[\dfrac{\partial^2 VH}{\partial x^2} + \dfrac{\partial^2 VH}{\partial y^2}\right]$ = depth-integrated momentum dispersion, y direction

E_{h_2} = horizontal eddy viscosity

λ = degrees longitude, east of Greenwich

ϕ = degrees latitude, north of Equator

R = radius of the Earth

A_c = minimum cross-sectional area of the inlet

Ω = tidal prism

a_b = the bay tide amplitude

A_b = the bay surface area

BACKGROUND:

Florida's Department of Transportation (FDOT) is responsible for designing, constructing, and maintaining most roadways in the State of Florida. In coastal areas, where the majority of the state's population resides, this responsibility extends to the development of bridges to ensure safe travel over intracoastal waterways. The design of these bridges is governed by a number of factors: wind, moving (vehicular), and hydro-dynamic loads, to name a few. In particular, the coastal circulation patterns are important in determining the amount of scour that may occur during extreme flow events (e.g. hurricane storm surge). At present, the FDOT employs local, two-dimensional depth averaged models to estimate both horizontal and vertical circulation patterns, and thus bridge scour, in the vicinity of coastal bridges. Typically, these models encompass the bay system where the bridge is located and extend seaward to shallow ocean regions beyond tidal inlets.

Under design conditions, these local circulation models incorporate storm surge hydrographs along the open ocean boundary. These open coast storm surge hydrographs are generated using either stochastic methods (e.g., statistical analysis of historical water elevation data) or deterministic methods (e.g., large-scale, ocean-based circulation models). The use of large-scale circulation models for coastal modeling has become more feasible due to recent advances in computational power and efficiency, and is the preferred method for generating open coast boundary conditions for a local circulation model. Questions, however, arise as to the effect of inlet and bay systems on the open coast storm surge hydrographs generated by a large-scale, ocean-based model.

The Florida coast is abundant with tidal inlets that allow for water to continuously circulate through embayment systems. This hydraulic connection provides a conduit for storm surge to enter the bay system during a hurricane event. Incorporating all of the inlet and bay systems along the Florida coast into the model domain is an arduous task at best and it significantly increases the computational nodes included in the model. Therefore, it is necessary to elucidate the effect, if any, that tidal inlets have on the open coast storm surge hydrographs. In order to accomplish this, a numerical parameter study is performed by employing various idealized inlet and continental shelf profiles that are representative of Florida tidal inlets. Each idealized inlet mesh is forced with a synthetic

wind field and pressure profile that is representative of Hurricane Ivan and the results of each simulation are compared to one another. By doing this, coastal modelers will be able to determine which inlets need to be included in the coastal circulation model, such that accurate open coast storm surge hydrographs can be generated.

Following is the methodology, results and conclusions for the numerical parameter study. The numerical codes used in this study (coastal circulation model and wind model), and the model domains and study area are presented in Section II. The results are presented in Section III, and, finally, the conclusions are discussed in Section IV.

METHODOLOGY

Model Description

The water surface elevations and circulation patterns are computed by the Advanced Circulation model (ADCIRC) for shelves, coasts, and estuaries (Luettich et al., 1992). In this study, barotropic dynamics are examined and density gradients are assumed to be relatively small, as these conditions are common near tidal inlets (Hench et al., 2002). These assumptions permit the use of the fully nonlinear two-dimensional, depth-integrated option of the model (ADCIRC-2DDI). Two forms of the governing equations are presented in this chapter: 1) in Cartesian coordinates and 2) in spherical coordinates, as both forms of the equations are used in this study. Wave setup was not included in this part of the study.

Circulation Model Formulation in Cartesian Coordinates

The numerical parameter study focuses on an idealized inlet domain that is constructed in the Cartesian coordinate system. Westerink et al., (1994) present the basic governing continuity, [1], and momentum equations, [2] and [3], in Cartesian coordinates that are used in the model:

$$\frac{\partial \zeta}{\partial t} + \frac{\partial UH}{\partial x} + \frac{\partial VH}{\partial y} = 0 \qquad [1]$$

$$\frac{\partial U}{\partial t} + U\frac{\partial U}{\partial x} + V\frac{\partial U}{\partial y} - fV = -\frac{\partial}{\partial x}\left[\frac{p_S}{\rho_0} + g(\zeta - \alpha\eta)\right] + \frac{1}{H}M_X + \frac{\tau_{SX}}{\rho_0 H} - \tau_* U \qquad [2]$$

$$\frac{\partial V}{\partial t} + U\frac{\partial V}{\partial x} + V\frac{\partial V}{\partial y} + fU = -\frac{\partial}{\partial y}\left[\frac{p_S}{\rho_0} + g(\zeta - \alpha\eta)\right] + \frac{1}{H}M_Y + \frac{\tau_{SY}}{\rho_0 H} - \tau_* V \qquad [3]$$

where:

t = time

x, y = horizontal coordinates, aligned in the East and North directions, respectively

ζ = free surface elevation, relative to the geoid

U = depth-averaged horizontal velocity, x direction

V = depth-averaged horizontal velocity, y direction

H = total water column depth, $h + \zeta$

h = bathymetric depth relative to the geoid

$f = 2\Omega \sin\phi$ = Coriolis parameter

Ω = angular speed of the earth

ϕ = degrees latitude

p_S = atmospheric pressure at the free surface

g = acceleration due to gravity

η = Newtonian equilibrium tide potential

α = earth elasticity factor

ρ_0 = reference density of water

τ_{SX} = applied free surface stress, x direction

τ_{SY} = applied free surface stress, y direction

$\tau_* = C_f \frac{\sqrt{U^2 + V^2}}{H}$ = bottom stress

C_f = bottom friction coefficient

$M_X = E_{h_2}\left[\frac{\partial^2 UH}{\partial x^2} + \frac{\partial^2 UH}{\partial y^2}\right]$ = depth-integrated momentum dispersion, x direction

$M_Y = E_{h_2}\left[\frac{\partial^2 VH}{\partial x^2} + \frac{\partial^2 VH}{\partial y^2}\right]$ = depth-integrated momentum dispersion, y direction

E_{h_2} = horizontal eddy viscosity

The governing equations are discretized in space by linear finite elements and in time by a finite difference scheme (Luettich et al., 1992). The finite element solution to the

shallow water equations gives rise to spurious modes and numerical instabilities. Hence, it becomes necessary to reformulate the equations into a form that provides a stable solution in its finite element representation. As a result, ADCIRC-2DDI employs the Generalized Wave Continuity Equation (GWCE) [4]. The result is a noise-free solution that is used in conjunction with the primitive momentum equations (equations [2] and [3]) to solve for the deviation from the geoid (ζ) and the velocities in the x and y directions (Westerink et al., 1994).

$$\frac{\partial^2 \zeta}{\partial t^2} + \tau_0 \frac{\partial \zeta}{\partial t} + \frac{\partial}{\partial x}\left\{ U\frac{\partial \zeta}{\partial t} - UH\frac{\partial U}{\partial x} - VH\frac{\partial U}{\partial y} + fVH \right.$$

$$\left. - H\frac{\partial}{\partial x}\left[\frac{p_S}{\rho_0} + g(\zeta - \alpha\eta)\right] - E_{h_2}\frac{\partial^2 \zeta}{\partial x \partial t} + \frac{\tau_{SX}}{\rho_0} - (\tau_* - \tau_0)UH \right\}$$

$$+ \frac{\partial}{\partial y}\left\{ V\frac{\partial \zeta}{\partial t} - UH\frac{\partial V}{\partial x} - VH\frac{\partial V}{\partial y} - fUH - H\frac{\partial}{\partial y}\left[\frac{p_S}{\rho_0} + g(\zeta - \alpha\eta)\right] \right.$$

$$\left. - E_{h_2}\frac{\partial^2 \zeta}{\partial y \partial t} + \frac{\tau_{SY}}{\rho_0} - (\tau_* - \tau_0)VH \right\} = 0 \qquad [4]$$

Circulation model formulation in Spherical Coordinates

The part of the study that examines Hurricane Ivan uses a real domain that is in the spherical coordinate system. Westerink et al., (1994) present the basic governing continuity, [5], and momentum equations, [6] and [7], in spherical coordinates that are used in the model:

$$\frac{\partial \zeta}{\partial t} + \frac{1}{R\cos\phi}\left[\frac{\partial UH}{\partial \lambda} + \frac{\partial (VH\cos\phi)}{\partial \phi}\right] = 0 \qquad [5]$$

$$\frac{\partial U}{\partial t} + \frac{1}{R\cos\phi}U\frac{\partial U}{\partial \lambda} + \frac{1}{R}V\frac{\partial U}{\partial \phi} - \left(\frac{\tan\phi}{R}U + f\right)V =$$

$$-\frac{1}{R\cos\phi}\frac{\partial}{\partial \lambda}\left[\frac{p_S}{\rho_0} + g(\zeta - \alpha\eta)\right] + \frac{1}{H}M_\lambda + \frac{\tau_{S\lambda}}{\rho_0 H} - \tau_* U \qquad [6]$$

$$\frac{\partial V}{\partial t} + \frac{1}{R\cos\phi}U\frac{\partial V}{\partial \lambda} + \frac{1}{R}V\frac{\partial V}{\partial \phi} + \left(\frac{\tan\phi}{R}U + f\right)U =$$

$$-\frac{1}{R}\frac{\partial}{\partial\phi}\left[\frac{p_S}{\rho_0}+g(\zeta-\alpha\eta)\right]+\frac{1}{H}M_\phi+\frac{\tau_{S\phi}}{\rho_0 H}-\tau_* V \qquad [7]$$

Where, R = radius of the Earth. In a similar manner as previously described, the finite element solution of these equations gives rise to numerical instabilities. Thus, the equations are reformulated into the GWCE [8] in spherical coordinates (Kolar et al., 1994).

$$\frac{\partial^2\zeta}{\partial t^2}+\tau_0\frac{\partial\zeta}{\partial t}-\frac{1}{R\cos\phi}\frac{\partial}{\partial\lambda}\left\{\frac{1}{R\cos\phi}\left(\frac{\partial UUH}{\partial\lambda}+\frac{\partial UVH}{\partial\phi}\right)-\left(\frac{\tan\phi}{R}U+f\right)VH\right.$$

$$\left.-\frac{H}{R\cos\phi}\frac{\partial}{\partial\lambda}\left[\frac{p_S}{\rho_0}+g(\zeta-\alpha\eta)\right]+\frac{E_{h_2}}{R\cos\phi}\frac{\partial^2\zeta}{\partial\lambda\partial t}+\frac{\tau_{S\lambda}}{\rho_0}-(\tau_*-\tau_0)UH\right\}$$

$$-\frac{1}{R}\frac{\partial}{\partial\phi}\left\{\frac{1}{R\cos\phi}\left[\frac{\partial HUV}{\partial\lambda}+\frac{\partial HVV\cos\phi}{\partial\phi}\right]+\left(\frac{\tan\phi}{R}U+f\right)UH-\frac{H}{R}\frac{\partial}{\partial\phi}\left[\frac{p_S}{\rho_0}+g(\zeta-\alpha\eta)\right]\right.$$

$$\left.+\frac{E_{h_2}}{R}\frac{\partial^2\zeta}{\partial\phi\partial t}+\frac{\tau_{S\phi}}{\rho_0}-(\tau_*-\tau_0)VH\right\}-\frac{\tan\phi}{R}\left(\frac{\partial VH}{\partial t}+\tau_0 VH\right)=0 \qquad [8]$$

Hurricane Ivan Wind Field Model

The state-of-the-art wind data for the Hurricane Ivan storm surge simulations was provided by Oceanweather, Inc. (http://www.oceanweather.com) using a tropical wind model developed by Cox and Cardone (2000). The model is a derivative of the TC96 model that was first implemented in the Ocean Data Gathering Program. The TC96 model provides snapshots that are blended into a synoptic-scale wind field using the Interactive Objective Kinematic Analysis algorithm (Cox et al., 1995) of the Wind Workstation (WWS). Using a numerical integration technique, the model solves the vertically averaged equations of motion for a boundary layer under horizontal and vertical stresses. Based on this principle, the numerical model provides a fairly thorough description of the time-space evolution of the wind speeds within the planetary boundary layer (PBL) during a tropical cyclone event (Thompson and Cardone, 1996).

The wind field model is driven by so-called “snapshots” in time of the storm’s intensity and is based on the assumption that the structure of the hurricane changes relatively slowly (Cox and Cardone, 2000). In addition to the TC96 model, these snapshots are also

obtained from the Hurricane Research Division Wind Analysis System (H*Wind), a distributed system that uses real-time tropical cyclone observations as input (Powell et al., 1998). The slow evolution of the storm's intensity is then interpolated from these snapshots. In addition, the model is also controlled by several input parameters: the storm's speed and direction, the geostrophic flow of the ambient PBL pressure field, a pressure profile parameter, and a scaling factor for the exponential radial pressure profile. The wind model is capable of simulating any type of storm for any particular region, and has been verified and validated for a number of test cases (Cox and Cardone, 2002).

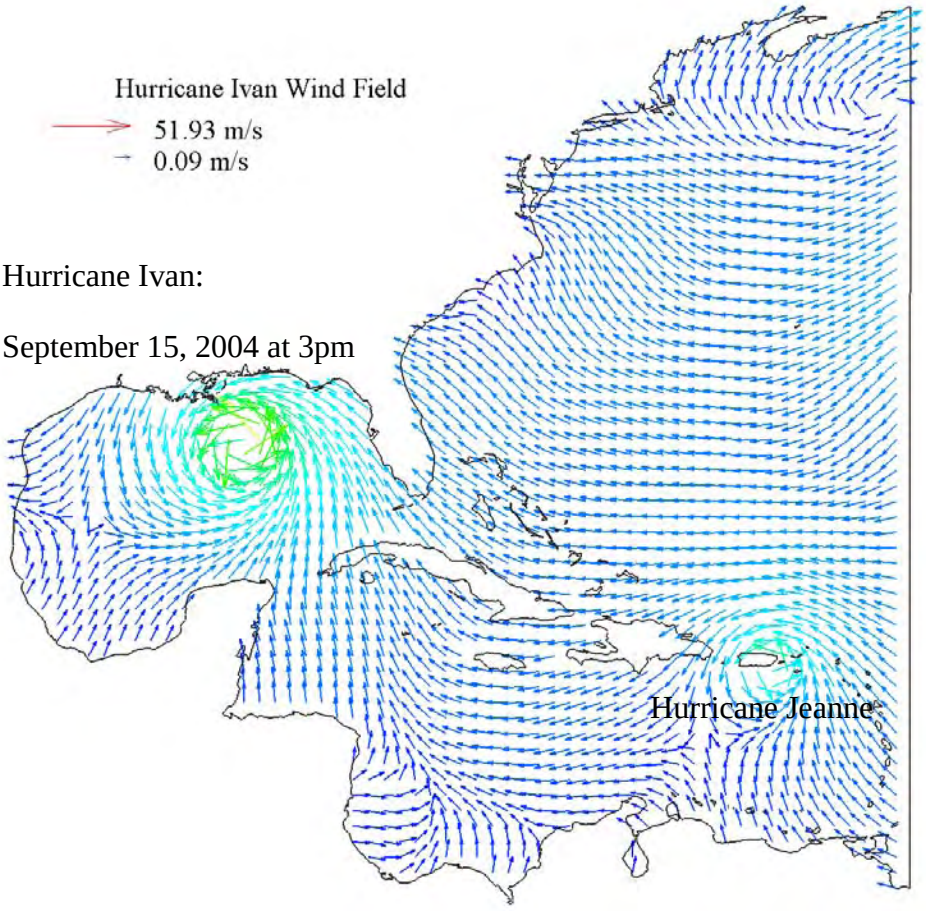

Figure P2- 1 Hurricane Ivan Wind Field just before Landfall.

Synthetic Wind Field Model

For the numerical parameter study, a synthetic hurricane wind field model is used to force the ADCIRC-2DDI model. The wind field model is parameterized according to the forward velocity and pressure field of Hurricane Ivan, and simulates a simplified,

circularly symmetric version of the storm. Compared to the wind field model used in the storm surge hindcast of Hurricane Ivan (previously discussed), the synthetic wind field model is much less sophisticated. However, the model does allow the user to specify the hurricane parameters and path of the storm, which makes it ideal for a numerical study such as this.

In all test cases presented herein, the wind field model is initialized to represent a typical worst-case scenario for coastal storm surge in the vicinity of the tidal inlet. First, the path of the storm is setup to traverse the coastline in a perpendicular manner (similar to how Hurricane Hugo made landfall on the South Carolina coast; Dietsche, 2004). Additionally, the eye of the storm makes landfall at a point 25 km west (or left) of the tidal inlet, placing the inlet in the upper right quadrant of the storm (see Figure P2-2). It is noted that many variations of the synthetic storm's parameters could have been adjusted, but was deemed inappropriate in the interest of time as this is not a sensitivity analysis.

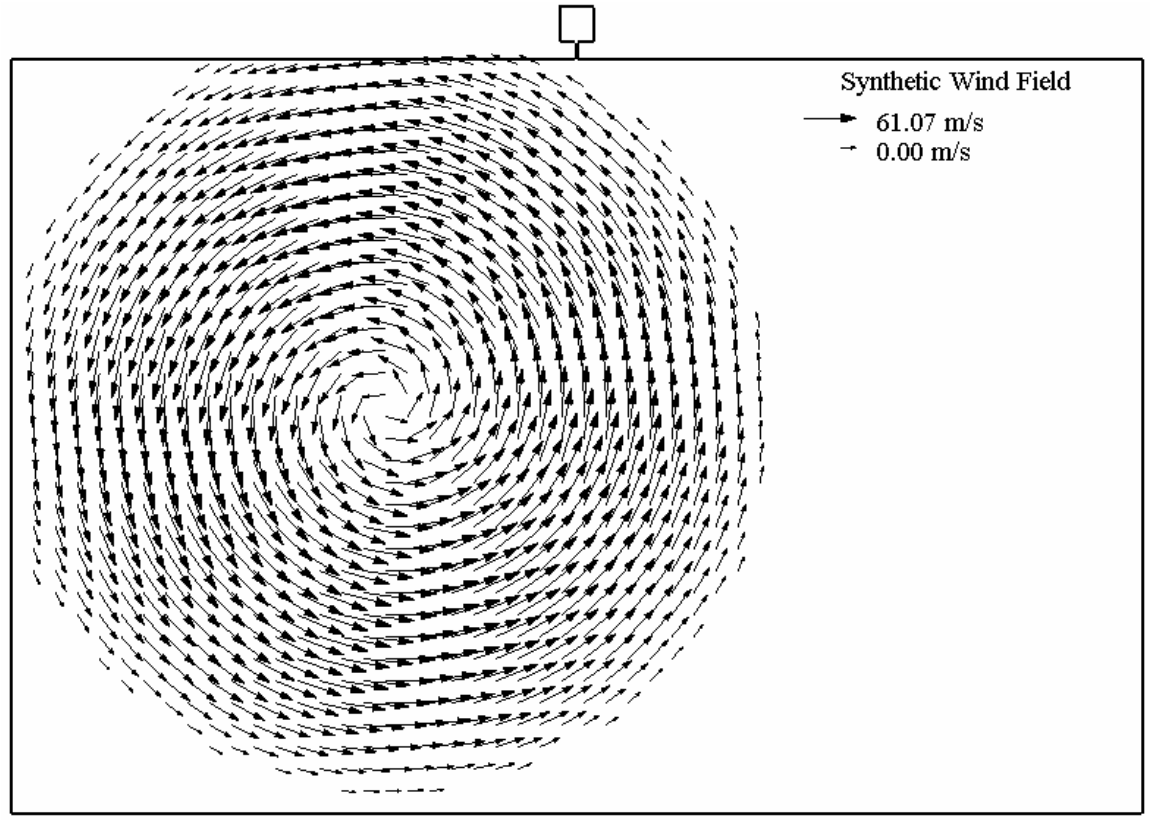

Figure P2- 2 Synthetic Wind Field Used in the Numerical Parameter Study.

Finite Element Mesh Development

In order to properly describe the physics of meteorological tides (storm surge), a numerical model must resolve coastal features that affect storm surge generation and propagation. Therefore, a model domain must describe complex coastal geometries (bathymetry and topography), large gradients in bathymetry along the continental shelf, and permit reasonable boundary conditions (i.e. tidal harmonics and/or water surface elevations). A finite element based model is ideal for such a task, as its flexibility allows for large spatial scales to be represented in the domain while allowing higher nodal resolution along the coastline (Blain et al., 1994).

Presented in this section is the development of finite element meshes for two different studies: a numerical study and a hindcast study. First, ten different finite element meshes are applied in an idealized setting to represent various inlet-bay configurations and continental shelf profiles. A statistical analysis is performed on existing data, such that the model domains are representative of coastal regions found along Florida's shoreline. Second, an ocean-based mesh is generated with coastline features in the vicinity of the Pensacola Inlet and Escambia Bay included in the model domain. This domain is used to generate open coast storm surge hydrographs in the vicinity of Pensacola Inlet during Hurricane Ivan.

Idealized Domains

Florida's tidal inlets

A thorough review of existing Florida tidal inlets is performed in order to properly design the idealized finite element meshes used in the numerical parameter study. A total of 74 tidal inlets are identified along the Florida coast, 26 on the east coast and 48 on the west coast (Carr de Betts, 1999). Figure P2-3 shows the location of each of these tidal inlets along the Florida coast.

Figure P2- 3 Location of Tidal Inlets along Florida's Coast (Carr de Betts, 1999).

A statistical analysis is performed on the hydrodynamic measurements associated with each tidal inlet. The mean, minimum, maximum, and standard deviation of each parameter dataset is determined (see Table P2-1). From this analysis it is noted that the variability amongst Florida tidal inlets is quite recognizable. For example, the average inlet length is 3142 meters, while the standard deviation is 6537 meters. This implies that a large range of inlet lengths is present in the dataset, which indicates that the mean values listed in Table P2-1 may not be representative of a typical Florida tidal inlet.

Table P2-1 Hydrodynamic Characteristics of Florida's Tidal Inlets.

Parameter	Unit	Mean	Minimum	Maximum	Standard Deviation
Width	[m]	557	18	5300	822
Depth	[m]	4.7	0.3	15.2	3.5
Length	[m]	3142	240	55000	6537
Area	[m^2]	2568	22	24000	4272
Tidal Prism	[m^3]	4.8E+07	2.8E+03	5.9E+08	1.0E+08

In lieu of this, a method to remove the statistical outliers is applied to each dataset. A standard *z*-score test is used to determine if any outliers exist as follows (Mendenhall and Sincich, 1995):

$$z = \frac{y - \mu}{\sigma} \qquad [9]$$

where, y = data point value, μ = mean, and σ = standard deviation. The values for μ and σ are obtained from Table P2-1. By definition, the *z*-score describes the location of the data point relative to the mean value. In order to determine whether a value is considered an outlier, the computed *z*-score for each data point is compared to a tabulated value of *z*-scores. If the computed value from the dataset is greater than the tabulated value, $|z| > |z_{table}|$, then the data point is considered to be an outlier. For this study, the 0.05 significance level is used for the tabulated *z*-score values.

This process is repeated for the width, depth, and length datasets (as these are the values used to design the finite element meshes), and the outliers from each dataset are removed. Next, another statistical analysis is performed on the revised dataset to determine mean values that are more representative of a typical Florida tidal inlet. Table P2-2 presents the results of this analysis.

Table P2-2 Modified Statistics of Florida's Tidal Inlets with Outliers Removed.

Parameter	Unit	Mean	Standard Deviation
Width	[m]	388	337
Depth	[m]	3.7	2.0
Length	[m]	2257	1814

Inlet-bay configuration

Four different inlet width profiles are used in the numerical parameter study: an average inlet width, a 100 meter inlet width, a 500 meter inlet width, and a 1000 meter inlet width. For each inlet width configuration, the inlet length and depth are held constant according to the average values determined in Table P2-2. However, the bay surface area varies between each inlet width configuration.

The bay surface area varies according to a relationship developed by Jarrett (1976):

$$A_c = 5.74 \times 10^{-5} \Omega^{0.95} \qquad [10]$$

where, A_c = minimum cross-sectional area of the inlet (ft^2), and Ω = tidal prism (ft^3). Equation [10] is an empirical relationship derived from a regression analysis of existing tidal inlets (both natural and man-made) along the United States coast (Jarrett, 1976). Converting Equation [10] to the SI unit system [(m^2) for the cross-sectional area and (m^3) for the tidal prism] yields the following equation:

$$A_c = 2.09 \times 10^{-5} \Omega^{0.95} \qquad [11]$$

This equation relates the minimum cross-sectional area of the inlet to the tidal prism for *stable* tidal inlets. As a comparison, data of Florida tidal inlets are compared to the solutions obtained from Equation [11]. Overall, Equation [11] provides an excellent fit to the raw data (Figure P2-4). Thus, Jarrett's relationship is deemed appropriate for Florida's tidal inlets.

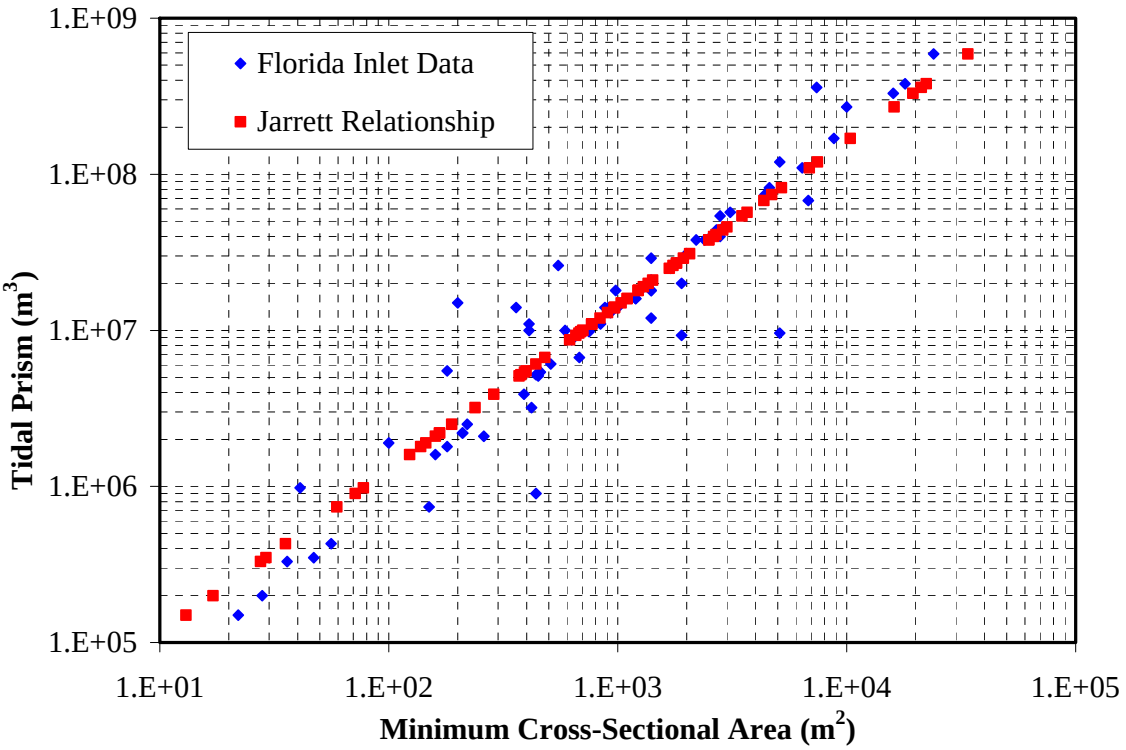

Figure P2- 4 Comparison of Jarrett's Relationship to Florida Tidal Inlet Data.

Additionally, the tidal prism is related to the bay surface area through the following relationship:

$$\Omega = 2a_b A_b \qquad [12]$$

where, a_b = the bay tide amplitude, and A_b = the bay surface area. The bay tide amplitude is defined as one half the tidal range; thus, Equation [12] relates the tidal prism to a product of the tidal range ($2a_b$) and the bay surface area. Substituting this relationship into Equation [12] yields the following solution:

$$A_c = 2.09 \times 10^{-5} \left(2a_b A_b\right)^{0.95} \qquad [13]$$

Furthermore, it's assumed that the tidal range ($2a_b$) is 1 meter, which is archetypical of the tidal range along the coast of Florida [see Kojima (2005) for a detailed tidal analysis along the United States coast]. Note that for the purpose of this study the precise value of the tidal range is not required. Substituting this assumption into Equation [13], and rearranging for the bay surface area, leads to the following equation:

$$A_b = \left(\frac{A_c}{2.09 \times 10^{-5}} \right)^{1/0.95} \quad [14]$$

This expression is used to develop the inlet-bay configurations in the finite element meshes of the numerical parameter study. A rectangular cross-sectional profile is assumed for the entire length of the inlet. Thus, the inlet cross-sectional area (A_c) can easily be determined based on the desired inlet width (average, 100 meters, 500 meters, and 1000 meters) and the constant inlet depth (3.7 meters). Following this procedure for each inlet width yields a unique bay surface area for each inlet configuration. The result of this process leads to the following inlet-bay configurations (Figure P2-5).

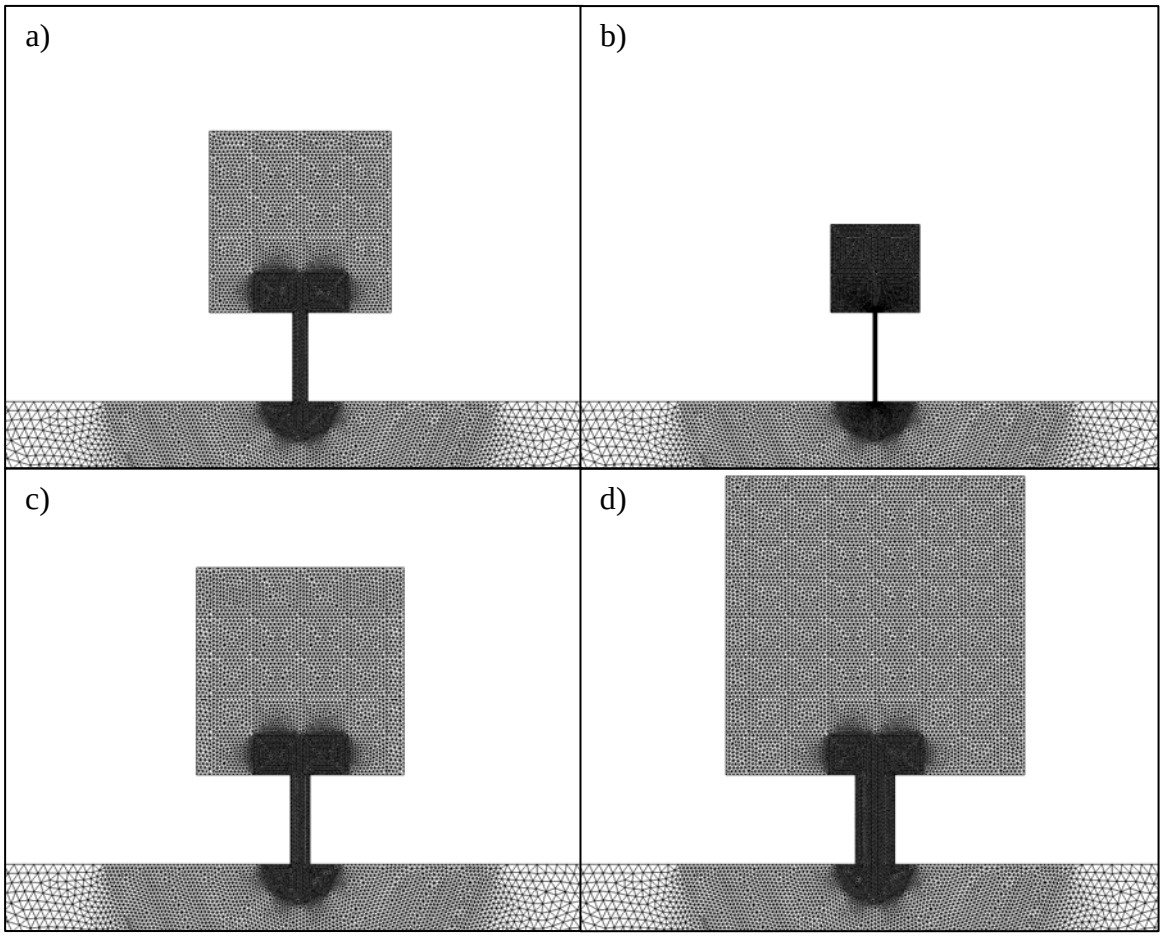

Figure P2- 5 Inlet-Bay Configurations for the Idealized Finite Element Meshes: a) Average Inlet Width; b) 100 meter Inlet Width; c) 500 meter Inlet Width; and d) 1000 meter Inlet Width

The node spacing ranges from 50 meters in the inlet to 100 meters in the bay for the average, 500 meter, and 1000 meter inlet configurations, and 25 meters in the inlet to 50 meters in the bay for the 100 meter inlet configuration. This level of resolution ensures that the inlet is represented by at least 4 elements across its width for all inlet-bay configurations.

Continental shelf profiles

In addition to four inlet-bay configurations, two different ocean basin profiles are developed: one that is representative of the western and northeastern coasts of Florida, and another that represents the southeastern coast of Florida. The distinction between these two regions is evident in the continental shelf width [legally, the continental shelf

break occurs at a depth of 600 fathoms, or 183 meters (Head and Marcus, 1987)]. The western and northeastern coasts of Florida are characterized by a relatively wide continental shelf (on the order of 150 km to 275 km wide), whereas the southeastern Florida coast is characterized by a relatively narrow continental shelf (on the order of 5 km to 25 km wide).

A high resolution finite element mesh for the Western North Atlantic Tidal model domain is used to obtain the bathymetry profiles extending seaward from tidal inlets in each of the two regions. The finite element mesh has approximately 333,000 nodal points with each node defined by its location (degrees longitude and latitude) and depth (in meters). Figures 6 and 7 show the level of mesh resolution and bathymetry, respectively, for both the east and west coasts of Florida. The domain has been used in previous modeling efforts [Parrish, 2001; Hagen and Parrish, 2004; and Kojima, 2005], and has faithfully reproduced the historic tidal signal along the coast of Florida. Thus, it is assumed that the domain provides a reasonably accurate representation of the bathymetry along the Florida coast.

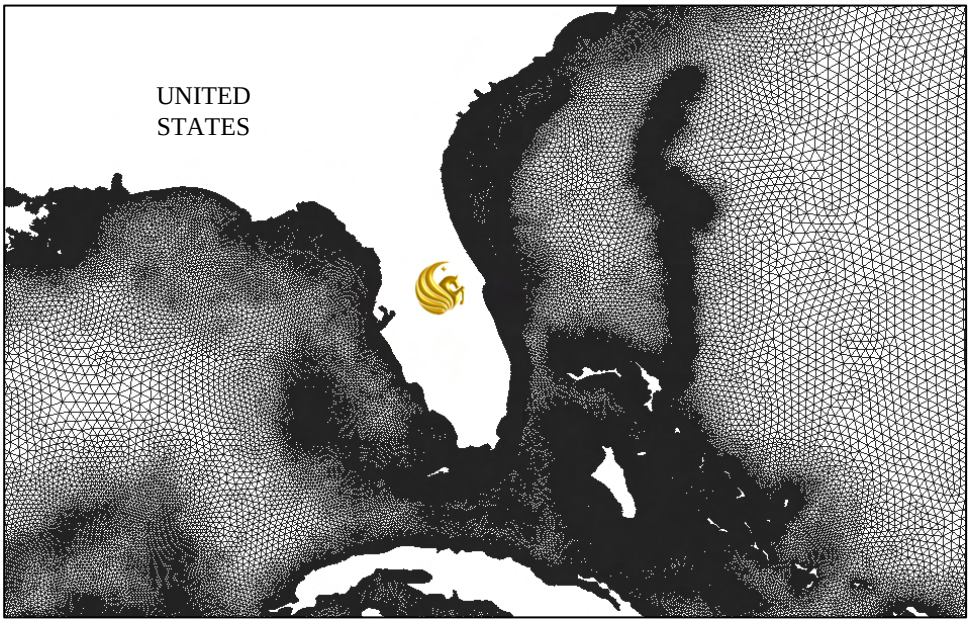

Figure P2- 6 High Resolution Finite Element Mesh along the Florida Coast.

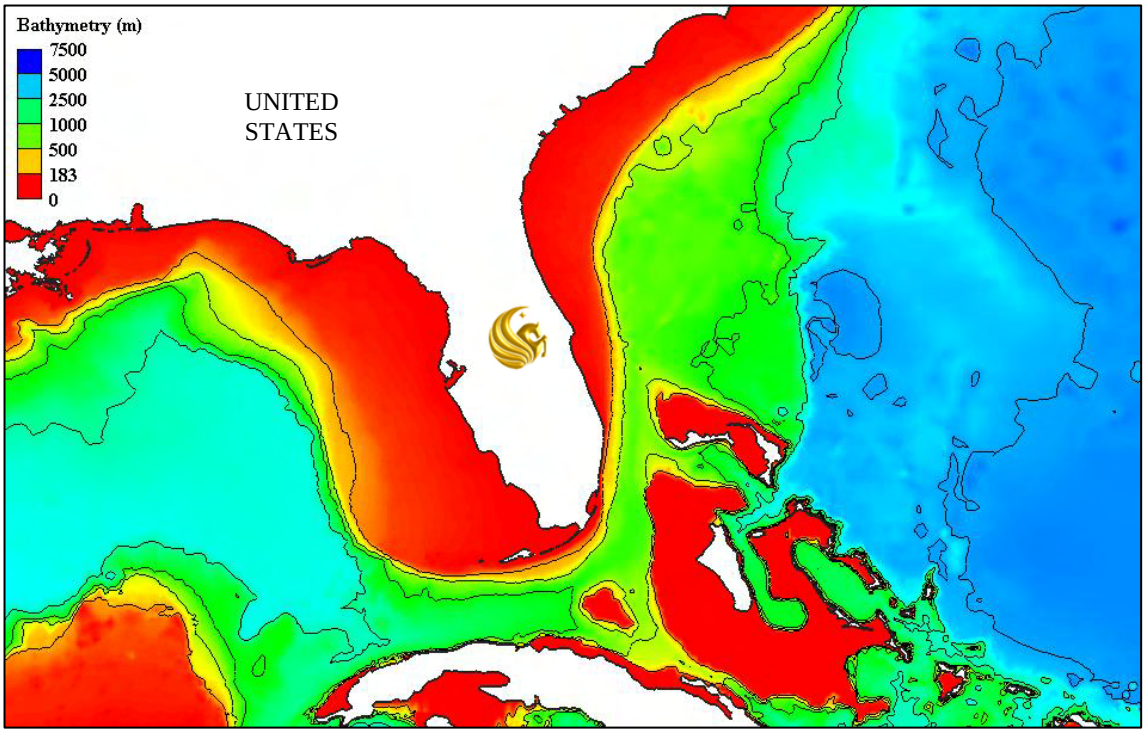

Figure P2- 7 Bathymetry Associated with the 333K Finite Element Mesh.

The Surface-water Modeling System (SMS) is used to extract the bathymetry information along the coast of Florida. SMS is a pre- and post-processor for a number of numerical surface-water models, and includes tools for developing both one- and two-dimensional models (Zundel, 2005). Among its capabilities are finite element mesh generation, finite difference grid generation, and cross-sectional area specification. Using SMS, observation arcs are extended seaward from each inlet into deeper waters in the Atlantic Ocean and Gulf of Mexico (Figure P2-8). Bathymetry information is then extracted from each of these observation arcs to get the ocean depth profile.

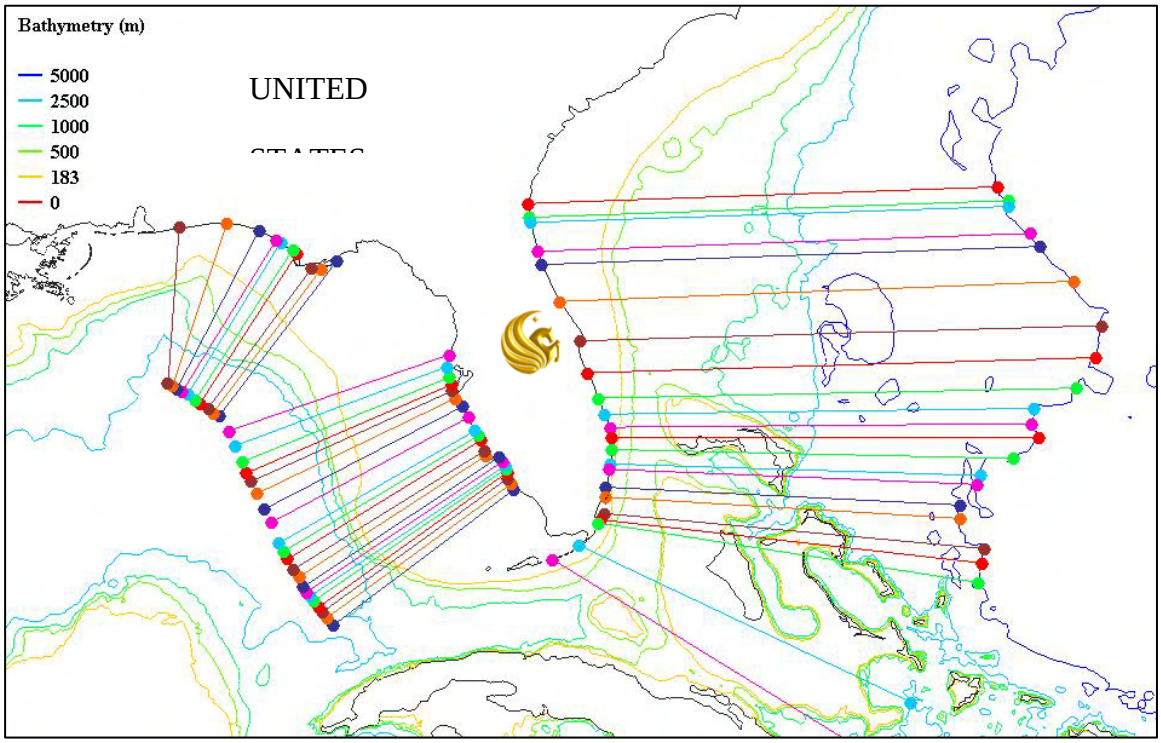

Figure P2- 8 Observation Arcs Used to Extract Bathymetry Information in SMS.

The bathymetry profiles are then grouped according to the location (western and northeastern Florida vs. southeastern Florida). Along the eastern seaboard, the boundary between northeast and southeast Florida is arbitrarily chosen to be the Ft. Pierce Inlet, i.e. any inlets located north of Ft. Pierce Inlet are considered to be in northeast Florida and any inlets located south of Ft. Pierce Inlet are classified as southeast Florida. A statistical analysis is then performed to determine the average location of the continental shelf break. Statistical outliers are removed using a *z*-score procedure similar to the analysis described in Section 2.1.1. Following this procedure, the average continental shelf width for the western and northeastern coast of Florida is determined to be 190 km, whereas the average continental shelf width for the southeastern coast of Florida is 13 km. The difference between these two values (177 km) provides a good basis for comparing two distinctly different shelf profiles in an idealized setting.

The open ocean boundary for the idealized finite element meshes is placed 100 km from the coastline. In order to appropriately design the idealized finite element meshes, the average depth at a distance of 100 km offshore is determined for each shelf profile. Using the bathymetry information extracted from the observation arcs in SMS, and following a statistical analysis procedure described in Section 2.1.1, leads to the

following average depths at 100 km offshore: 73 meters for the western and northeastern Florida shelf profile, and 457 meters for the southeastern Florida shelf profile. Comparing these two values to the average continental shelf width for the two different profiles indicates that the entire western/northeastern Florida domain is contained entirely up on the continental shelf, whereas the southeastern Florida domain includes the shelf break along with deeper water. The difference between each profile can easily be seen in Figure P2-9.

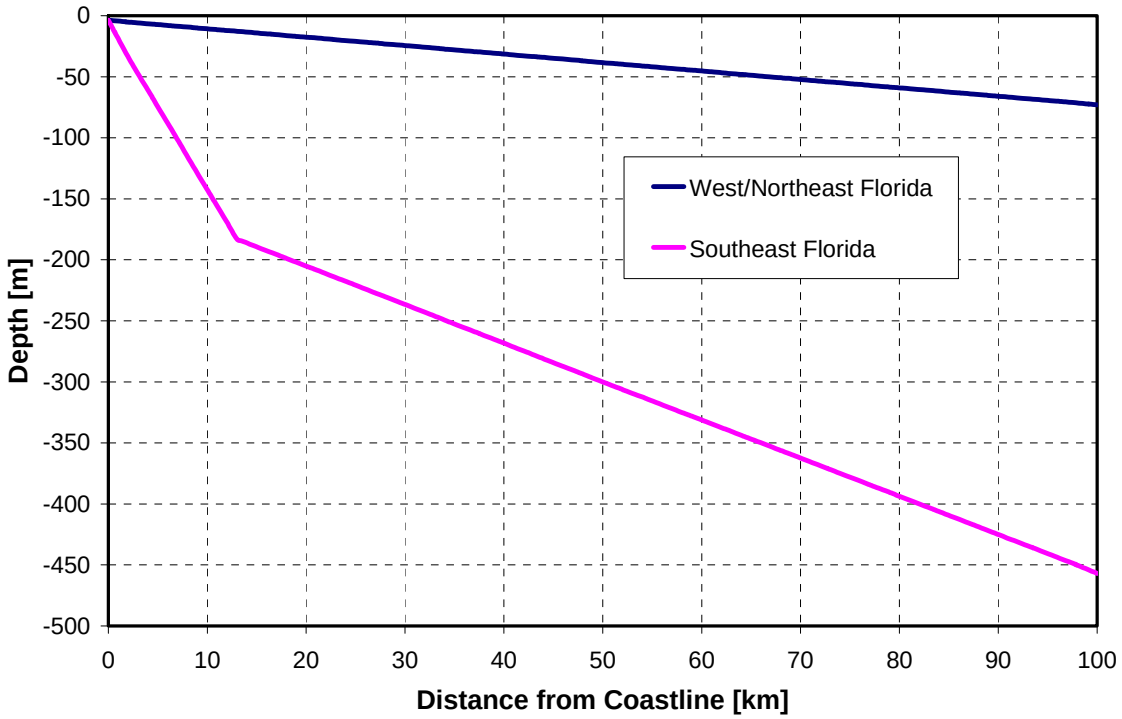

Figure P2- 9 Comparison of the West/Northeast Florida and Southeast Florida Idealized Bathymetry Profiles.

Figures 10 and 11 show an example of the bathymetry profile for the idealized finite element meshes for the western and northeastern coast of Florida and the southeastern coast of Florida, respectively. Included in each figure are several bathymetry profiles for Florida tidal inlets located within each region. It is noted from each figure, that the idealized shelf profiles provide a good representation of the variability found in Florida tidal inlets.

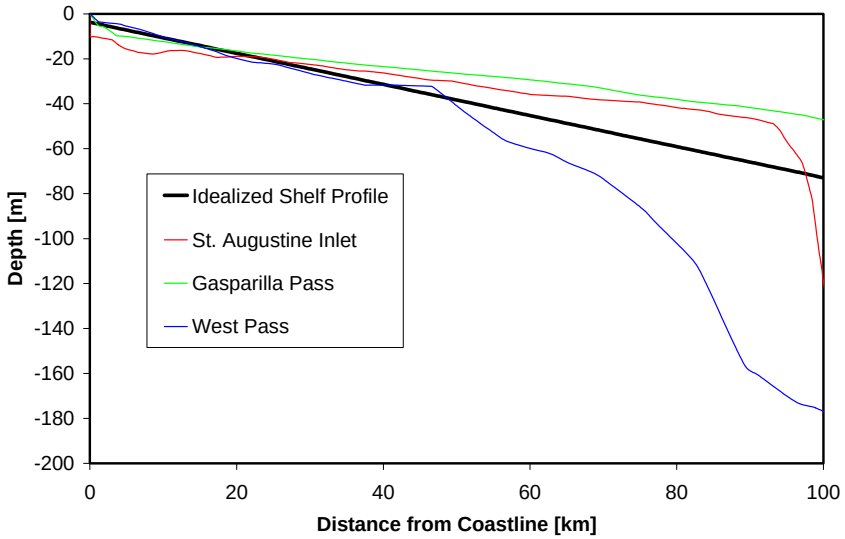

Figure P2- 10 Comparison of Idealized Shelf Profile with Actual Florida Shelf Profiles for the West/Northeast Florid a Domain.

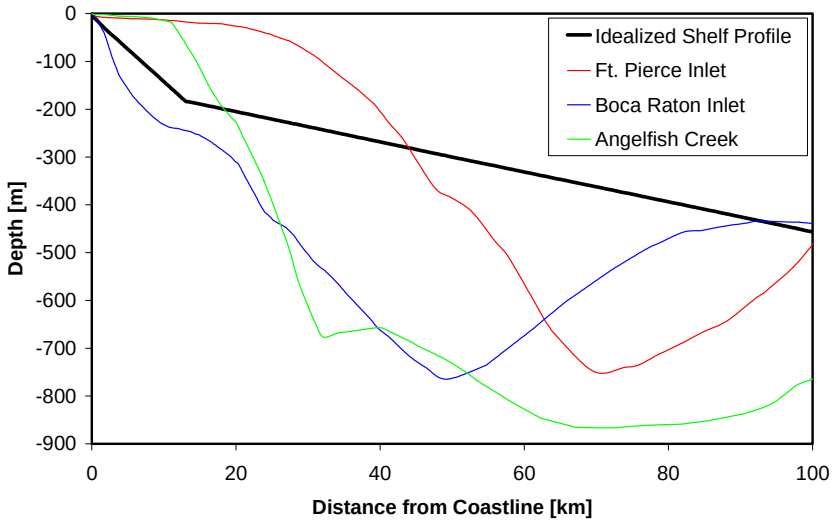

Figure P2- 11 Comparison of Idealized Shelf Profile with Actual Florida Shelf Profiles for the Southeast Florida Domain.

The two different shelf profiles are used in conjunction with the four different inlet-bay configurations to produce eight different finite element meshes. Additionally, two control meshes are built (one for each shelf profile) that do not include any inlet-bay system. These meshes are used as control cases for comparing the effect that tidal inlets have on the open coast storm surge hydrograph. The idealized shelf profile for the Florida Southeast Coast has approximately an average slope out to about 200 m water

depths. Beyond that depth the slope is less than the measured values at the three locations. This should have little impact on the results since the vast majority of the shoaling takes place in water depth less than 200 m.

In the interest of clarity and brevity, each finite element mesh is referenced based on the inlet-bay configuration (first term in the name) and the shelf profile (second term). Hence, the mesh that pairs the average inlet-bay configuration with the west/northeast Florida shelf profile is referred to as the Average-WNEFL mesh. Similarly, the mesh that pairs the average inlet-bay configuration with the southeast Florida shelf profile is referred to as the Average-SEFL mesh.

Figures 12 and 13 present the finite element discretization and the bathymetry for the Average-WNEFL mesh. Figures 14 and 15 continue with the finite element discretization and bathymetry for the Average-SEFL mesh. For all meshes, the node spacing at the open ocean boundary is 2500 meters and transitions down to 25m-50m in the inlet channel. The 25 m to 50 m resolution was dictated by the width of the inlets considered (i.e. several nodes required within the inlet width). Furthermore, all domains measure 150 km alongshore and 100 km seaward.

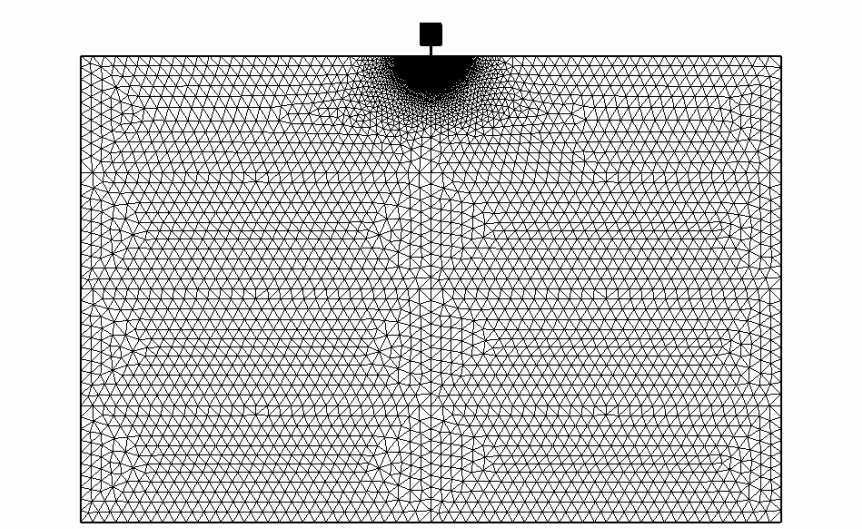

Figure P2- 12 Finite element mesh for the average inlet-bay configuration and the West / Northeast Florida shelf profile (Average-WNEFL mesh).

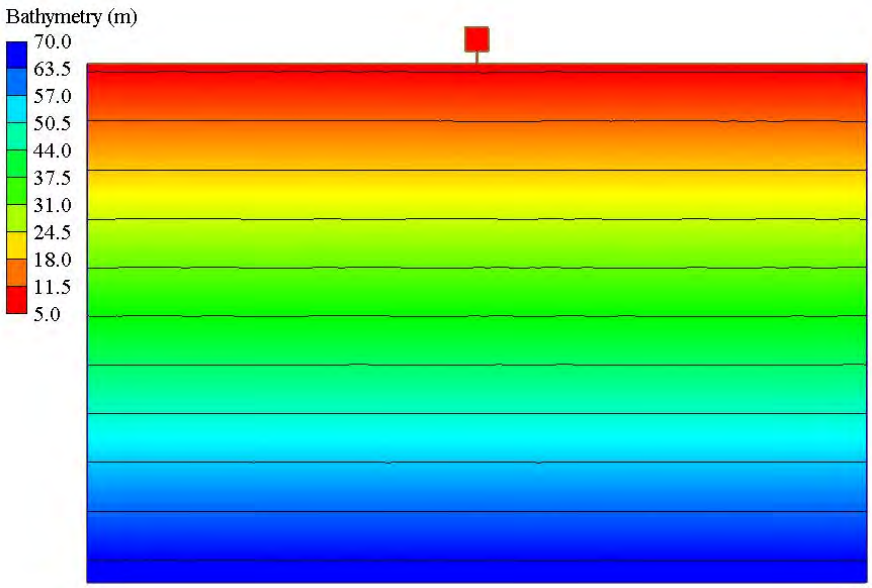

Figure P2- 13 Bathymetry for the Average Inlet-Bay Configuration and the West / Northeast Shelf Profile (Average-WNEFL mesh).

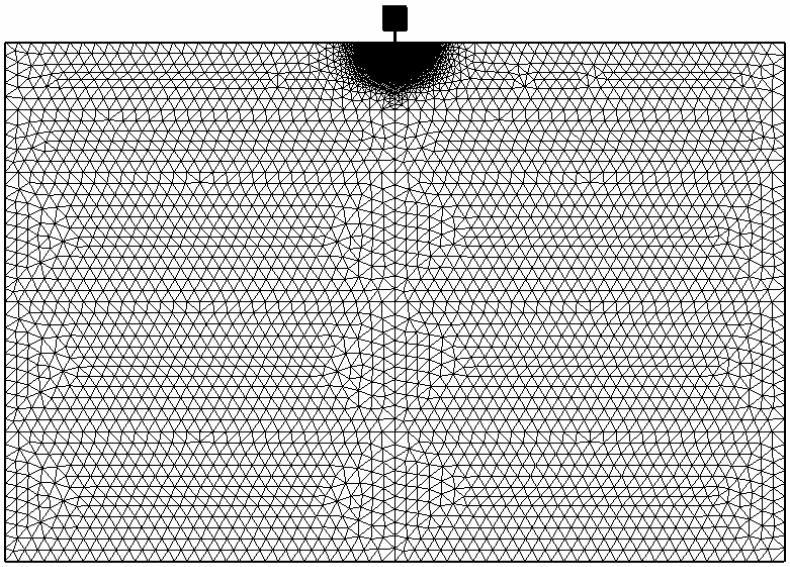

Figure P2- 14 Finite Element Mesh for the Average Inlet-Bay Configuration and the Southeast Florida Shelf Profile (Average-SEFL mesh).

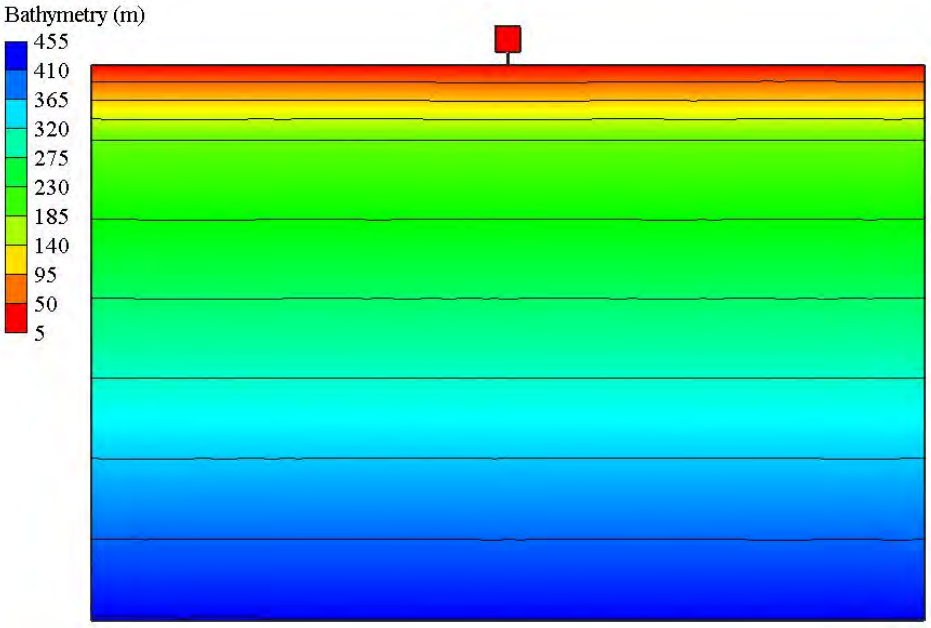

Figure P2- 15 Bathymetry for the Average Inlet-Bay Configuration and the Southeast Florida Shelf Profile (Average-SEFL mesh).

Escambia Bay Meshes

Study location

The study area is located along the Panhandle of Florida in the northwestern portion of the state of Florida. The main focus of this study is an inlet-bay system that was devastated by storm surge from Hurricane Ivan in September 2004. The system includes the Pensacola Inlet, Pensacola Bay, Escambia Bay, Blackwater Bay and East Bay (Figure P2-16). The system is connected to two adjacent bay systems via a Gulf Intracoastal Waterway (GIW): Perdido Bay to the west and Choctawatchee Bay to the east.

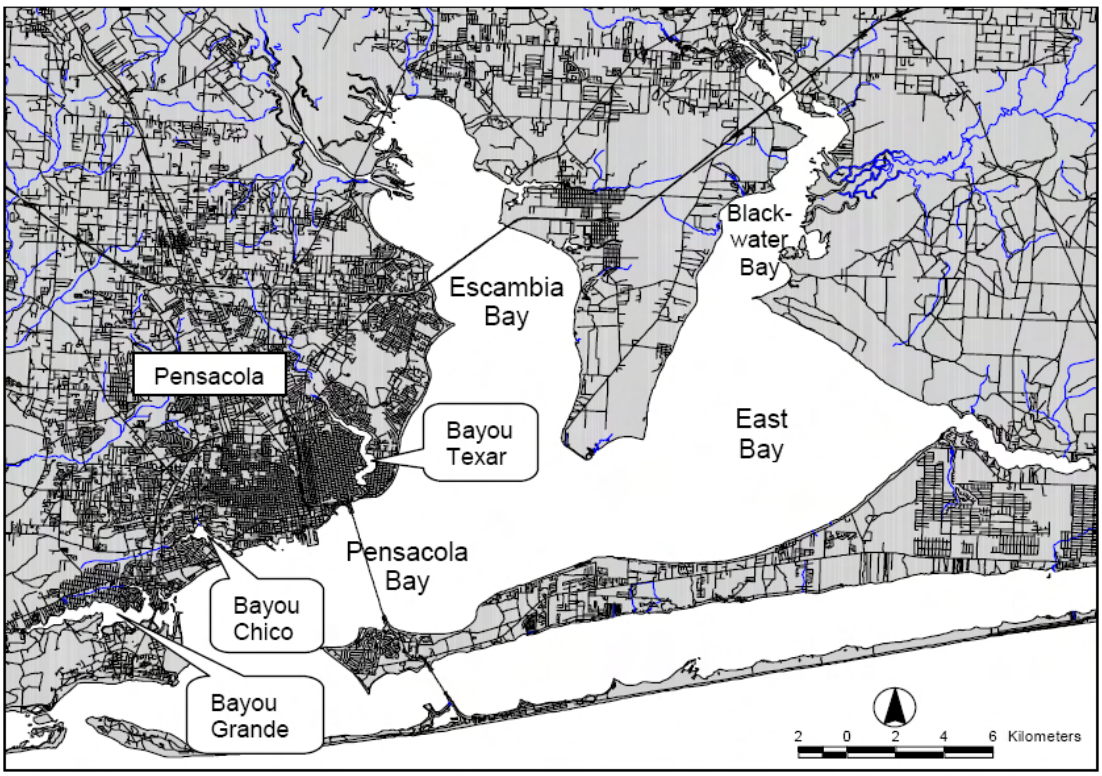

Figure P2- 16 Escambia Bay Study Location (DeBusk et al., 2002).

Pensacola Inlet is a relatively deep inlet that connects the Escambia Bay to the Gulf of Mexico. The inlet is part of Escambia County, and is bordered by two low-lying, sandy barrier islands: Perdido Key to the west and Santa Rosa Island to the east. The inlet became a federal navigation project in 1881 and is regularly dredged to a depth of approximately 15 meters to accommodate U.S. Navy aircraft carriers (Carr de Betts, 1999).

Model domains for Escambia Bay

An ocean-based domain is used to simulate storm surge due to Hurricane Ivan in the vicinity of Escambia Bay. The domain encapsulates portions of the Atlantic Ocean found west of the 60º West Meridian, the Gulf of Mexico, and the Caribbean Sea. The mesh was developed by incorporating the Escambia Bay coastline features into an existing 52,774 (53K) node mesh for the Western North Atlantic Tidal model domain [see Kojima (2005) for verification of the existing 53K mesh]. The new mesh includes 88,318 nodes and 165,137 elements, and covers a horizontal surface area of approximately 8.347×10^6 km^2.

Bathymetry for the Escambia Bay region was obtained via the National Geophysical Data Center (NGDC) Coastal Relief CD-ROM, Volume 3. The database consists of a combination of 3-arc second digital elevation maps (via the United States Geological Survey) and hydrographic soundings (via the National Ocean Service). For regions extending beyond the Escambia Bay and Pensacola Inlet, the bathymetry was interpolated from an existing high resolution Western North Atlantic mesh (333K mesh). Figures 17 through 22 present the finite element discretization and bathymetry for the domain with zoomed in views of the Escambia Bay and Pensacola Inlet.

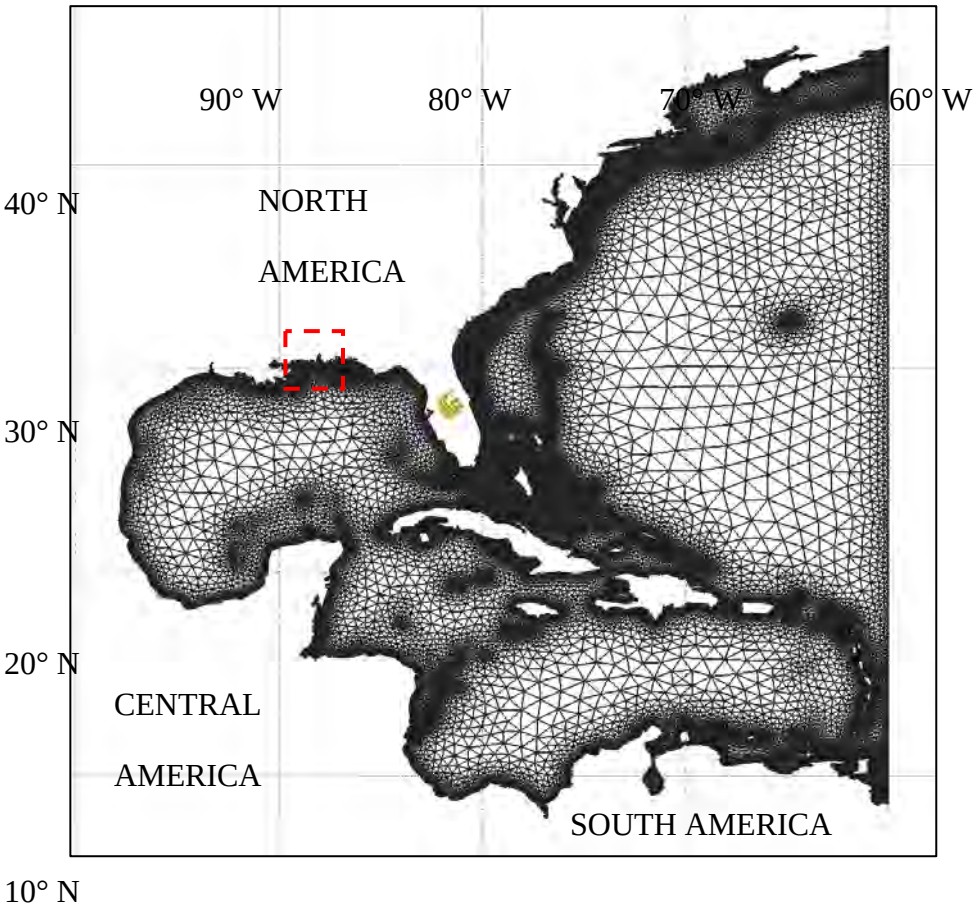

Figure P2- 17 Finite Element Discretization for the Ocean-Based Domain.

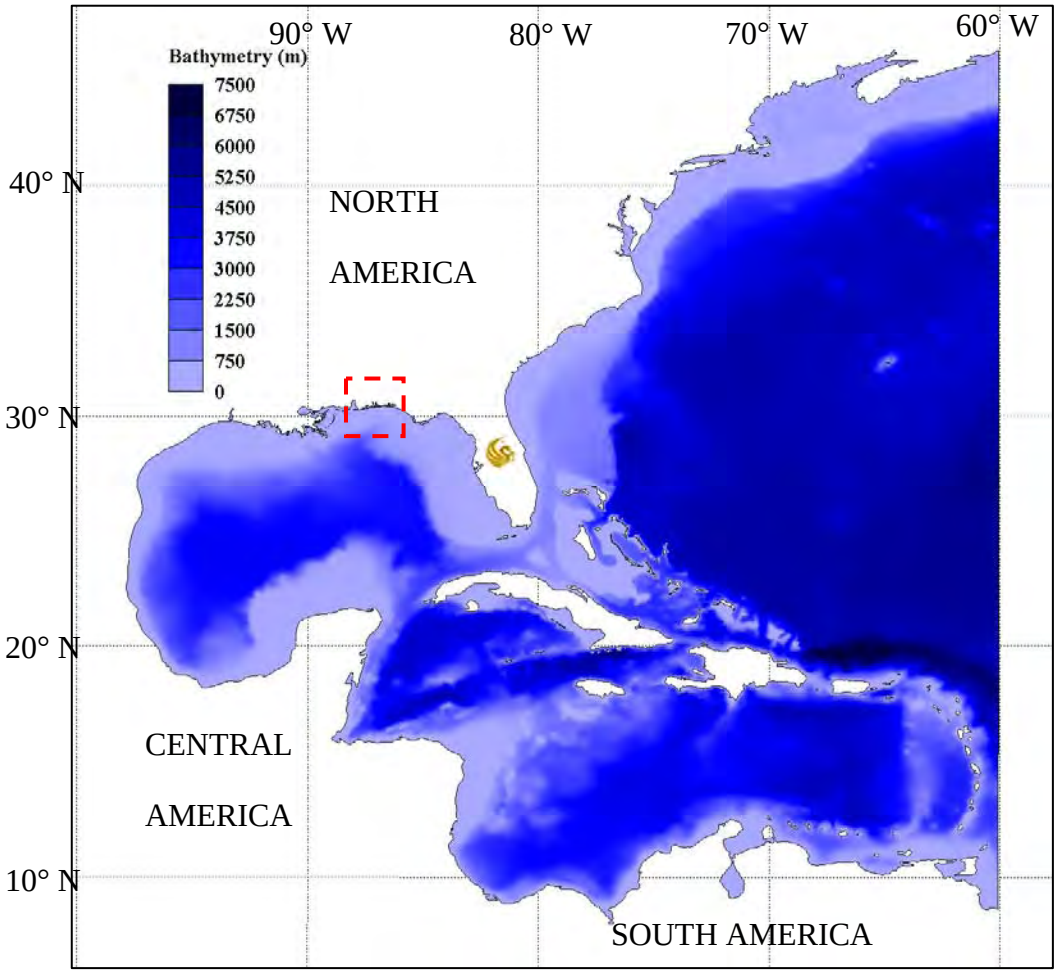

Figure P2- 18 Bathymetry for the Ocean-Based Domain.

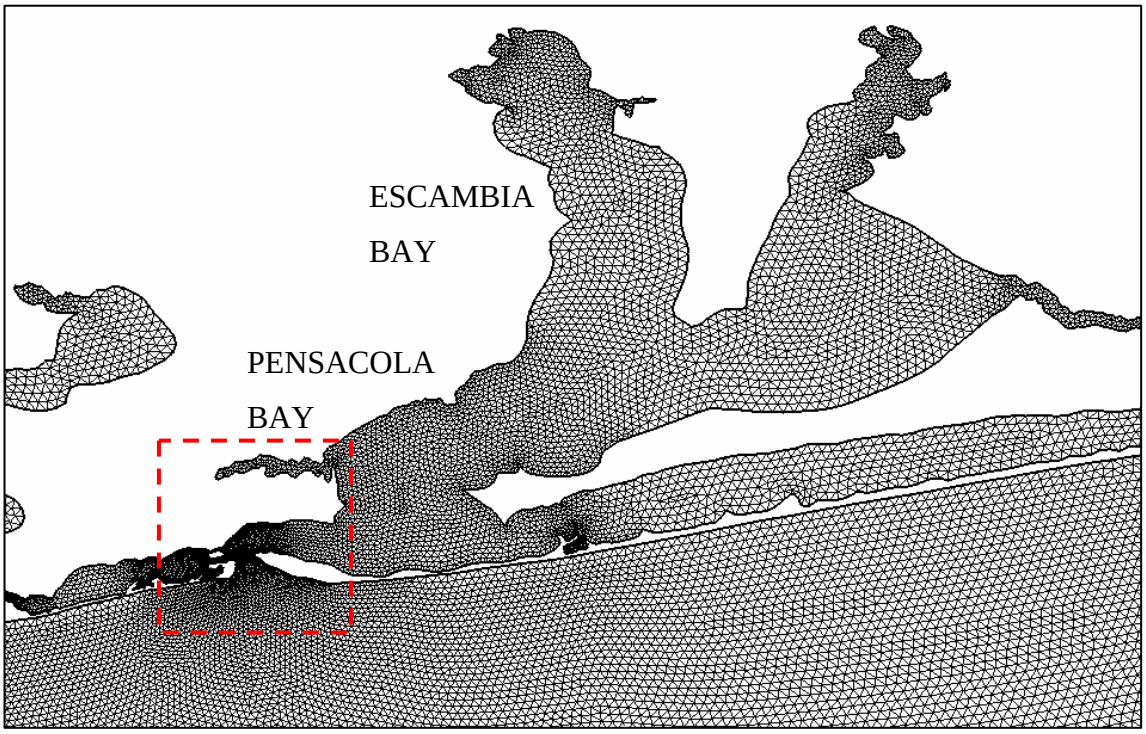

Figure P2- 19 Finite Element Discretization near the Escambia Bay.

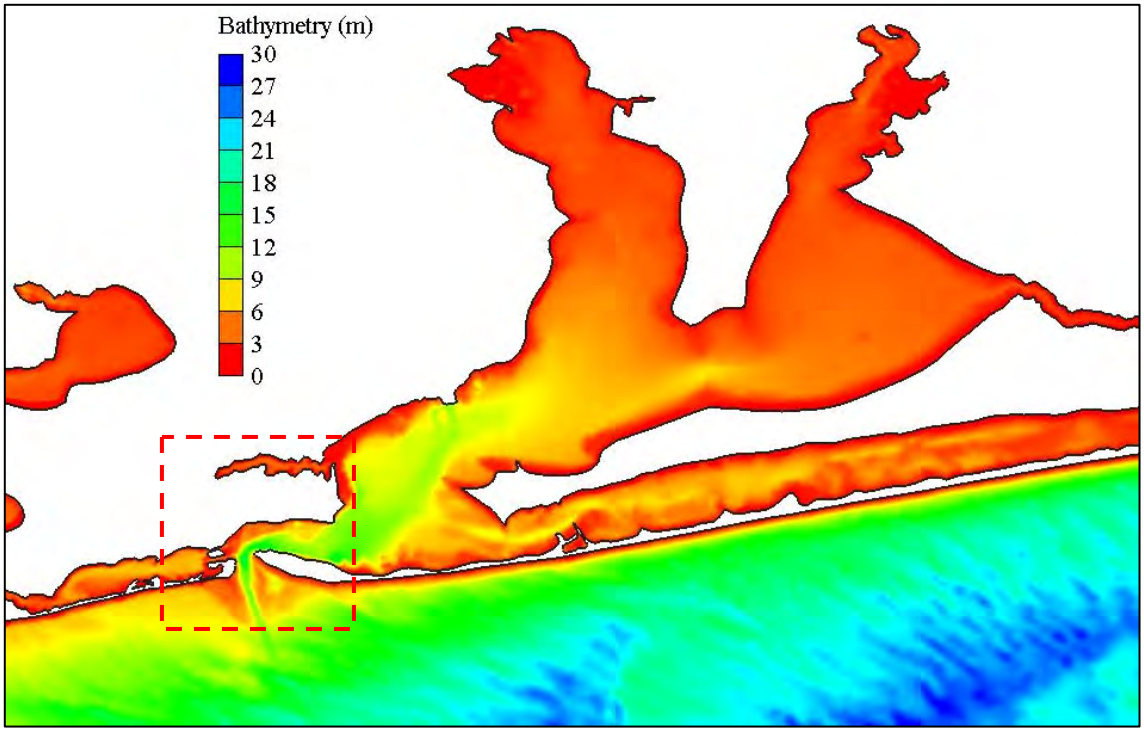

Figure P2- 20 Bathymetry for Coastal Areas near the Escambia Bay.

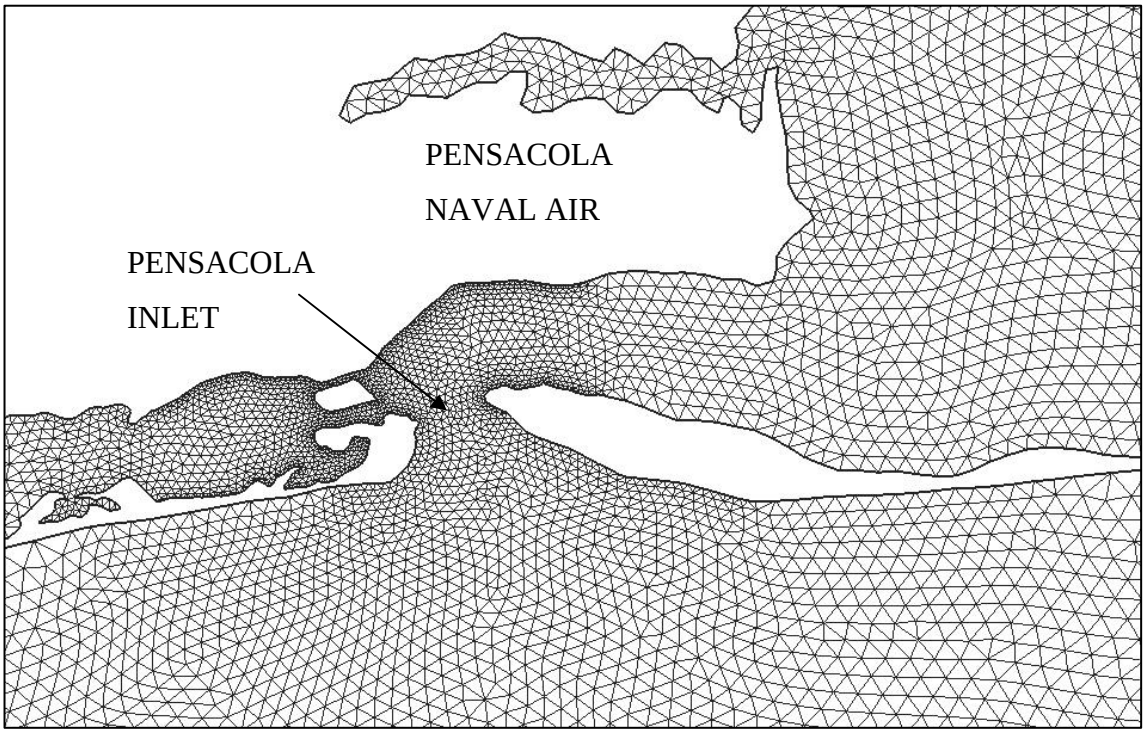

Figure P2- 21 Finite Element Discretization Near Pensacola Inlet.

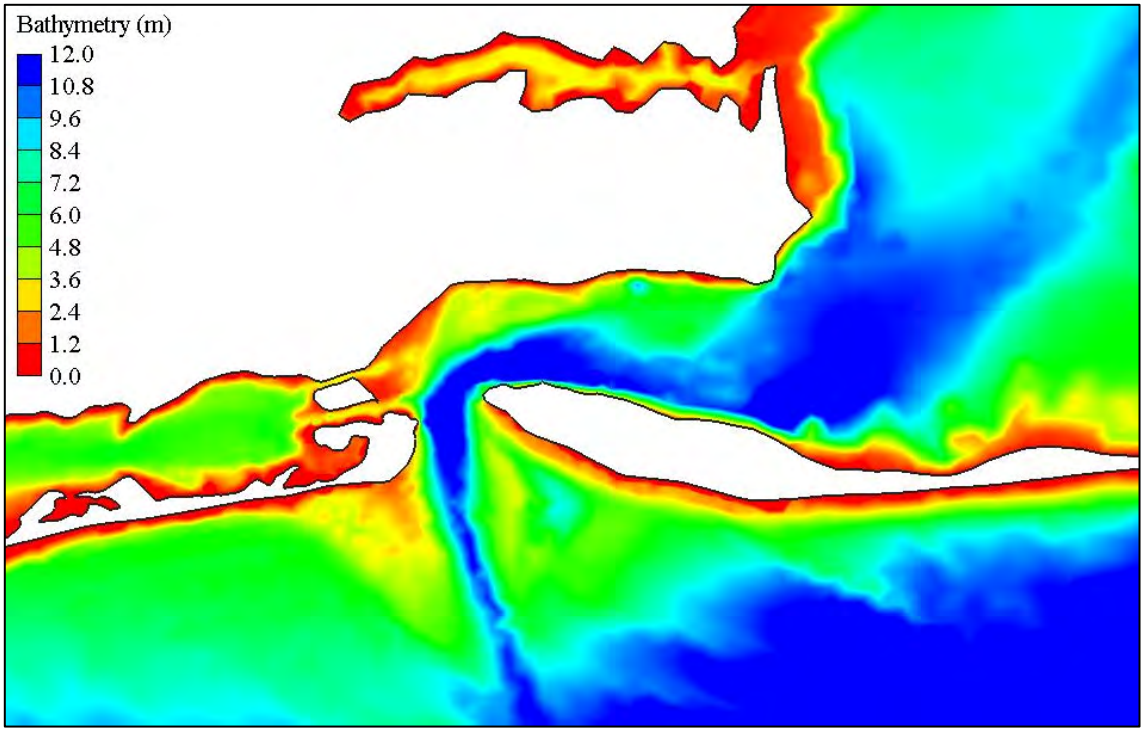

Figure P2- 22 Bathymetry for Coastal Areas Near the Pensacola Inlet.

Inundation areas

In addition, the inclusion of inundation areas near the Escambia Bay is examined. More specifically, the effect of treating the low-lying barrier islands that are adjacent to Pensacola Inlet (Perdido Key and Santa Rosa Island) as model boundaries versus inundation areas is studied. Figure P2-23 presents a digital elevation model (DEM) for the inland coastal area surrounding the Escambia Bay and Pensacola Inlet.

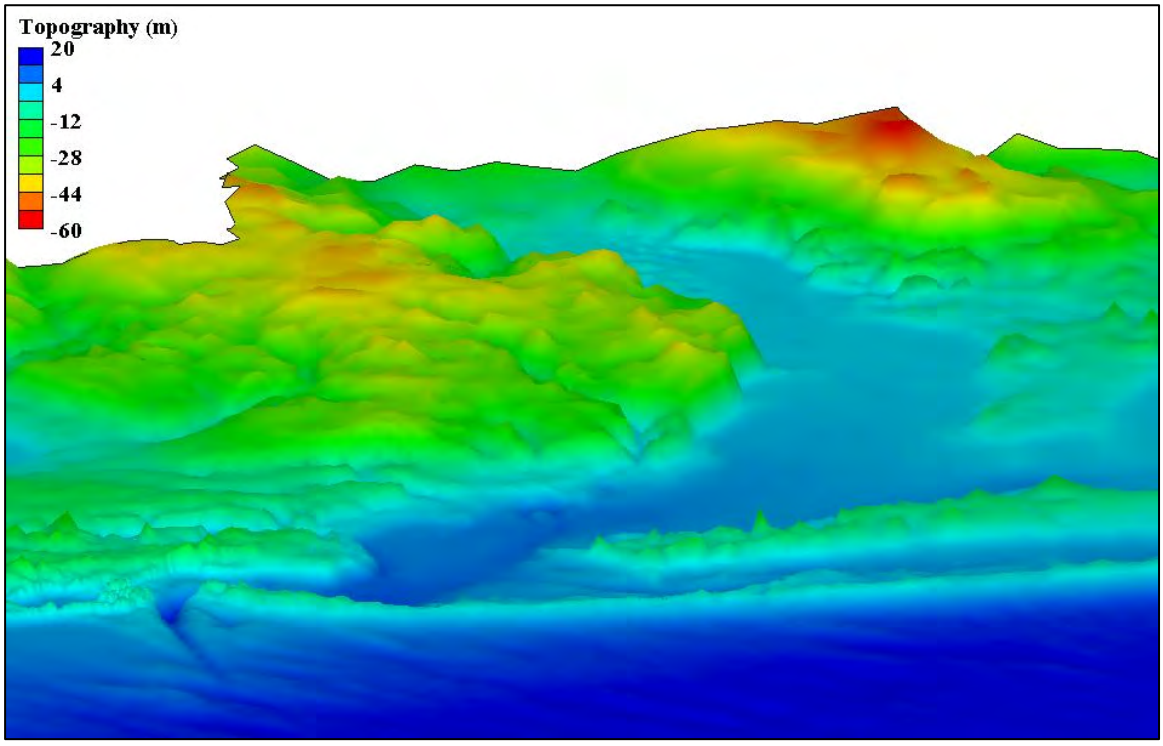

Figure P2- 23 Topography Surrounding the Escambia Bay and Pensacola Inlet.

The negative values shown in Figure P2-23 indicate elevations that are above mean sea level (the green colors represent elevations that are 10 meters above MSL or greater). In lieu of the fact that the recorded storm surge in Escambia Bay was on the order of 3-4 meters, it is evident from Figure P2-23 that including a detailed floodplain mesh in the vicinity of Escambia Bay is not necessary. Thus, only the effect of including the low-lying barriers islands as inundation areas is examined, and is incorporated into the model domain. The finite element mesh that includes the barrier islands as inundation areas is shown below (Figure P2-19 shows the finite element mesh that treats the barriers islands as model boundaries).

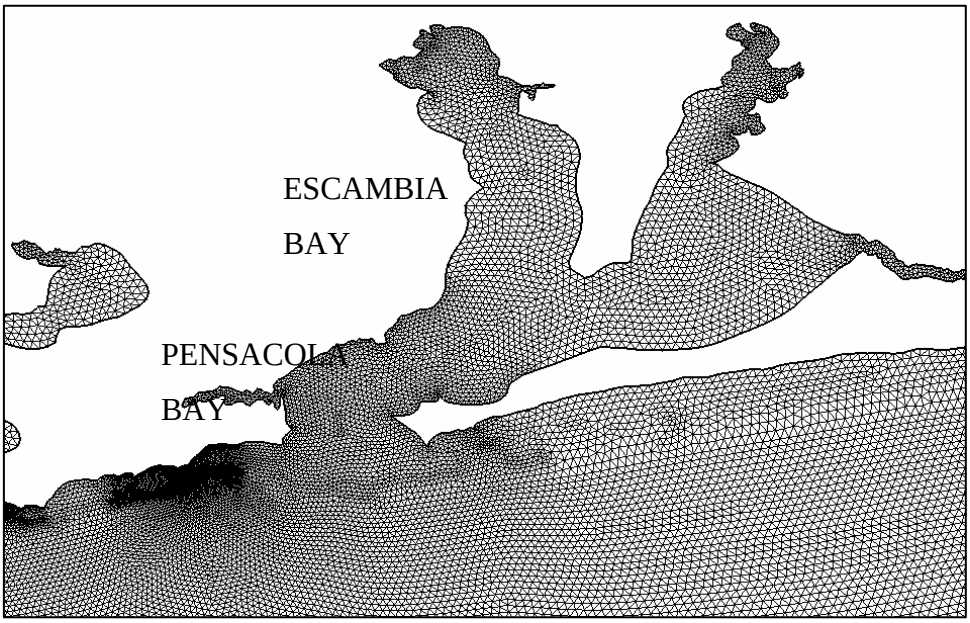

Figure P2- 24 Finite Element Mesh for the Escambia Bay Region with the Barrier Islands Treated as Inundation Areas.

Model Setup

Two different domains are used in this study: an idealized domain and a real domain. As such, the ADCIRC model parameters must be set according to the domain type and study specifications. For example, parameters that specify the run time, time step, wetting and drying process, forcing frequencies, etc. must be included in the Model Parameter and Periodic Boundary Condition file (fort.15). Furthermore, the water elevation output locations must be specified in the input file for each domain. Presented herein are the model parameters and output locations for both the idealized domains and the Escambia Bay domain.

Idealized Domain

Model parameters for idealized domain

For the idealized study, the inlet-bay configuration and continental shelf profile are isolated to examine their influence on the model results. Consequently, the model parameters are held constant for each simulation and are specified according to the

following: The equations are solved in the Cartesian coordinate system. Simulations are spun up from rest over a 2 day period via a hyperbolic ramp function. Total simulation time is 4 days, with a 0.25 second time step used to ensure model stability. A hybrid bottom friction formulation is employed with the following specifications: $C_{f_{\min}}$ = 0.0025, H_{break} = 10 meters, θ = 10, and λ = 1/3. The horizontal eddy viscosity coefficient is set to 5 m^2/sec. A constant Coriolis parameter corresponding to 27.5° N (approximately the middle latitude of Florida) is used. One harmonic forcing frequency corresponding to the M_2 (principal lunar) constituent is applied to the system with an amplitude of 0.5 meters and 0° phasing (since the timing is not important in an idealized setting). This produces a tidal range of approximately 1 meter near the coastline, which is representative of the tidal range characteristics along the Florida coast. Meteorological forcings (wind stress and surface pressure) are read into the simulation every 30 minutes, with the eye of the synthetic hurricane making landfall approximately three days into the simulation.

Model output locations for idealized domain

In lieu of the fact that previous bridge scour modeling efforts have incorporated open coast boundaries at varying distances from the mouth of the inlet, a wide range of semi-circular arcs are created with output stations located along each arc. These arcs have radii ranging from 1 km to 15 km from the mouth of the inlet, and are representative of typical open coast boundary locations used in bridge scour modeling. Water surface elevations are recorded at each of these stations over the entire duration of the simulation at six minute intervals. Figure P2-25 displays the semi-circular arcs with the output locations for the different radii.

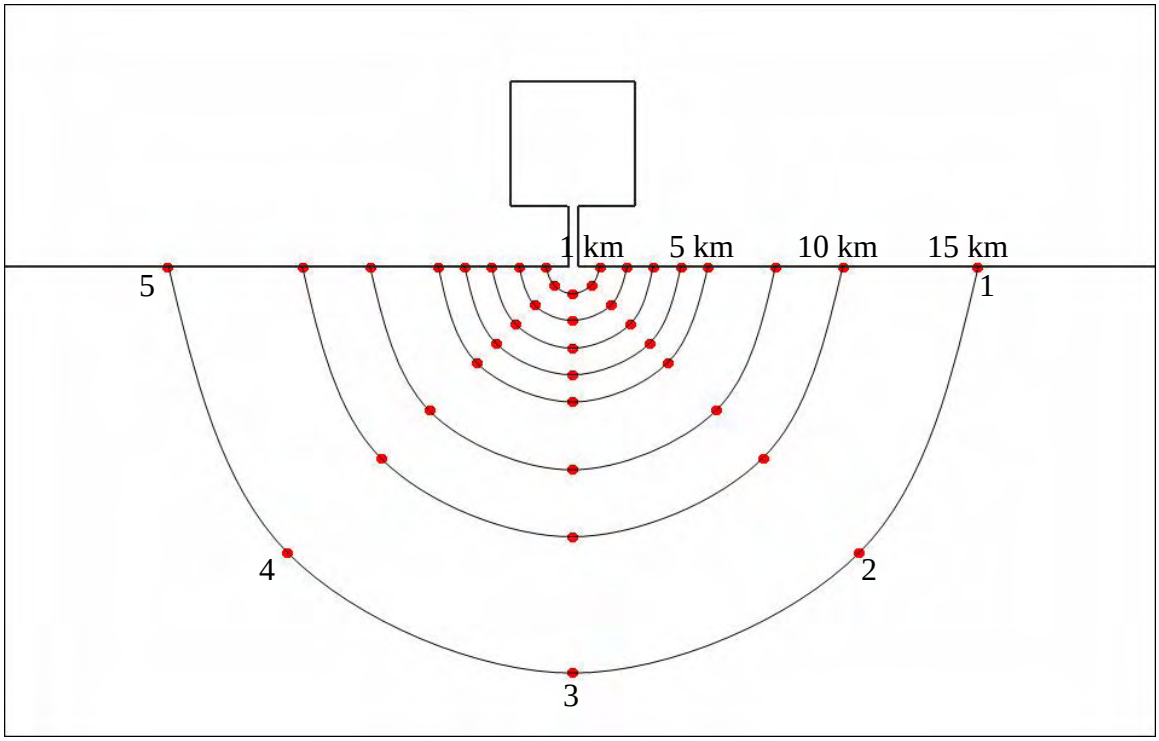

Figure P2- 25 Semi-circular arcs with output locations for idealized domain.

Five output stations are located along each semi-circular arc: east (1), southeast (2), south (3), southwest (4), and west (5). The directions are oriented such that the "up" direction is north; however, the directions (e.g. east, west, etc.) are used only as a convenience and the subsequent hydrograph plots in the results section use the numbering system to identify the location along the arc. These output locations are used to compare the effect that inlets have on the open coast storm surge hydrographs and to examine the spatial variance of the hydrographs along each arc.

Additional locations within the inlet and bay are also specified in the input file (Figure P2-26). Stations are located along the centerline of the inlet at three locations (mouth of the inlet, middle of the inlet, and end of the inlet), and at multiple sites within the bay. These locations are consistent between the inlet-bay configurations and are used to examine the influence of inlet width on the surge levels within the inlet and bay.

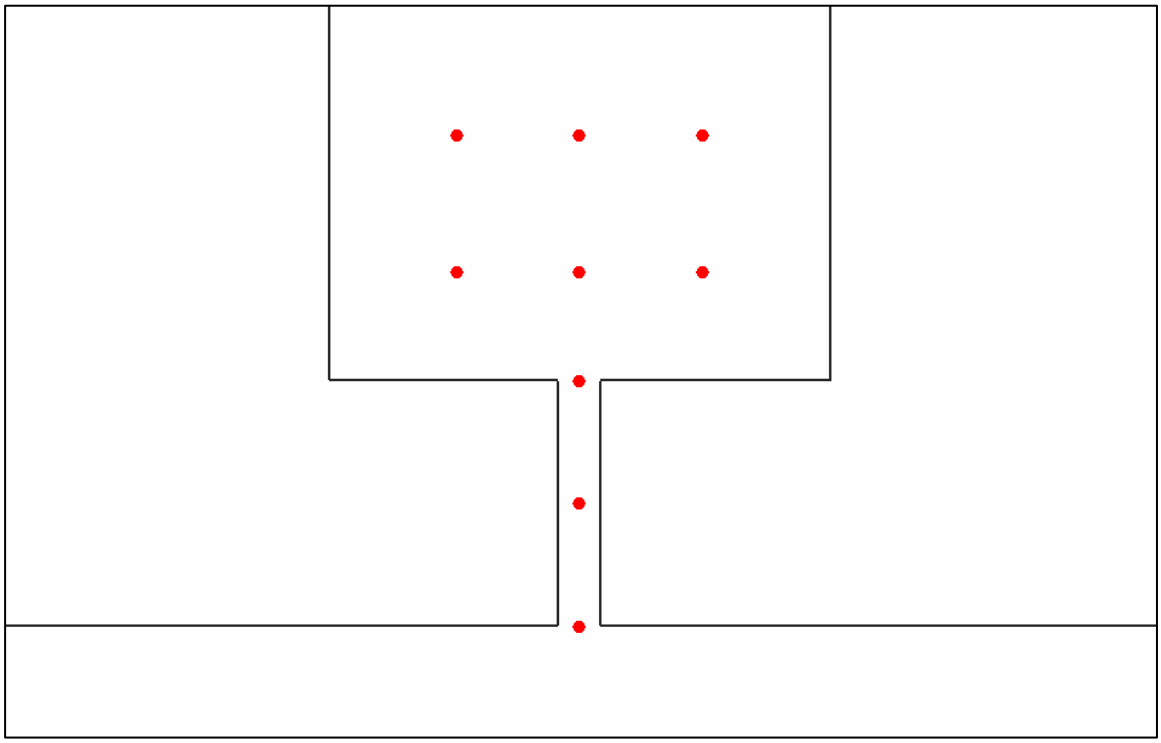

Figure P2- 26 Output locations within the inlet-bay system.

Escambia Bay Domain

Model parameters for Escambia Bay domain

Astronomic tides are included for each of the Escambia Bay domains; however, the astronomic tides and storm surge are computed separately due to the differences in simulation length. The total water elevation is computed by superimposing the storm surge output with a resynthesis of the astronomic tides (adjusted in time to match the storm surge output). The results are then compared to historical National Ocean Service (NOS) gauge data located within Pensacola Bay to verify the model.

The model parameters for the astronomic tidal simulations are set as follows: The coordinate system is set to spherical. Simulations are begun from a cold start. Seven harmonic forcings are applied simultaneously along the ocean boundary (M_2, K_1, O_1, N_2, K_2, Q_1, and S_2) and are ramped over a 20-day period. The hybrid bottom friction formulation is employed with the following settings: $C_{f_{\min}}$ = 0.0025, H_{break} = 1 meter, θ = 10, and λ = 1/3. The horizontal eddy viscosity coefficient is set at 5 m^2/sec, and a time step of 5 seconds is used to ensure model stability.

Similarly, the model parameters for the storm surge simulations are set as follows: A spherical coordinate system is applied. Simulations are begun from a cold start. A ten day simulation is performed (September 7, 2004 at 6 p.m to September 17, 2004 at 6 p.m.), with a 2.5-day ramp period. Meteorological forcings (wind stress and pressure) are read into the model every 30 minutes. The wetting and drying of elements is employed with the minimum depth set to 0.1 meters. A 1.25 second time step is used for each model domain to ensure stability. A hybrid bottom friction formulation is used with the following settings: $C_{f_{\min}} = 0.001$, $H_{break} = 10$ meters, $\theta = 10$, and $\lambda = 1/3$, and the horizontal eddy viscosity coefficient is set to 5 m^2/sec.

Model output locations for Escambia Bay domain

In a similar manner to the idealized domain, semi-circular arcs of varying radii are extended seaward from the mouth of Pensacola Inlet (arcs range from 1 km to 15 km in radial distance). Figure P2-27 shows the observation points along each semi-circular arc extending seaward from Pensacola Inlet.

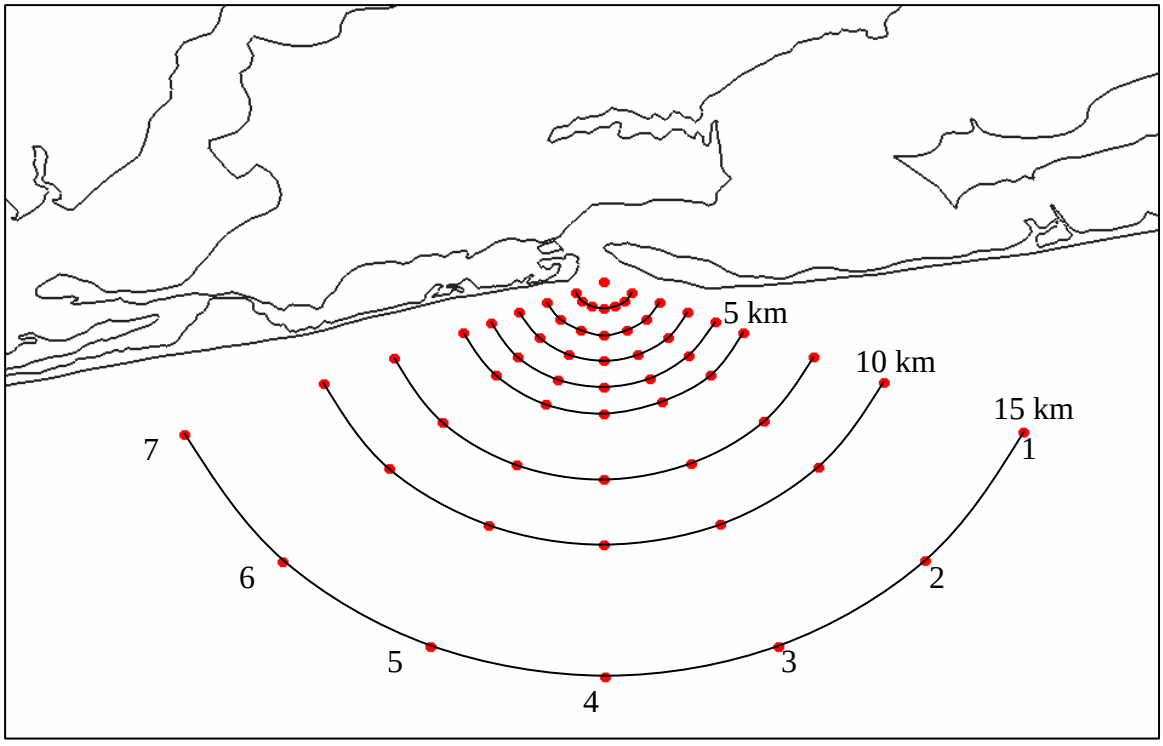

Figure P2- 27 Semi-circular arcs with output locations for Escambia Bay domain.

Observation points for locations due east and west from the mouth of the inlet are not included as some of the points would either be outside of the model boundaries or within

the bay system. In this case, seven output stations are located on each semi-circular arc: east-southeast (1), southeast (2), south-southeast (3), south (4), south-southwest (5), southwest (6), and west-southwest (7). These output locations are used to compare the effect that the Pensacola Inlet has on the open coast storm surge hydrographs and to examine the spatial variance of the hydrographs along each arc.

Additional output locations are specified within the Escambia Bay system. In particular, model output is provided at the NOS tide gauge location in Pensacola Bay (Figure P2-28).

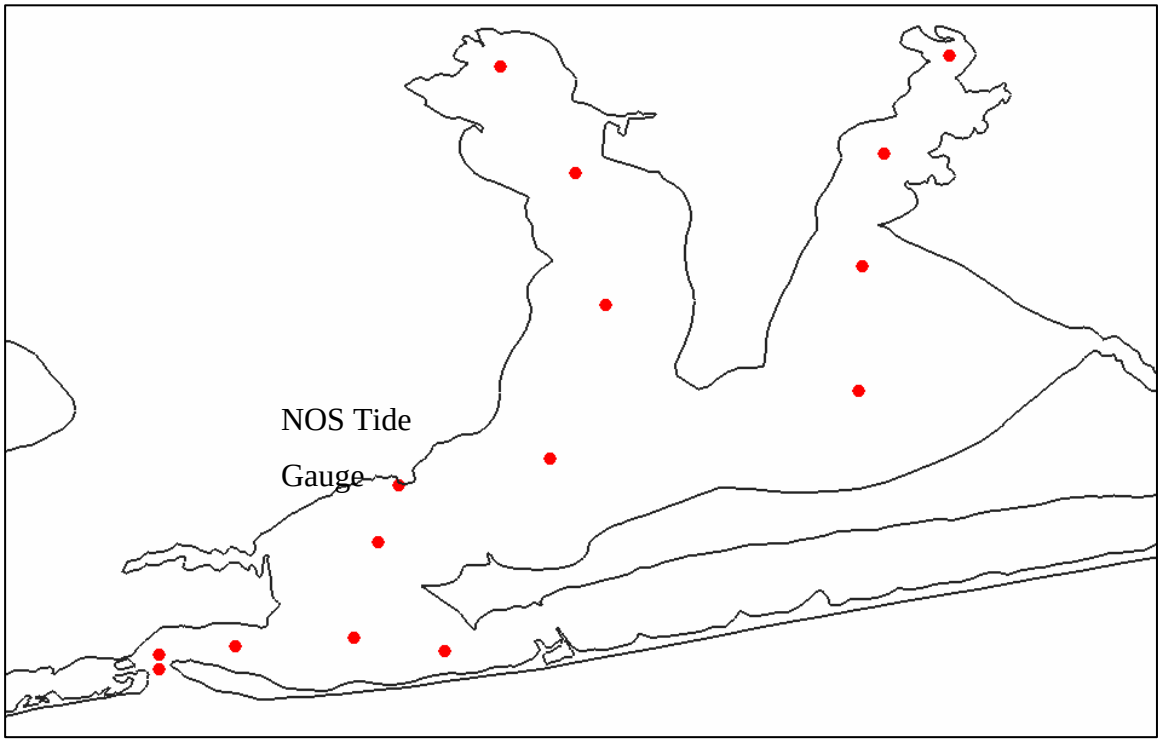

Figure P2- 28 Observation stations within Escambia Bay.

SIMULATION RESULTS

Primary focus is given to the effect that inlet-bay configurations have on the open coast storm surge hydrographs. Two different studies are presented in this section to illustrate these results: 1) a numerical parameter study, where the effect of four different inlet widths (average, 100 meter, 500 meter, and 1000 meter widths) on the open coast storm surge hydrographs are isolated and compared; and 2) a hindcast study that focuses on the effect of the Pensacola Inlet and Escambia Bay system on the open coast storm surge hydrographs produced from Hurricane Ivan. Additional discussion is provided on two secondary results: 1) the spatial variance of the open coast storm surge along the observation arcs; and 2) the significance of the continental shelf profile on the peak open coast surge levels.

The numerical parameter study results are presented in Section 1, and the hindcast results are presented in Section 2. A discussion is provided at the end of the section (Section 3) that qualitatively compares the idealized domain results with the real domain results. The findings and conclusions presented herein have implications for developing more accurate open coast boundary conditions for bridge scour models and other inlet-based storm surge models (as used herein, bridge scour model refers to any local, high resolution 2- or 3-dimensional model used to compute velocities and circulation patterns within an inlet and bay that could be used to determine scour levels near coastal bridges).

Idealized Domain Results

First, a numerical parameter study is performed to elucidate the behavior of open coast storm surge hydrographs in an idealized setting. In contrast to a hindcast study, a numerical study allows certain domain variables (e.g. inlet width and bathymetry) to be isolated and examined. The overall behavior of the model to changes in these numerical parameters is extrapolated by comparing simulation results to one another. Historical data is not available for such a study, thus model results are qualitatively compared to better clarify overall hydrograph behaviors.

Inlet comparisons

Ultimately, the results and conclusions from this study will be used to determine whether an inlet and bay system (e.g. the Pensacola Inlet and Escambia Bay system) should be

included in a large-scale ocean circulation model (e.g. the Western North Atlantic Tidal model domain) for generating open coast boundary conditions for local bridge scour models. In order to accomplish this, four inlet-bay configurations and a control case are developed in an idealized setting. The control mesh does not include an inlet-bay system along the coastline and provides a test case for better determining the influence of the inlet-bay system on the open coast storm surge hydrographs.

Observation points along semi-circular arcs of varying radii (1 km to 15 km) are extended seaward from the mouth of the inlet and are the same in each simulation. Model output is then compared at each of the observation points for all of the inlet-bay configurations. Figure P2-29 shows the observation points along the 1 km and 5 km arc radii. Figures 30 and 31 show model results for each of the inlet-bay configurations at point #3 (perpendicular to the coast) on both of these arcs for the west/northeast Florida shelf profile. Figures 32 and 33 display model results at the same locations for the southeast Florida shelf profile.

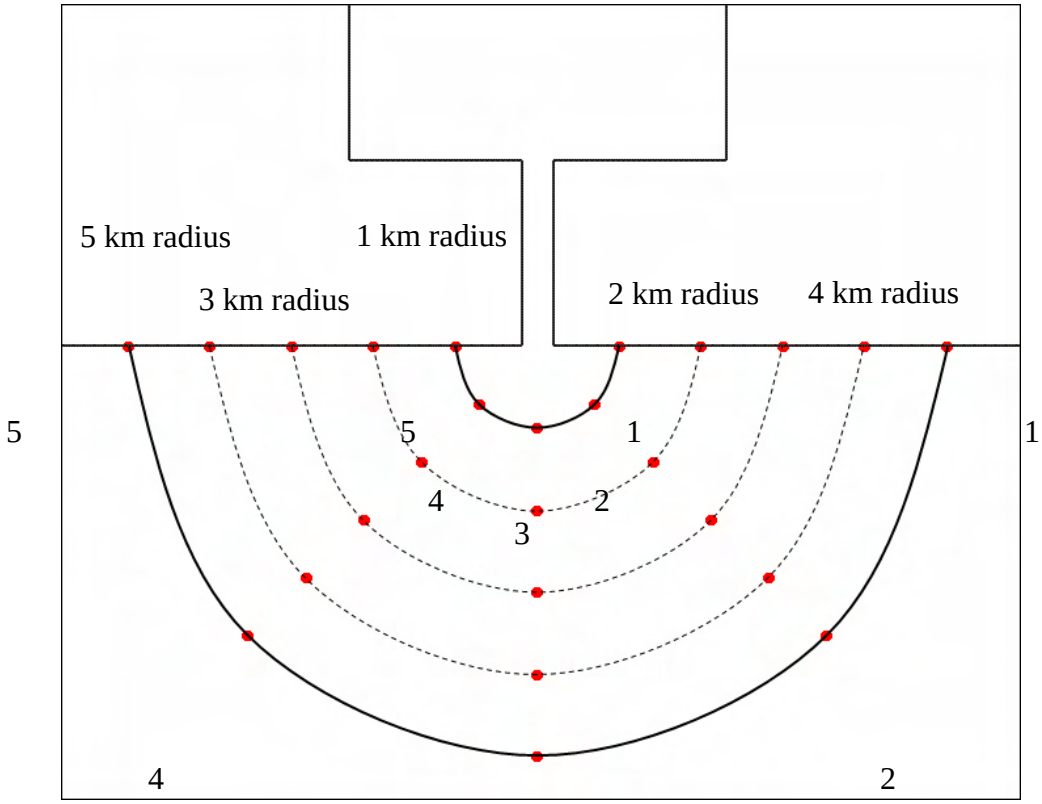

Figure P2- 29 Observation points along the 1 km and 5 km arc radii.

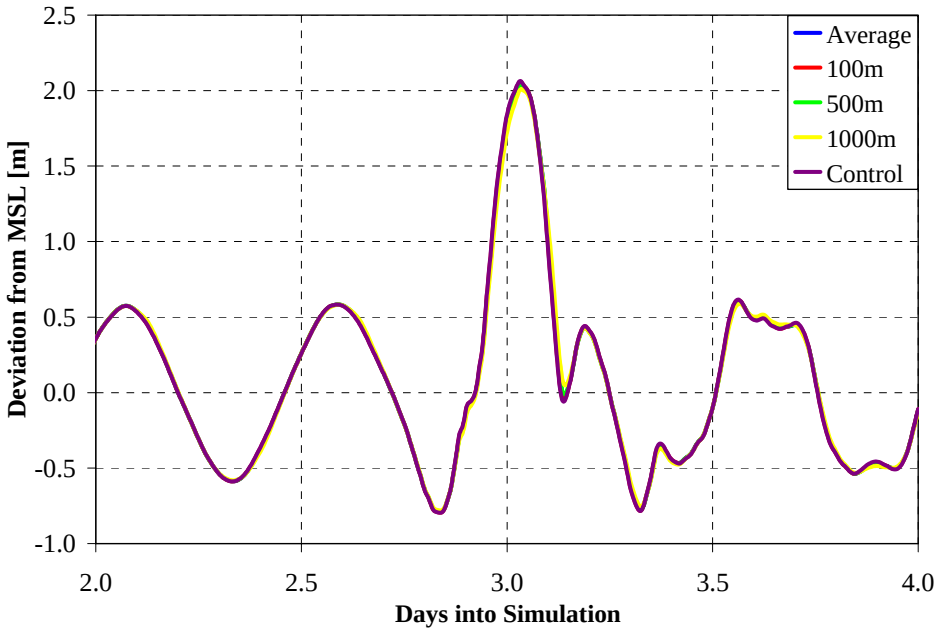

Figure P2- 30 Storm surge hydrographs at point #3 on the 1 km radius observation arc for each of the inlet-bay configurations (west/northeast Florida shelf profile).

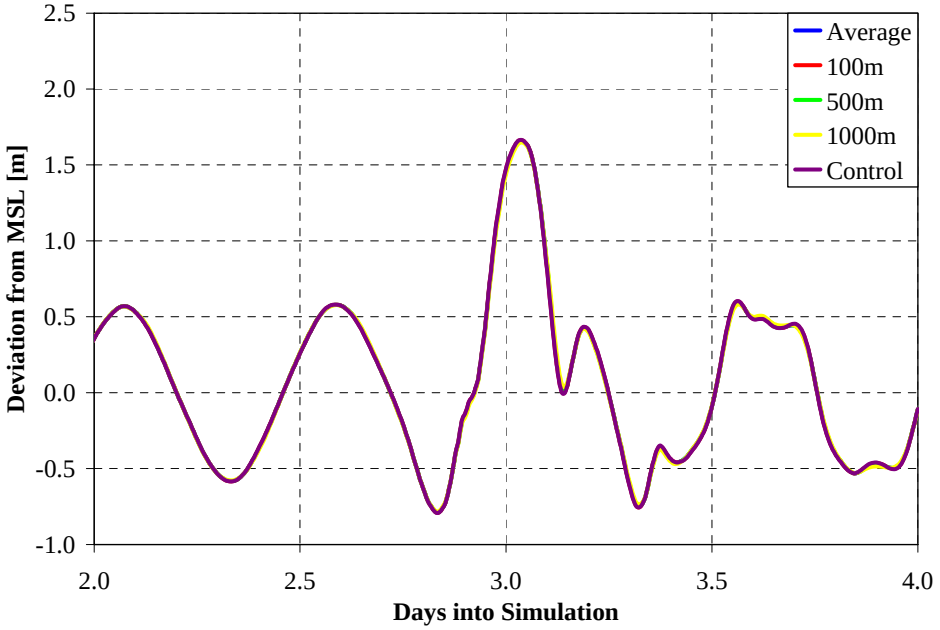

Figure P2- 31 Storm surge hydrographs at point #3 on the 5 km radius observation arc for each of the inlet-bay configurations (west/northeast Florida shelf profile).

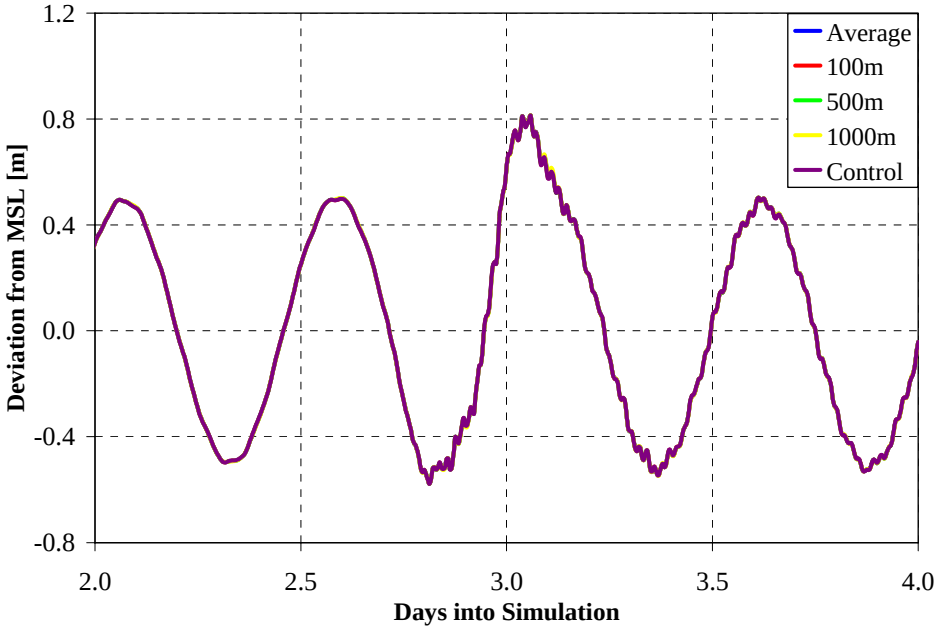

Figure P2- 32 Storm surge hydrographs at point #3 on the 1 km radius observation arc for each of the inlet-bay configurations (southeast Florida shelf profile).

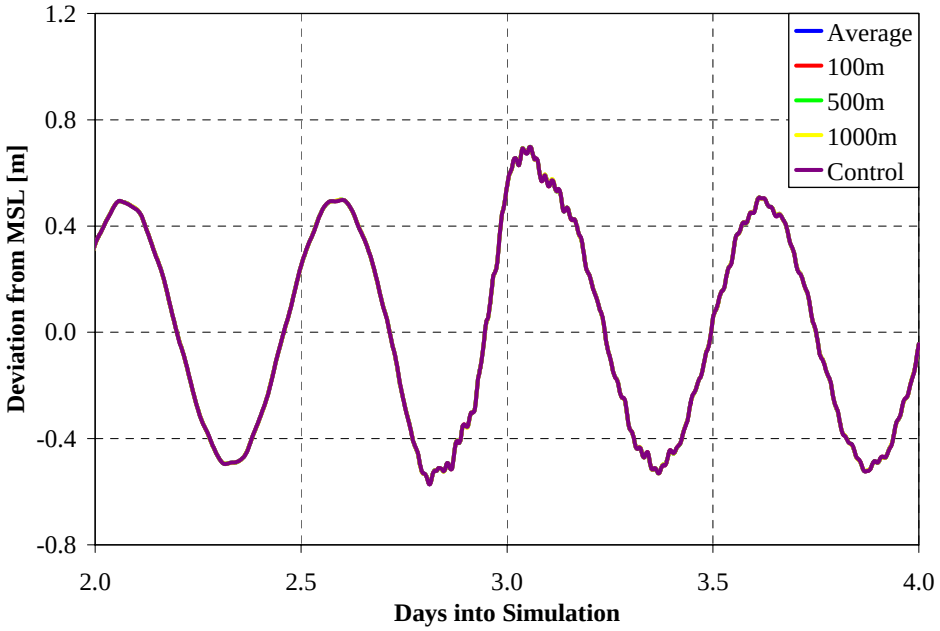

Figure P2- 33 Storm surge hydrographs at point #3 on the 5 km radius observation arc for each of the inlet-bay configurations (southeast Florida shelf profile).

It is evident from the plots that no appreciable difference exists in the storm surge hydrographs between the inlet-bay configurations. A difference of 5 cm is recognizable in Figure P2-30 (1 km radius, west/northeast Florida profile) for the 1000 meter inlet

width (yellow line), but the difference is practically negligible at the 5 km radius (Figure P2-31). Overall, the inlet-bay configurations do not appear to create a significant difference in the open coast storm surge hydrographs. Model output at all of the other observation points show similar results as Figures 30 through 33, and are presented in their entirety in Appendix A. It should be noted that this study was directed at storm surge elevations. Current velocities are very sensitive to water elevation differences and thus even though the elevation differences are small the current differences are most likely larger. However present methods for driving coastal storm surge models with open coast storm surge hydrographs do not input current velocities at the outer boundary (since this information is not available).

Results from the model domain that incorporates the southeast Florida bathymetry profile appear to contain a periodic oscillation in water surface elevations as the hurricane makes landfall, but are not noticeable prior to the surge event (i.e. before day 2.75 of the simulation). A possible reason for the oscillations is the steep bathymetry profile described in the model domain. As the surge propagates closer to the coastline, the steep bathymetry profile tries to counteract the rise in sea level by drawing down the surge. Since the two-dimensional, depth-integrated option of the ADCIRC model is chosen for this study, vertical circulation patterns within the water column are not computed. Thus, the steep bathymetry profile tries to draw down the entire water column, rather than generate vertical circulation patterns, creating the oscillations in the surge hydrographs.

Spatial variance

Previous research indicates that storm surge hydrographs vary spatially in the vicinity of a tidal inlet. Dietsche (2004) employed semi-circular arcs with radii ranging from 2.5 km to 10 km from the center of the Winyah Bay Inlet in South Carolina. Results showed that the storm surge hydrographs varied significantly both along these arcs and extending radially outward (i.e. going from the 2.5 km radius to the 10 km radius). Work is undertaken in this study to verify these results in an idealized setting.

The following figures are based on the mesh with the average inlet width for both the west/northeast Florida shelf profile and the southeast Florida shelf profile. As indicated in Section 1.1, the hydrographs produced for the various inlet-bay configurations are nearly identical. Consequently, similar results are produced with the other inlet-bay

configurations. Two different results are presented in this section: 1) hydrographs along both the 1 km radius and 5 km radius arcs for each continental shelf profile; and 2) hydrographs for point #3 (perpendicular to the coast) on each arc ranging from 1 km to 5 km in radius for both continental shelf profiles.

Figure P2-34 shows recorded sea stages along the 1 km radius observation arc for the Average-WNEFL mesh. The highest peak (recorded at point #5) is 2.16 meters above MSL, whereas the lowest (recorded at point #3) is 2.04 meters above MSL, a difference of 0.12 meters. The peaks reveal that the points (#4 and #5) closest to the eye of the storm produce the greatest surge. Overall, the behavior of the storm surge hydrographs shows that a spatial variance exists along this observation arc during the surge event. However, the hydrographs also show that the astronomic tide signals are identical prior to hurricane landfall (i.e. before day 2.75 of the simulation), thus indicating that the spatial variance is limited to the surge event.

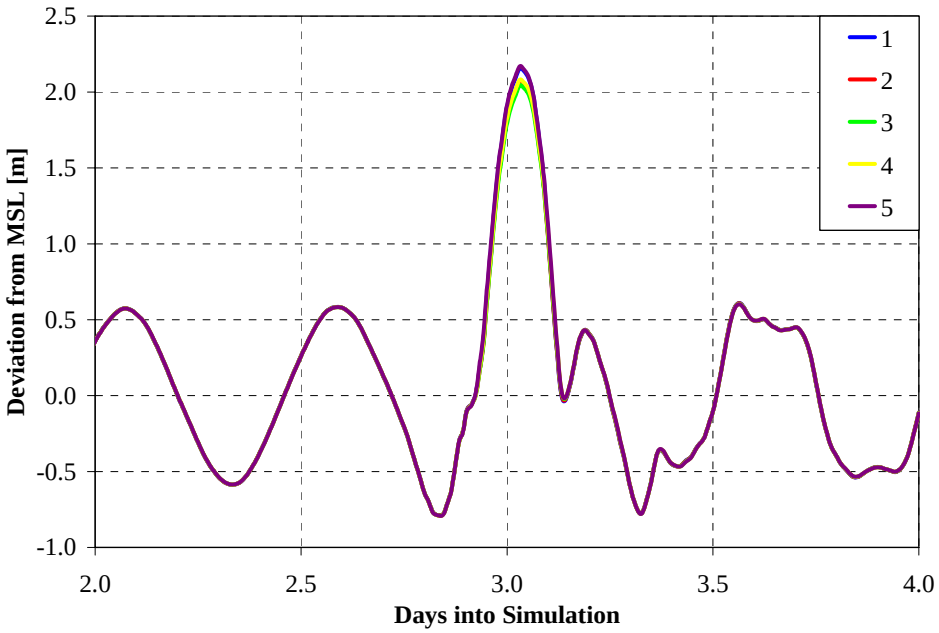

Figure P2- 34 Storm surge hydrographs along the 1 km radius observation arc for the Average-WNEFL mesh.

Similarly, Figure P2-35 presents computed water elevations along the 5 km radius observation arc for the Average-WNEFL mesh. The highest peak (recorded at point #5) is 2.18 meters above MSL, whereas the lowest (recorded at point #3) is 1.66 meters above MSL, a difference of 0.52 meters. This difference is comparable to what Dietsche

(2004) found for the Winyah Bay in South Carolina. Compared to the 1 km radius, the difference between the highest and the lowest peak values is much greater for the 5 km radius (0.52 meters for the 5 km radius compared to 0.12 meters for the 1 km radius). It is also noted that the peak values are less along the 5 km radius than along the 1 km radius, indicating that storm surge is greater nearer to the coastline. Furthermore, the astronomic tide signals at each location are identical prior to hurricane landfall.

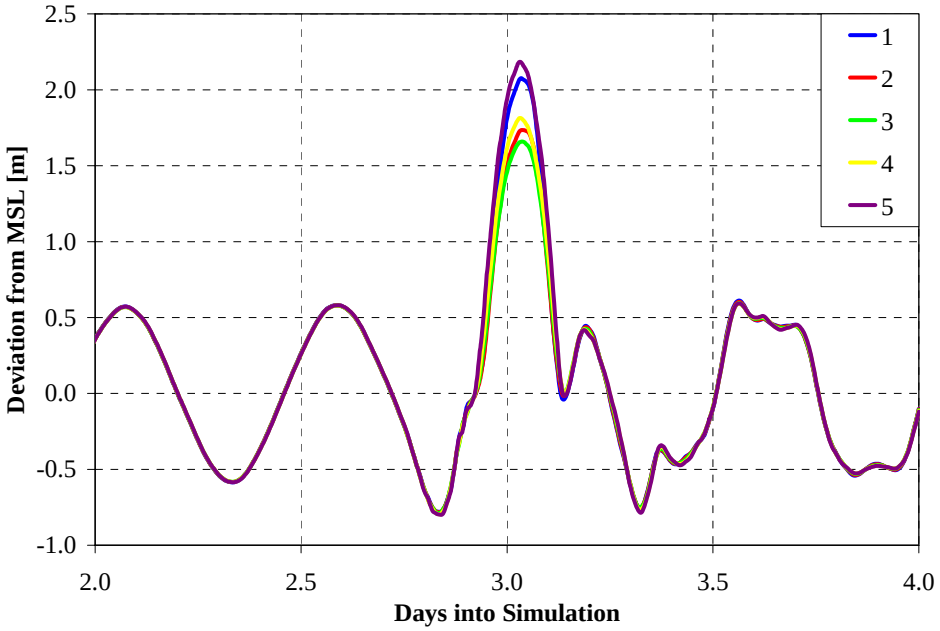

Figure P2- 35 Storm surge hydrographs along the 5 km radius observation arc for the Average-WNEFL mesh.

Figures 36 and 37 display computed storm surge elevations for the southeast Florida shelf profile for the 1 km radius and the 5 km radius, respectively. A trend similar to the west/northeast profile is observed for both radii. For the 1 km radius, the highest peak (recorded at point #5) is 0.90 meters above MSL, whereas the lowest (recorded at point #3) is 0.81 meters above MSL, a difference of 0.09 meters. Furthermore, the highest peak for the 5 km radius is 0.92 meters (recorded at point #5), whereas the lowest is 0.62 meters at point #2, a difference of 0.30 meters.

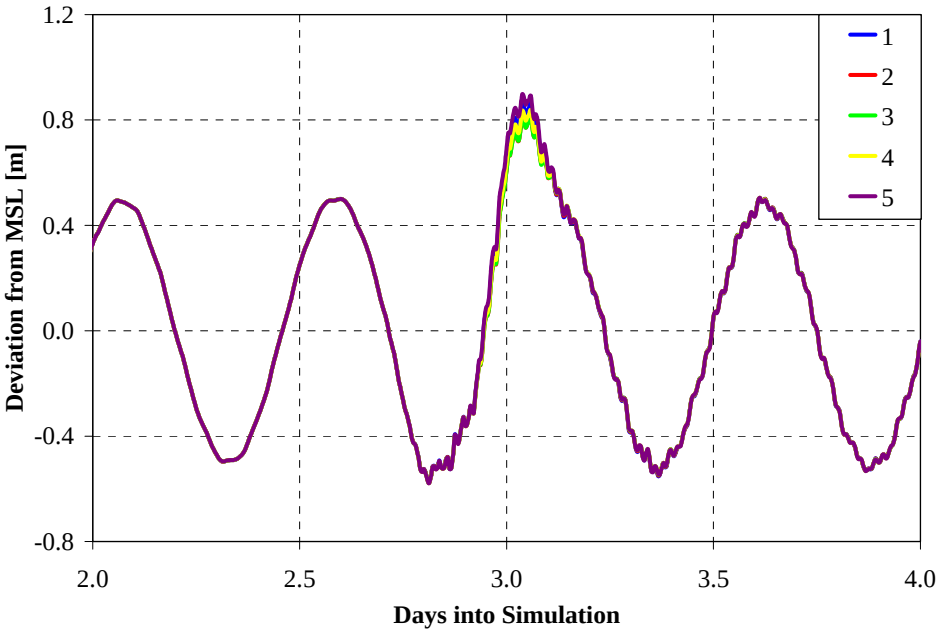

Figure P2- 36 Storm surge hydrographs along the 1 km radius observation arc for the Average-SEFL mesh.

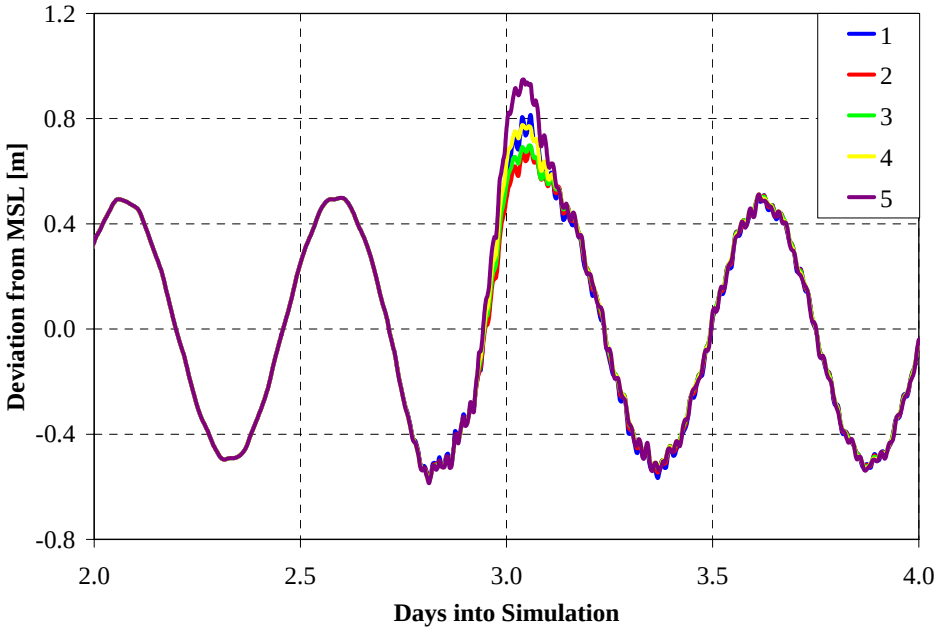

Figure P2- 37 Storm surge hydrographs along the 5 km radius observation arc for the Average-SEFL mesh.

Results presented thus far potentially have huge implications for local bridge scour modeling. Previous research (Edge et al., 1999 and Zevenbergen et al., 1999) has applied a single design hydrograph at the open coast boundary (distance of the ocean boundaries

from the inlet was not specified in each study, but they appeared to be within a few kilometers of the coast) for bridge scour studies. Results presented herein show that the hydrographs vary spatially over this open coast boundary, thus indicating that individual hydrographs should be applied at each open boundary node.

Furthermore, results presented in Section 1.1 show that the open coast boundary should be placed far enough from the inlet to remove the influence of the inlet from the open coast storm surge hydrographs. By doing so, the spatial variance along the open coast boundary becomes greater, which may lead to significantly different scour predictions when applying individual hydrographs compared to applying a single design hydrograph at each open boundary node. In addition, if a coastal modeler were to place the open coast boundary of a bridge scour model nearer to the inlet (e.g. 1 km), then momentum flux problems will most likely influence the model solution. Typically, the open ocean boundary is placed far enough away from the area of interest to remove any negative effects that may arise close to the boundary. Taking this into account, the open coast boundary should be placed farther from the inlet, creating a greater level of spatial variance amongst the storm surge hydrographs along the boundary.

Spatial variance is also recognized at the same point on different observation arcs. Results show that the peak storm surge increases as the surge wave propagates into shallower waters. Figures 38 and 39 display recorded water elevations at point #3 (perpendicular to the coast) on observation arcs ranging from 1 km to 5 km in radius for both the Average-WNEFL mesh and the Average-SEFL mesh, respectively. The peak water elevation for the Average-WNEFL mesh is about 2.05 meters at the 1 km radius arc, and the lowest peak elevation is 1.66 meters at the 5 km radius arc. Similarly, the peak water elevation for the Average-SEFL mesh is 0.76 meters at the 1 km radius arc, whereas the lowest peak elevation is 0.66 meters along the 5 km radius. In both cases, it is evident that the peak water elevation increases closer to the coastline.

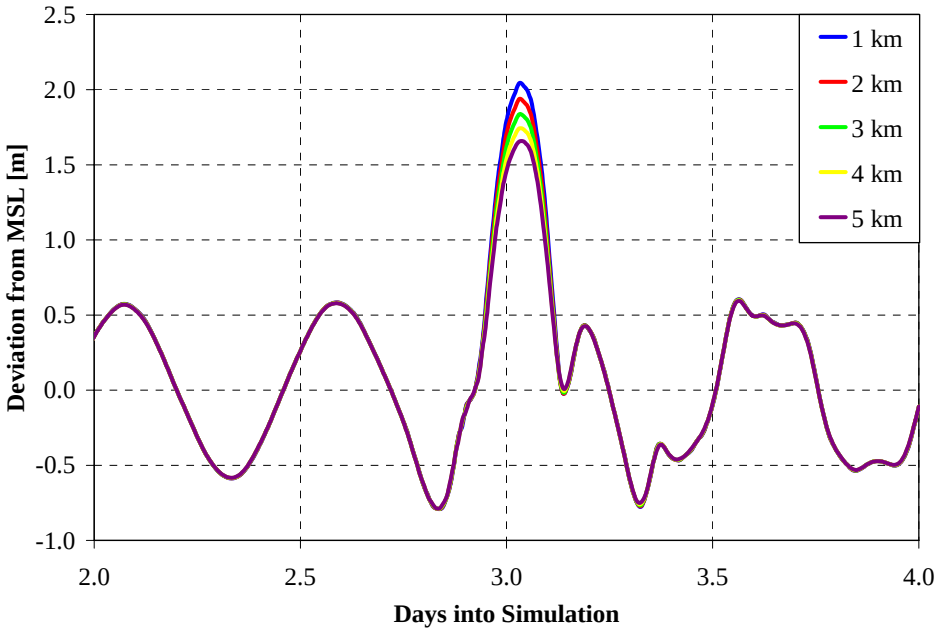

Figure P2- 38 Storm surge hydrographs at point #3 on radii extending from 1 km to 5 km for the Average-WNEFL mesh.

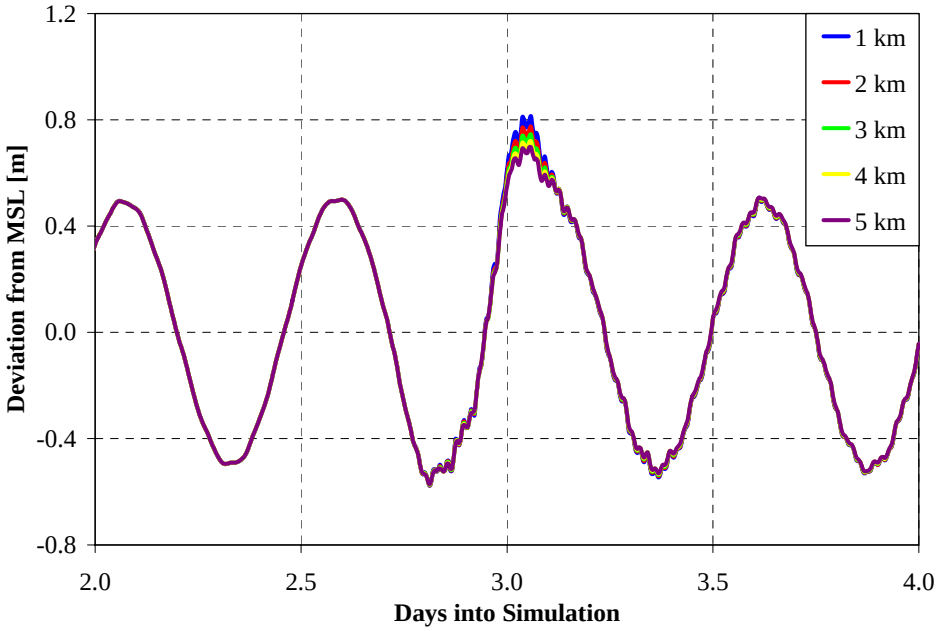

Figure P2- 39 Storm surge hydrographs at point #3 on radii extending from 1 km to 5 km for the Average-SEFL mesh.

It is evident from the results presented herein that the open coast storm surge hydrographs can vary greatly depending on location. The peak water elevations can vary by as much as 0.5 meters or more, which indicates that placement of the open coast boundary

location is critical. How much of a difference these variations would make in bridge scour predictions is uncertain, but intuitively it appears that the results could have a significant impact on scour studies.

Comparison of bathymetry profiles

Previous research (Weaver and Slinn, 2004) has shown that a shallow, wide shelf profile produces greater surge levels along the coast than a steep, narrow shelf profile. Results presented herein verify this conclusion for the two bathymetry profiles used in the numerical parameter study. Figure P2-40 shows a comparison between model results for both the west/northeast Florida shelf profile (blue line) and the southeast Florida shelf profile (red line) at point #3 along the 1 km radius boundary locations. In this case, the west/northeast Florida shelf profile produced a significantly greater (over 1 meter) surge level than the southeast Florida shelf profile. Similar results are obtained at the other output locations.

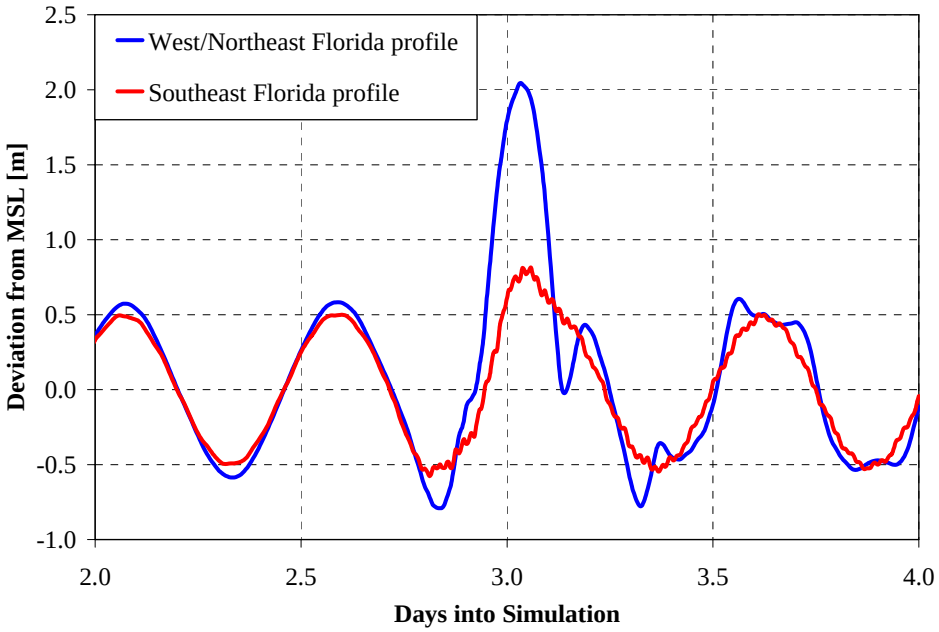

Figure P2- 40 Comparison between shelf profiles at point #3 along the 1 km radius arc.

Large tidal inlet

A limitation with results presented thus far is the maximum inlet width included in the study (1000 meter width). The results presented indicate that the tidal inlets used in this study do not have a significant impact on the open coast storm surge hydrographs. In lieu

of this, a very large inlet-bay configuration (5000 meter inlet width) is developed to determine if an inlet can, indeed, have a significant effect on the open coast hydrographs. This inlet width is consistent with the largest Florida tidal inlet (San Carlos), but is not typical of all other Florida tidal inlets. The mean (388 meters) and standard deviation (337 meters) from the statistical analysis show that an inlet width of 5000 meters is well outside of three standard deviations away from the mean value (a typical cutoff point for detection of outliers). Thus, an inlet of this size represents an extreme case and is not typical of most Florida tidal inlets.

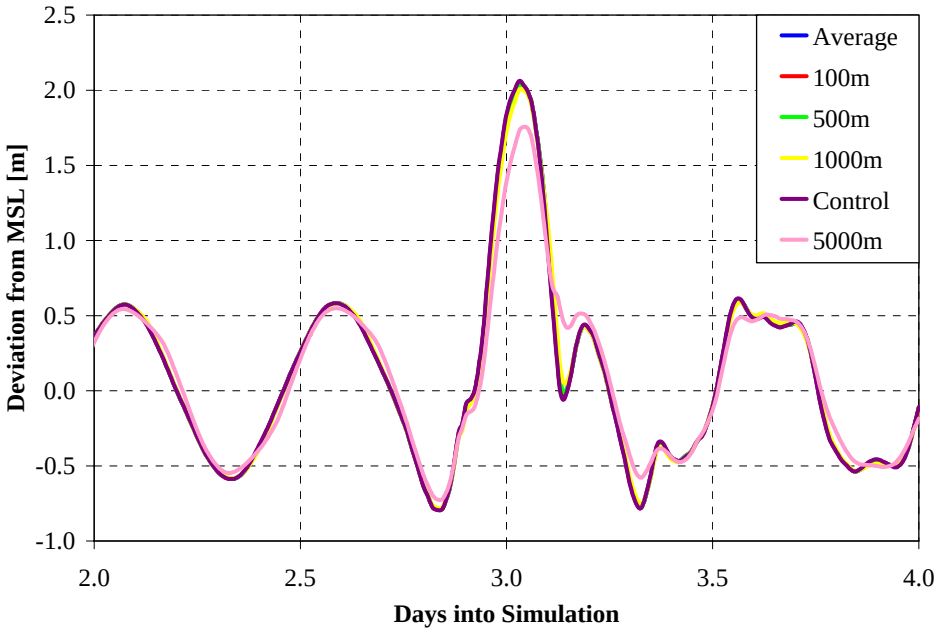

Figure P2- 41 Comparison of the large inlet results to the results for the inlet-bay configurations used in this study at point #3 on the 1 km radius arc.

The same model parameters and observation points are included in the simulation. Figure P2-41 shows a comparison of the 5000 meter inlet model results to the model results for the other inlet-bay configurations at point #3 (perpendicular to the coast) on the 1 km radius observation arc. The results clearly indicate that the 5000 meter inlet width has an effect on the open coast storm surge hydrographs. The peak surge level for the large inlet is less than the other inlet-bay configurations (a difference of 30 cm between the 5000 meter inlet width and the control mesh), and the recession behavior is different due to a greater volume of water receding from the bay. Thus, an inlet of this size would need to be included in the model domain.

Inlet comparisons within the inlet and bay

This section examines the influence of inlet width on surge levels within the inlet and bay. Two comparisons are made to elucidate this behavior. First, model results for each of the inlet-bay configurations are compared at a point in the middle of the inlet (point #1 in Figure P2-42). Next, the inlet-bay configurations are compared at a location that is 1 km into the bay (point #2 in Figure P2-42). For both comparisons, the west/northeast Florida shelf profile is used since it produces a greater level of surge along the coast.

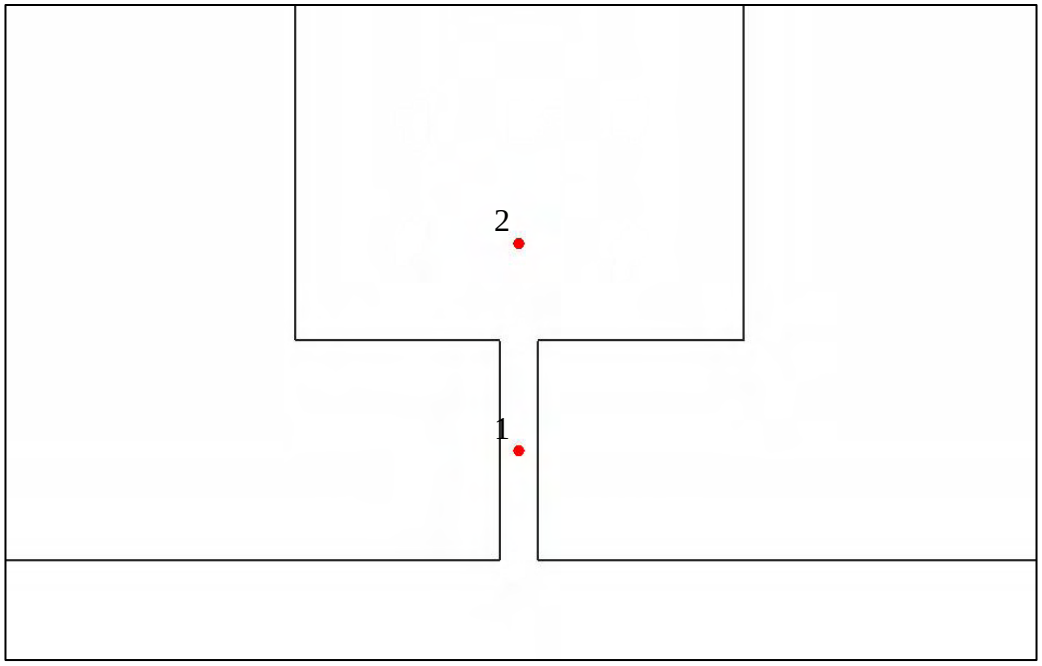

Figure P2- 42 Model output locations used to study the influence of inlet width on the surge levels within the inlet-bay system.

Comparing model output for each of the inlet-bay configurations (Figure P2-43) at point #1 indicates that the smallest inlet width (100 meters) produces a greater peak surge level (2.10 meters) than the other inlet widths (1.97 meters for the average inlet width; 1.93 meters for the 500 meter inlet width; and 1.79 meters for the 1000 meter inlet width). At first glance, it appears that the 100 meter width allows more storm surge to enter the inlet; however, examination of the velocities through each inlet indicates that the opposite effect is true. The velocity in the inlet for each of the inlet-bay configurations is approximately 3.10 m/s during the peak surge event. Taking into account the difference in cross-sectional areas between the inlet configurations, it is evident that a greater

amount of flow enters the bay for the large inlet width than the small inlet width. Thus, a slightly higher water elevation is recognized in the inlet for the 100 meter width, but considerably more water is flowing through the inlet for the 1000 meter width.

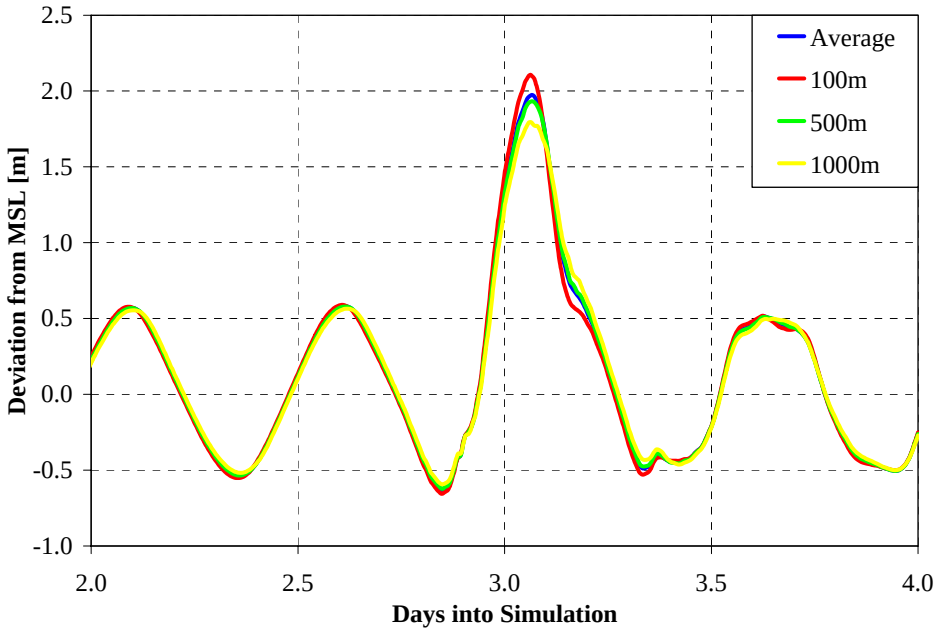

Figure P2- 43 Comparison of model output in the middle of the inlet (see Figure P2-42, point #1) for each of the inlet-bay configurations.

Next, all four inlet-bay configurations are compared at a point 1 km into the bay (Figure P2-44). Similar to the previous analysis, the 100 meter inlet width produces a higher peak surge elevation than the other inlet widths. Furthermore, the plots reveal that a slight phasing difference is recognized relative to the peak values (30 minutes between the peak values for the 100 meter width and the 1000 meter width). This difference can be attributed to the increase in bay surface area, creating a delay in the peak surge for the 1000 meter width compared to the 100 meter width.

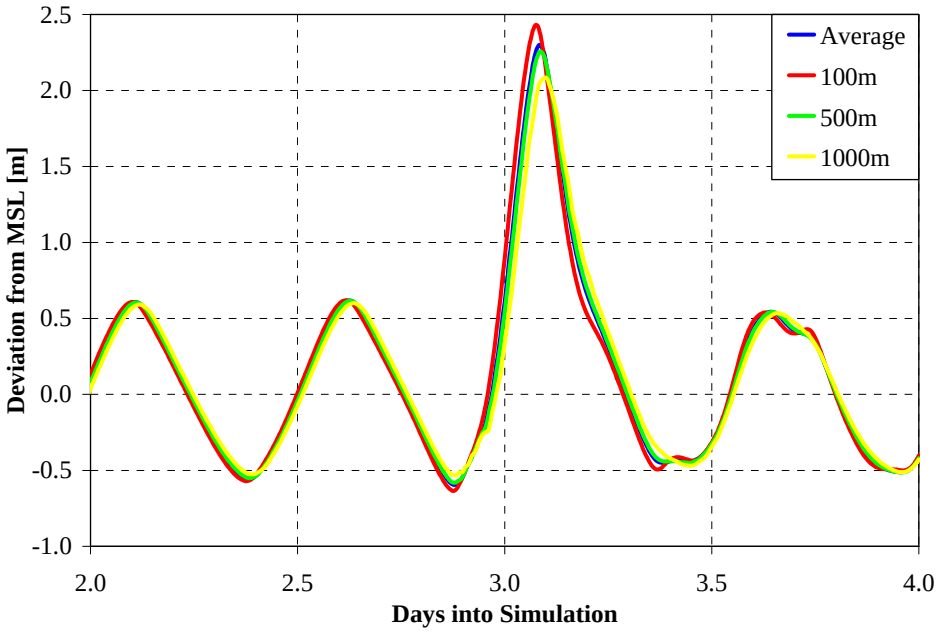

Figure P2- 44 Comparison of model output at a location 1 km into the bay (see Figure P2-42, point #2) for each of the inlet-bay configurations.

Escambia Bay Domain Results

A hindcast study is undertaken to determine if conclusions from the numerical parameter study can be extrapolated to a real-life scenario. In contrast to the numerical parameter study, historical water elevation data is available to compare model results as a means of verification. First, an astronomic tide verification and a storm surge hindcast of Hurricane Ivan are performed to validate the model domains in the coastal region of the Pensacola Inlet and Escambia Bay. Next, the effect of the Pensacola Inlet-Escambia Bay system on the open coast storm surge hydrographs and the spatial variance of the storm surge hydrographs along the open coast are evaluated. The width (980 meters) of Pensacola Inlet and the size (6.8×10^8 m^2) of the adjoining bay indicate that the domain is similar to the inlet-bay configuration with the 1000 meter inlet width used in the numerical parameter study.

Astronomic tide verification

First, the model domain is verified through an astronomic tide comparison. A National Ocean Service tide gauge located within Pensacola Bay provides historical tidal constituent data (Figure P2-45). A 14-day resynthesis of model results is compared to a

resynthesis of historical constituents at the NOS tide gauge in Pensacola Bay. The 14-day resynthesis period is chosen to allow for a complete spring-neap tide cycle.

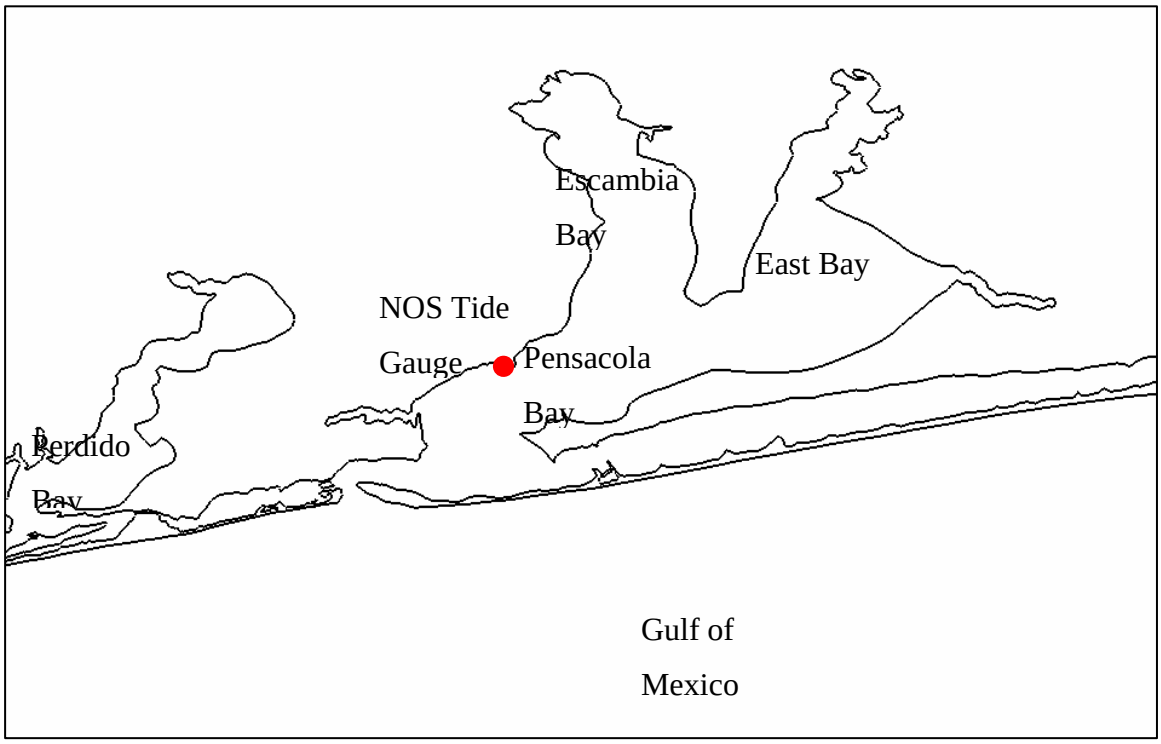

Figure P2- 45 NOS tide gauge used to compare model results with historical data in Pensacola Bay.

The results (Figure P2-46) indicate that the model domain performs reasonably well at this location. A slight discrepancy is recognized in phasing between days 8 and 14, as well as the troughs through most of the resynthesis. Overall, however, the model domain faithfully simulates the tidal dynamics within the Pensacola Inlet-Escambia Bay system.

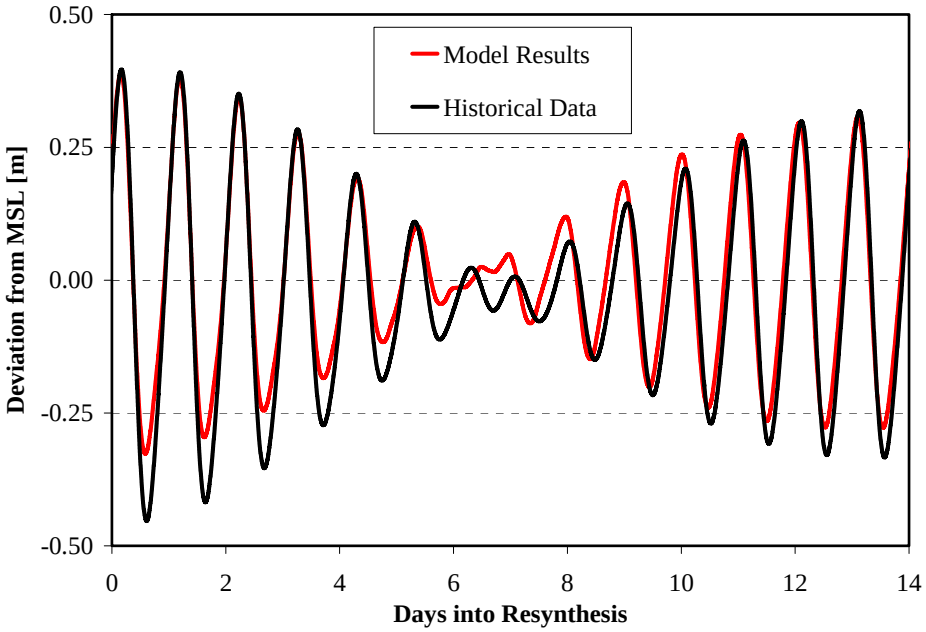

Figure P2- 46 Astronomic tide comparison at the NOS station in Pensacola Bay.

In addition, the astronomic tide variance is examined along the open coast observation arcs extending seaward from the mouth of Pensacola Inlet. Similar to the tide verification at the NOS station in Pensacola Bay, a 14-day resynthesis is performed at each of the model output locations along the observation arcs. Figure P2-47 shows a resynthesis of the astronomic tide signal at each of the output locations along the 5 km radius observation arc. The results indicate that the tide signal is nearly identical at each of these locations. Similar results are obtained along the other semi-circular observation arcs, indicating that the astronomic tides do not display a spatial variance near the inlet. As a result, the spatial variance recognized amongst the storm surge hydrographs in the following sections is a result of the storm surge phenomenon rather than the astronomic tides.

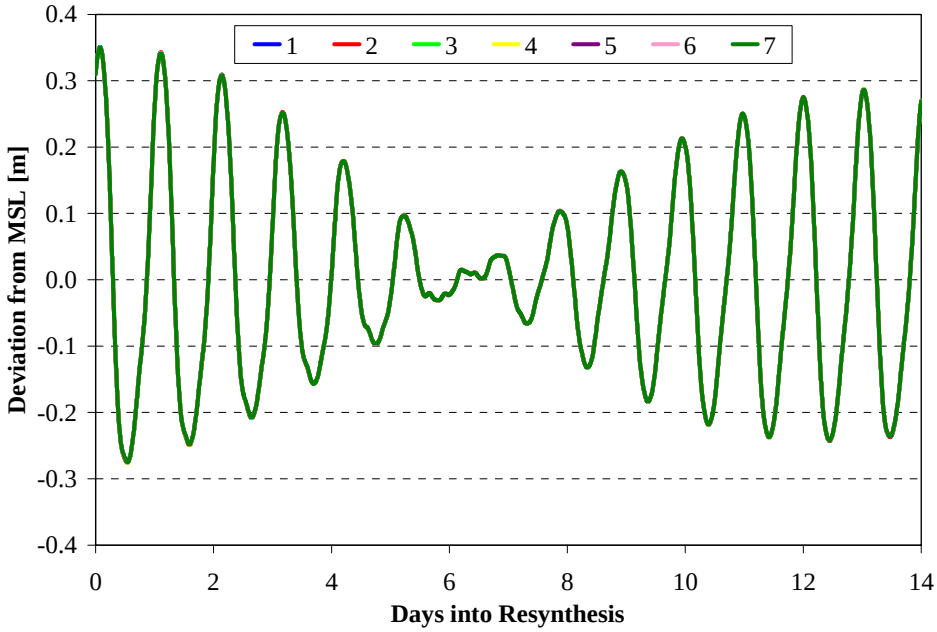

Figure P2- 47 Astronomic tide comparison along the 5 km radius observation arc extending seaward from the mouth of Pensacola Inlet.

Hurricane Ivan hindcast

This section presents a storm surge hindcast from Hurricane Ivan in the vicinity of Escambia Bay. Two different results are presented herein: 1) a comparison of model output at the NOS station in Pensacola Bay; and 2) a comparison of model output to high water marks in the vicinity of the Interstate-10 Bridge in Escambia Bay.

The model domain is used to simulate storm surge within Escambia Bay for September 7, 2004 at 6 p.m. through September 17, 2004 at 6 p.m. A zero elevation boundary condition is applied along the ocean boundary, the wind and pressure field is read into the simulation every 30 minutes, and water elevations are output every six minutes at the NOS station within Pensacola Bay. Figure P2-48 displays storm surge elevations at the NOS station for the model results (red line) and the historical water elevations (black line).

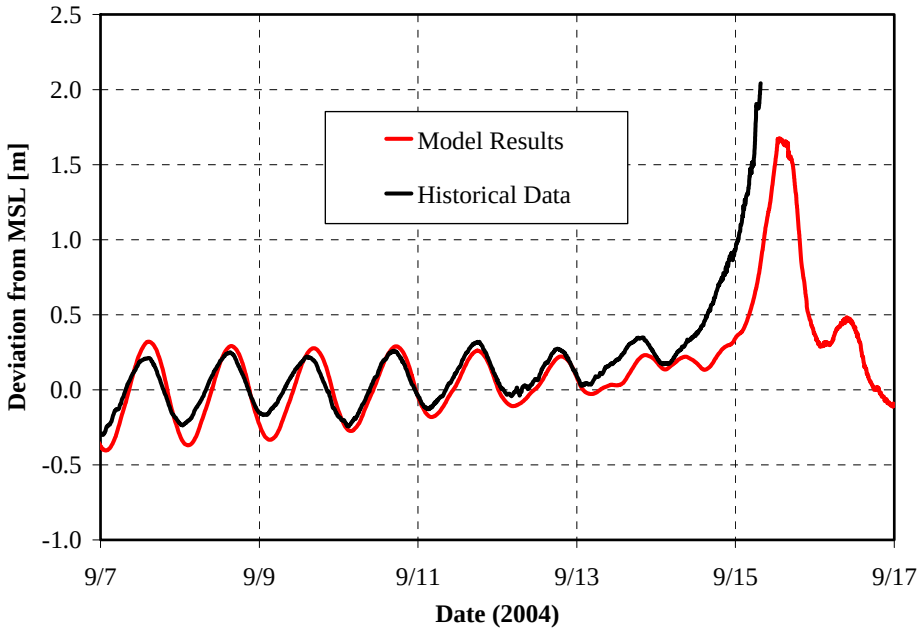

Figure P2- 48 Hurricane Ivan water elevations at the NOS station in Pensacola Bay.

Several noticeable results are obtained from this figure. First, the NOS tide gauge appears to have stopped recording close to the time of hurricane landfall. As a result, the peak surge level and the set-down behavior at this location are not shown in the historical data, making a comparison throughout the entire hurricane event impossible. In lieu of this, it is evident that the model under predicts the peak storm surge level. However, high water marks in Escambia Bay suggest a peak water level of 3-4.5 meters near the Interstate 10 Bridge in Escambia Bay (Douglass et al., 2004). A plot of the maximum surge contours within the bay (Figure P2-49) indicates that model results produce peak surge levels that are slightly less (2.5-3 meters) than the high water marks near the bridge.

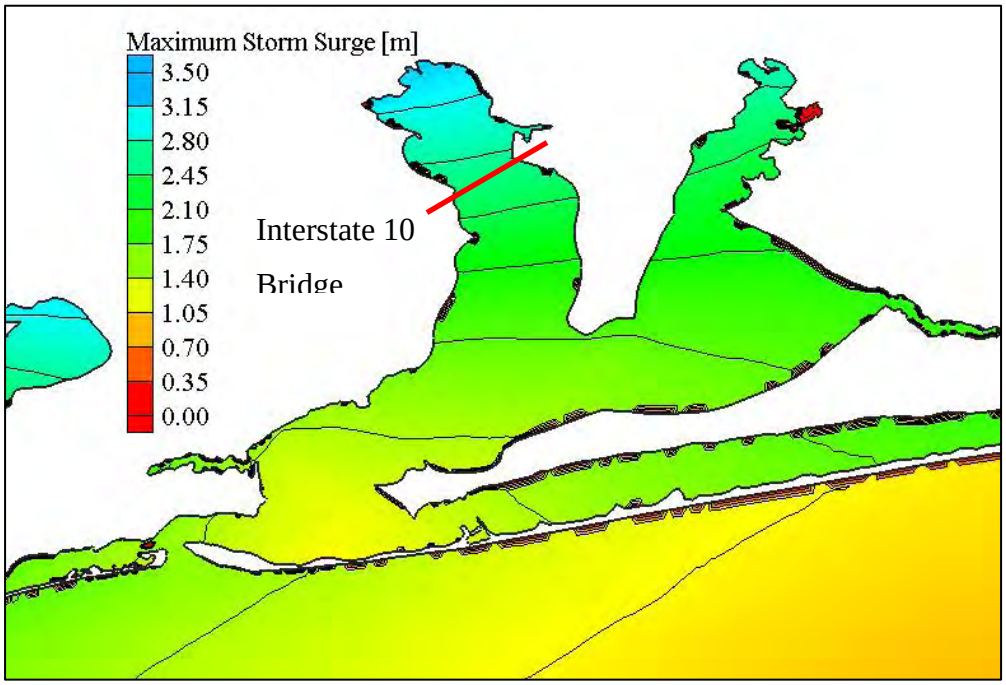

Figure P2- 49 Maximum storm surge contours within Pensacola Bay and Escambia Bay.

Second, the lack of short-wave processes (wind-waves) in the modeling approach is evident. Typically, wind-induced waves travel ahead of the storm surge, creating water elevations to rise before the hurricane makes landfall. In this case, the difference between the historical data and the ocean-based domain results prior to landfall (between 9/13 and 9/15) can be attributed to the lack of wind-waves included in the modeling process. Assuming accurate wind fields, the lack of including short-wave processes is likely the reason the model under predicts the peak storm surge.

Effect of inundation areas

The influence of inundation areas on the storm surge predictions within the bay and along the open coast is examined in this section. The same wind field and pressure profile is applied to the system, and results are compared at the NOS tide gauge located in Pensacola Bay.

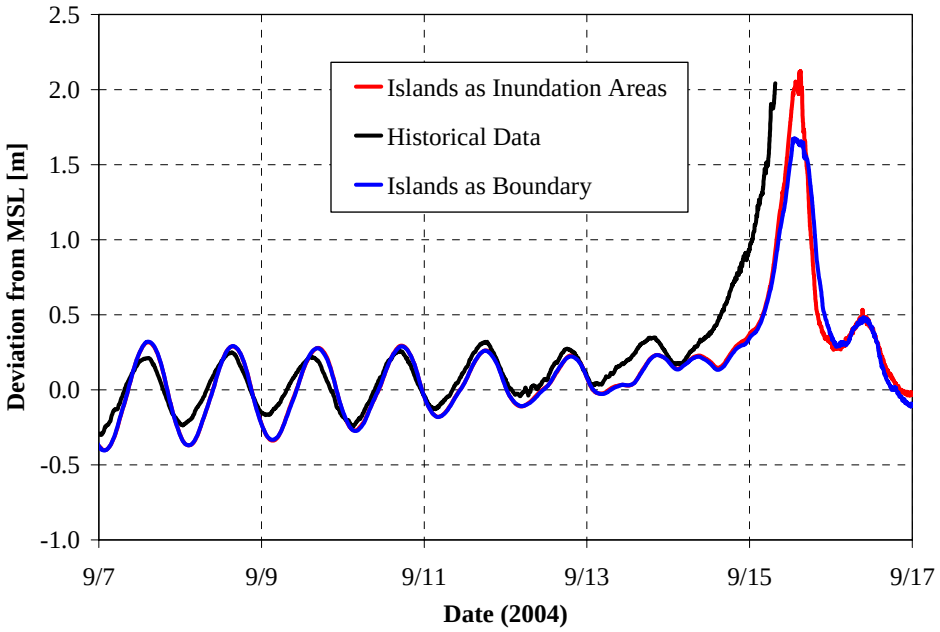

Figure P2- 50 Storm surge hydrographs for the ocean-based domain: treating barrier islands as inundation areas (red line) and treating barrier islands as model boundaries (blue line).

Figure P2-50 shows a comparison between treating the barrier islands as model boundaries (blue line) versus treating the barrier islands as inundation areas (red line). The results clearly indicate that allowing the storm surge to flood over the barrier islands creates greater water elevations within the bay. In this case, the highest surge value for treating the barrier islands as inundation areas is 2.12 meters, whereas the highest surge value for treating the barrier islands as model boundaries is 1.66 meters, a difference of 0.46 meters. The rising limbs and recession limbs are similar to one another, but both hydrographs clearly lack important short-wave action prior to landfall. Furthermore, the tide gauge stopped recording close to hurricane landfall, making an accurate assessment of peak historic water elevations impossible. However, it is evident that including barrier islands as inundation areas produces a peak surge level that is more consistent with historical data.

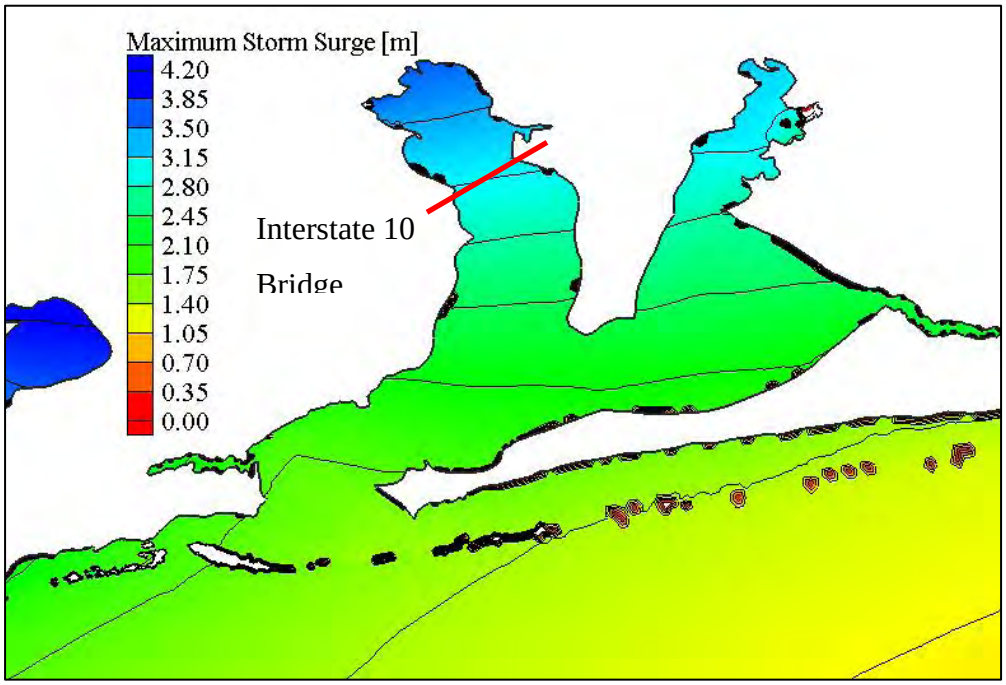

Figure P2- 51 Maximum storm surge contours within Pensacola Bay and Escambia Bay with the barrier islands included as inundation areas.

Comparing the maximum storm surge contours within Escambia Bay to high water marks (3-4.5 meters) recorded near the Interstate 10 Bridge indicates that including the barrier islands as inundation areas creates maximum surge levels that are more consistent with historical records (Figure P2-51). The results shown in this figure (3-4 meters near the bridge) compare more favorably with the high water marks than the results shown in Figure P2-49 (barrier islands are treated as model boundaries). Thus, including the barrier islands as inundation areas creates more realistic surge levels within the bay than treating them as model boundaries.

The primary focus of this study is the surge levels along the open coast. In lieu of this, the effect of treating the barrier islands as inundation areas is examined along the open coast observation arcs extending seaward from the mouth of the inlet (Figure P2-52).

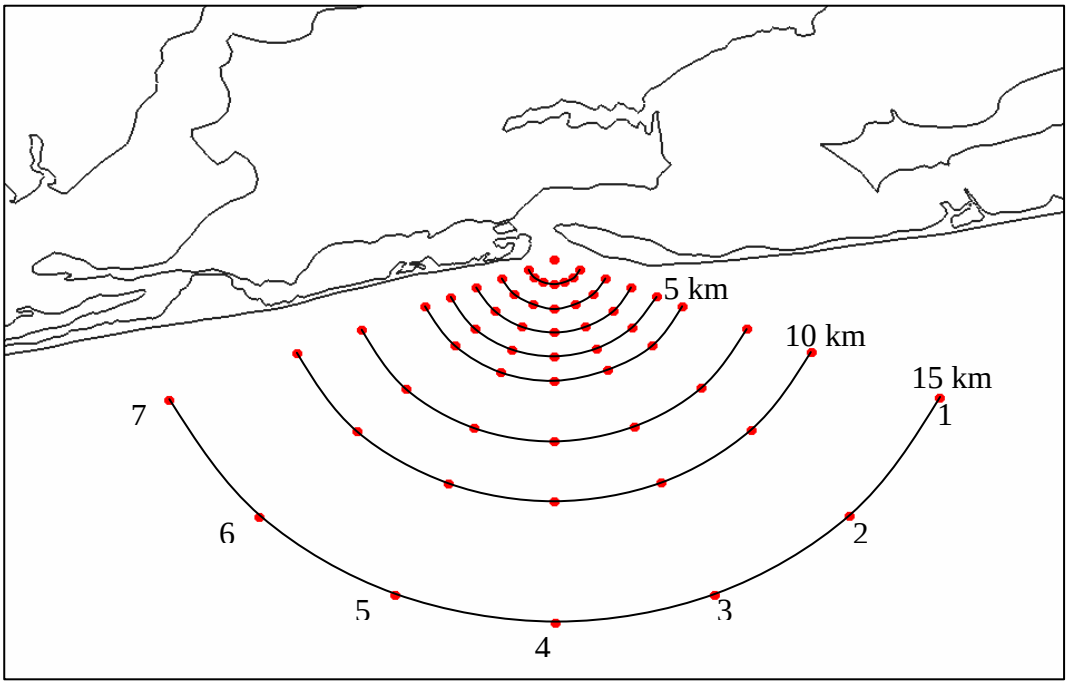

Figure P2- 52 Open coast observation arcs for the Escambia Bay domain.

Model results are compared at point #4 (due south) along the 1 km radius observation arc (Figure P2-53; only September 14, 2004 through September 17, 2004 is shown to provide a clearer view of the peak surge). The hydrographs show a minimal difference in the water surface elevations at this location. The peak elevation for the domain that treats the barrier islands as model boundaries is 1.86 meters; whereas the peak surge for the domain that treats the barrier islands as inundation areas is 1.89 meters (a difference of only 3 cm). Furthermore, the rising limb and recession limb behavior of the two hydrographs is nearly identical. Figures 54- 56 show similar results at point #4 on the 5 km radius, 10 km radius, and 15 km radius observation arcs, respectively. Therefore, it is concluded that the inundation areas do not significantly alter the open coast storm surge hydrographs.

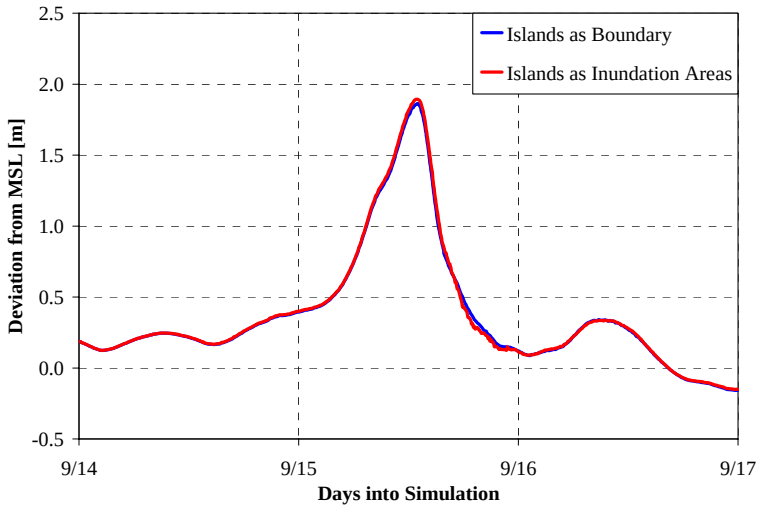

Figure P2- 53 Comparison between treating barrier islands as inundation areas versus model boundaries at point #4 along the 1 km radius observation arc.

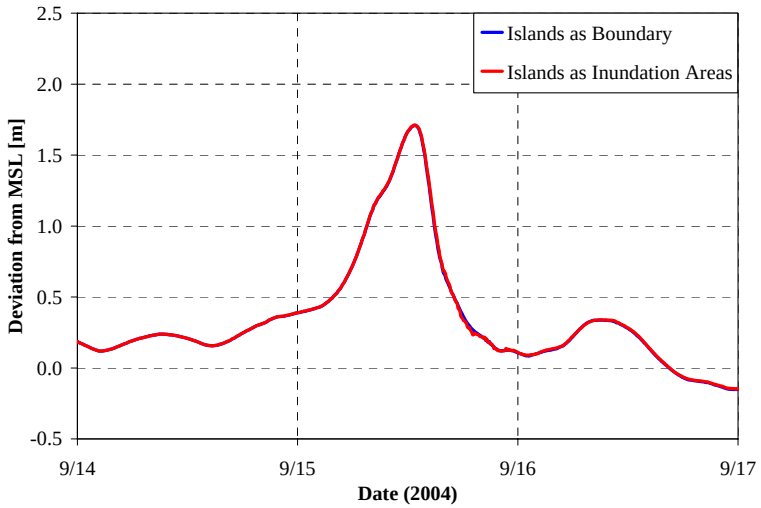

Figure P2- 54 Comparison between treating barrier islands as inundation areas versus model boundaries at point #4 along the 5 km radius observation arc.

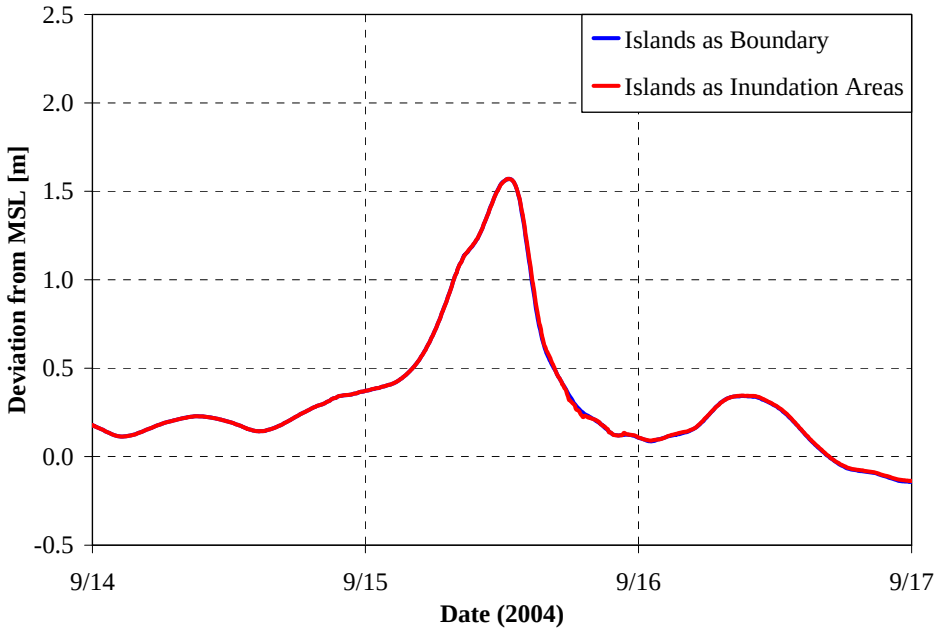

Figure P2- 55 Comparison between treating barrier islands as inundation areas versus model boundaries at point #4 along the 10 km radius observation arc.

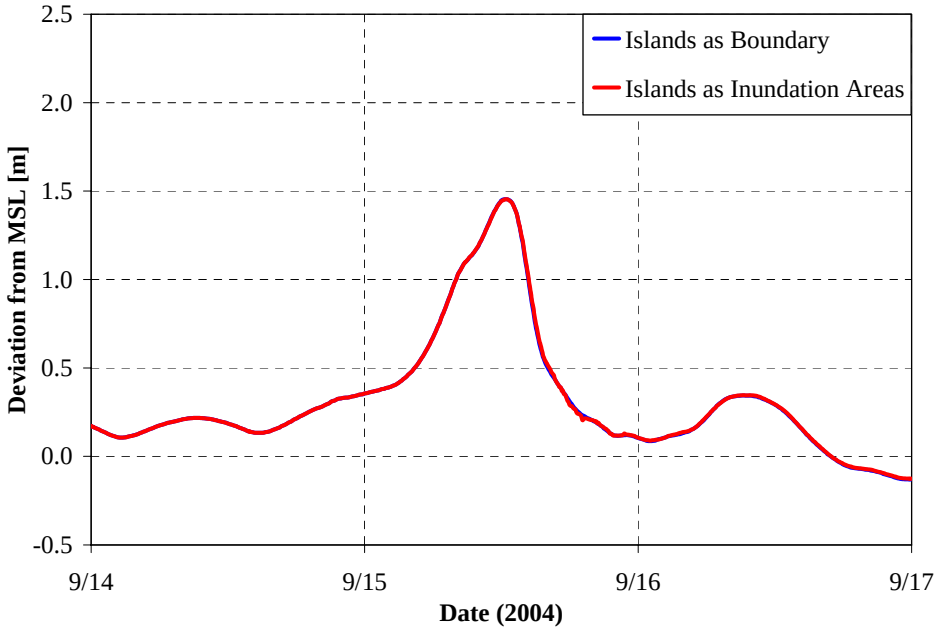

Figure P2- 56 Comparison between treating barrier islands as inundation areas versus model boundaries at point #4 along the 15 km radius observation arc.

Effect of Pensacola Inlet on open coast storm surge hydrographs

The main conclusion from the numerical parameter study is that the effect of tidal inlets on open coast storm surge hydrographs is negligible. The implication of this conclusion is that a large-scale ocean circulation model does not need to include an inlet-bay system in the computational domain when generating open coast boundary conditions for a local bridge scour model. This section verifies this conclusion for the case of Pensacola Inlet during Hurricane Ivan.

Two computational domains are used in this analysis: 1) a finite element mesh of the Western North Atlantic Tidal model domain that *does not* include the Pensacola Inlet-Escambia Bay system; and 2) a finite element mesh of the same region that *does* include the Pensacola Inlet-Escambia Bay system. The domain that does not include the Pensacola Inlet-Escambia Bay system has been optimized in previous research for storm surge applications (Hagen et al., 2005 and Kojima, 2005), and is representative of a model domain that would be used to generate open coast boundary conditions for a local bridge scour model if the inlet-bay system is not included in the domain. In contrast, the domain that does include the Pensacola Inlet-Escambia Bay system is typical of a model domain that would be used to generate the open coast boundary conditions if the inlet-bay system is included in the domain. Model output is generated along the semi-circular observation arcs extending seaward from the mouth of the inlet.

Figure P2-57 shows sea stages at point #4 (due south) on the 5 km radius observation arc. Model results for the domain that do not include the Pensacola Inlet (blue line) indicate a peak surge level of 1.79 meters; whereas model results for the domain that do include the Pensacola Inlet (red line) indicate a peak surge of 1.71 meters (a difference of 8 cm). Similar results are obtained at the other open coast observation locations.

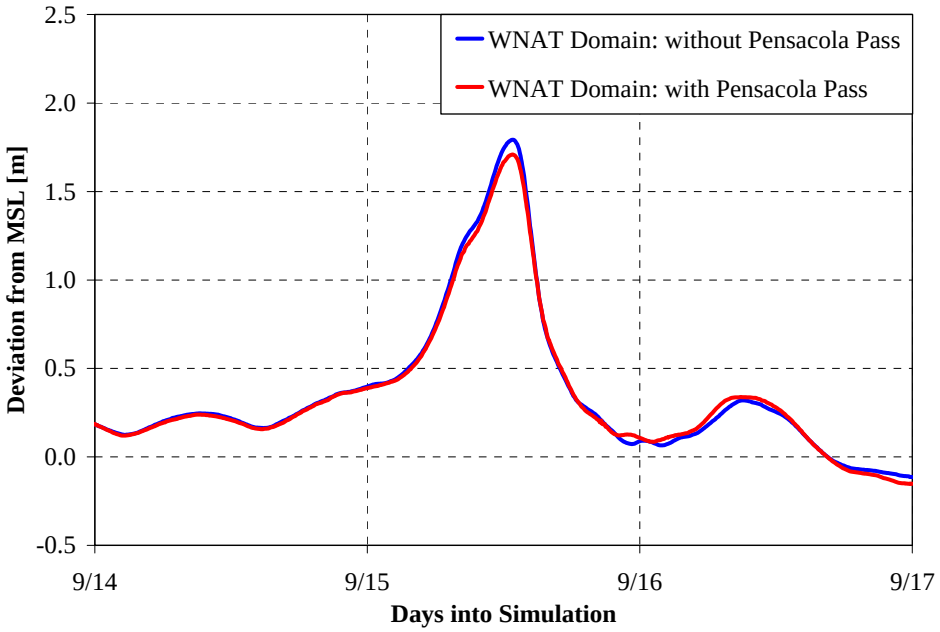

Figure P2- 57 Storm surge hydrographs at point #4 along the 5 km radius observation arc for the model domain that does not include the Pensacola Inlet (blue line) and the model domain that does include the Pensacola Inlet (red line).

At this point, it is impossible to state that this difference would or would not have an appreciable effect on the performance of a bridge scour model. However, clearly it is unlikely that a difference of 8 cm (4.5% relative to the peak value) would significantly alter the model's performance, especially since the rising and falling limbs of the hydrographs are nearly identical. These results are consistent with the conclusions from the numerical parameter study, i.e. tidal inlets do not appear to have a significant influence on the open coast storm surge hydrographs.

Spatial variance along the open coast boundary locations

This section verifies the spatial variance results shown in the numerical parameter study with a real-life scenario (e.g. Pensacola Inlet). The 1 km radius and 5 km radius observation arcs are used to verify these findings. Figure P2-58 displays the storm surge hydrographs along the 1 km radius extending seaward from the mouth of Pensacola Inlet.

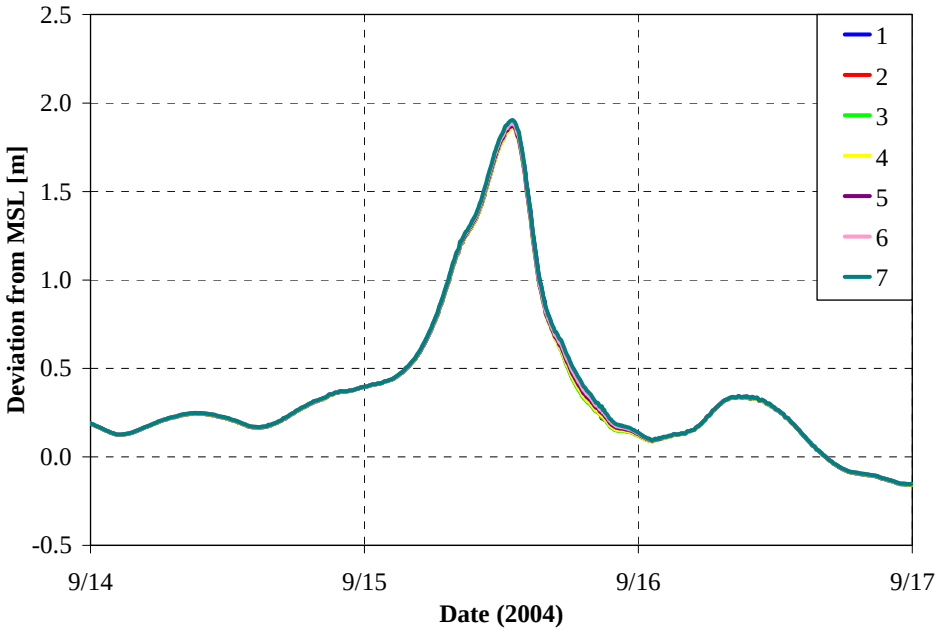

Figure P2- 58 Storm surge hydrographs along the 1 km radius observation arc extending seaward from Pensacola Inlet.

The plots indicate that a minimal difference exists between the hydrographs along this observation arc. The highest peak surge value is 1.87 meters at point #7 (west-southwest), whereas the lowest peak value is 1.83 meters at point #3 (south-southeast), a difference of only 4 cm. Compared to the results obtained in the numerical parameter study, a smaller spatial variance is noted along the 1 km radius for the Hurricane Ivan storm surge hindcast.

Figure P2-59 shows the water elevation recordings along the 5 km arc radius. In contrast to the 1 km radius, a noticeable spatial variance is evident in the plots. The greatest peak surge value is 1.94 meters (point #7) and the lowest peak surge value is 1.65 meters (point #3), a difference of 0.29 meters. The spatial variance along the 5 km radius is much greater than the spatial variance along the 1 km radius, which is consistent with the results from the numerical parameter study.

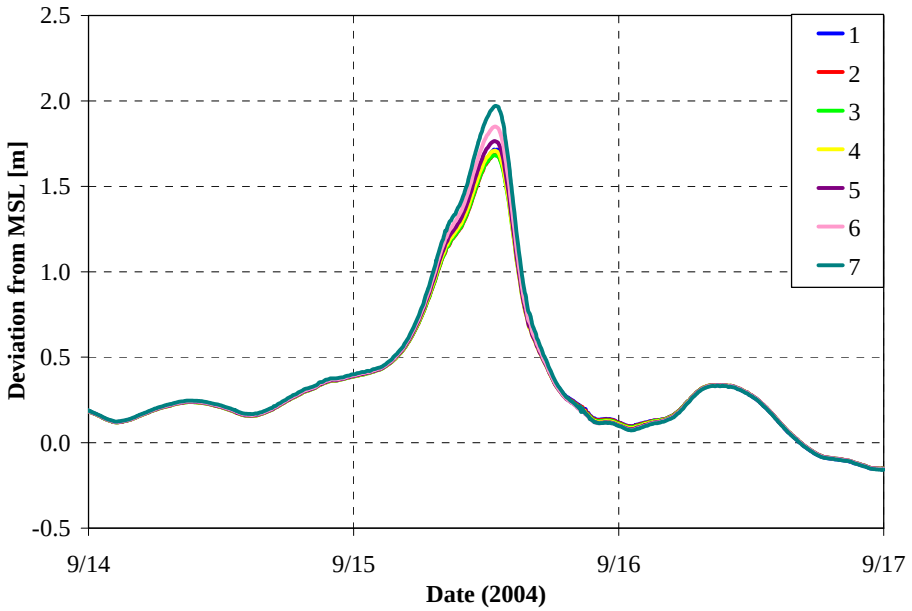

Figure P2- 59 Storm surge hydrographs along the 5 km radius observation arc extending seaward from Pensacola Inlet.

In addition, spatial variance is also recognized as the radius of the observation arc is increased. Figure P2-60 shows hydrographs at the same location (point #4, due south) along observation arcs ranging from 1 km (blue line) to 5 km (purple line) in radius. Similar to the numerical parameter study results, the peak storm surge increases nearer to the coastline.

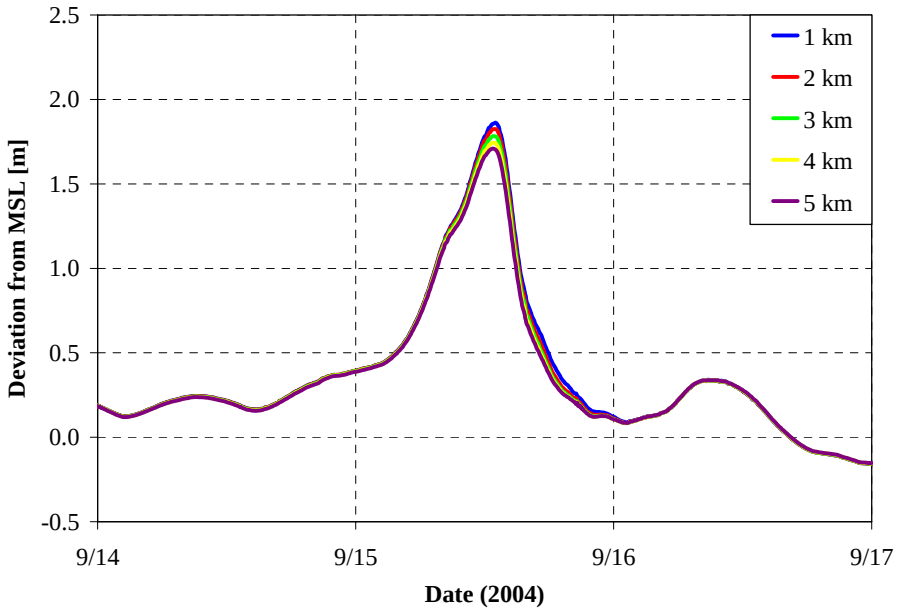

Figure P2- 60 Storm surge hydrographs at the same location (point #4, due south) on each observation arc from 1 km to 5 km in radius.

Discussion

Comparing the hindcast study results to the numerical parameter study results indicates that the main conclusions drawn in the idealized study are verified in a real-life scenario. In both cases, the inclusion of an inlet-bay system in the model domain did not have a significant impact on the open coast storm surge hydrographs. This finding was noted for both shelf profiles in the idealized domain study and for the case of Pensacola Inlet during Hurricane Ivan. Thus, tidal inlets that fall into the range of widths used in this study do not need to be included in a large-scale ocean circulation model when generating open coast boundary conditions for a local, high resolution model.

In addition, a spatial dependence is recognized for storm surge hydrographs along open coast boundary locations extending seaward from the mouth of the inlet. The magnitude of this variance becomes greater as the radial distance of the open coast boundary increases. Similar behavior is noted for both the numerical parameter study and the hindcast study. The magnitude of the spatial difference appears to be greater in the numerical parameter study than in the hindcast study. This is likely due to the controlled environment (i.e. simple linear bathymetry, location of hurricane landfall relative to the inlet, etc.) built into the idealized domains. Nevertheless, spatial variance is recognized for all domains presented herein.

CONCLUSIONS

Presented in this report is a numerical parameter study focusing on the effect that tidal inlets have on open coast storm surge hydrographs. Four different inlet-bay configurations are constructed based on a statistical analysis of existing Florida tidal inlets. Furthermore, two different continental shelf profiles are developed that represent the bathymetry profiles found along the west/northeast coast of Florida and the southeast coast of Florida. The inlet-bay configurations and continental shelf profiles allow for a number of test cases to elucidate the influence that tidal inlets have on open coast boundary conditions. A secondary focus of this study is the spatial variance of the storm surge hydrographs near tidal inlet boundary locations. The conclusions from this study have implications toward future bridge scour modeling efforts.

Numerical parameter study conclusions

Two primary conclusions are drawn from the numerical parameter study: 1) the effect of tidal inlets on open coast storm surge hydrographs is minimal; and 2) a noticeable spatial variance of storm surge hydrographs exists along the open coast boundary locations.

The effect of including inlet-bay systems on the open coast storm surge hydrographs is negligible for both the west/northeast Florida shelf profile and the southeast Florida shelf profile. Comparing model output for all four inlet-bay configurations to the control mesh indicates that including an inlet-bay system in the model domain does not significantly alter the open coast hydrographs. Taking this into account, a large-scale model domain (e.g. the WNAT model domain) would not need to include the inlet-bay system in the computational domain to generate open coast boundary conditions for a local inlet-based model (a significant time-saving benefit for coastal modelers).

Another significant finding in this study is the spatial variance of the storm surge hydrographs along the open coast boundary locations. Nearer to the inlet, the spatial variance of the hydrographs is minimal; however, the spatial variance increases further from the inlet (i.e. going from the 1 km radius to the 15 km radius). Depending on the continental shelf profile, the difference in peak elevations along the open coast boundary can be as much as 0.5 meters or more. This contradicts previous bridge scour modeling studies, whereby a single design hydrograph was applied along the open coast boundary

(as a point of reference, the open coast boundary in these studies appeared to be several kilometers offshore). If the open ocean boundary is placed close to the inlet so that a single hydrograph can be used at each node, then momentum flux problems may arise from the boundary being placed near the area of interest. By placing the boundary further from the inlet and applying individual hydrographs at each node, the cross-basin hydrodynamics of storm surge propagation can be artificially incorporated into the inlet-based model. Results from this study imply that current modeling practices can be improved upon by incorporating spatially varying hydrographs along the open coast boundary.

Hurricane Ivan hindcast conclusions

Two main conclusions can be drawn from the Hurricane Ivan storm surge hindcast; 1) including the barrier islands as inundation areas in the model significantly improved the storm surge levels within the bay, however, it did not have an appreciable effect on the open coast storm surge hydrographs; and 2) similar open coast storm surge hydrographs are generated when including the Pensacola Inlet-Escambia Bay system in the model domain compared to not including the inlet-bay system in the domain.

First, the inclusion of barrier islands as inundation areas allowed more storm surge to enter the bay. By comparison, the peak surge elevation within the bay was approximately half a meter greater when the inundation areas are included than when they are not included. Furthermore, no significant difference was recognized in the open coast storm surge hydrographs when the barrier islands were included as inundation areas compared to treating the barrier islands as model boundaries. This analysis indicates that a coastal modeler would not need to include barrier islands as inundation areas when generating open coast boundary conditions for a local bridge scour model.

Second, the effect that the Pensacola Inlet-Escambia Bay system has on the open coast storm surge hydrographs was examined. The results are consistent with the conclusions from the numerical parameter study, such that including the Pensacola Inlet-Escambia Bay system in the model domain does not have a significant impact on the open coast storm surge hydrographs. Furthermore, a spatial variance is also recognized along the observation arcs extending seaward from the mouth of Pensacola Inlet. Similar to the behavior recognized in the numerical parameter study, the magnitude of the spatial

variance increases as the open coast boundary locations are extended farther from the mouth of the inlet. Thus, it is apparent that applying a single design hydrograph along the open coast boundary is inappropriate and may lead to erroneous results.

APPENDIX A - NUMERICAL PARAMETER STUDY RESULTS: INLET COMPARISONS

Presented in this appendix are storm surge hydrographs along each of the open coast boundary locations (observation arcs) for both continental shelf profiles. Each figure contains plots that compare storm surge hydrographs for all of the inlet-bay configurations at five points along each observation arc [east (1), southeast (2), south (3), southwest (4), and west (5)]. The figures contain hydrographs for the average inlet width (blue line), 100 meter inlet width (red line), 500 meter inlet width (green line), 1000 meter inlet width (yellow line), and the control mesh (purple line). In all cases, the plots are nearly identical, indicating that the inlet-bay configurations do not have a significant impact on the open coast storm surge hydrographs

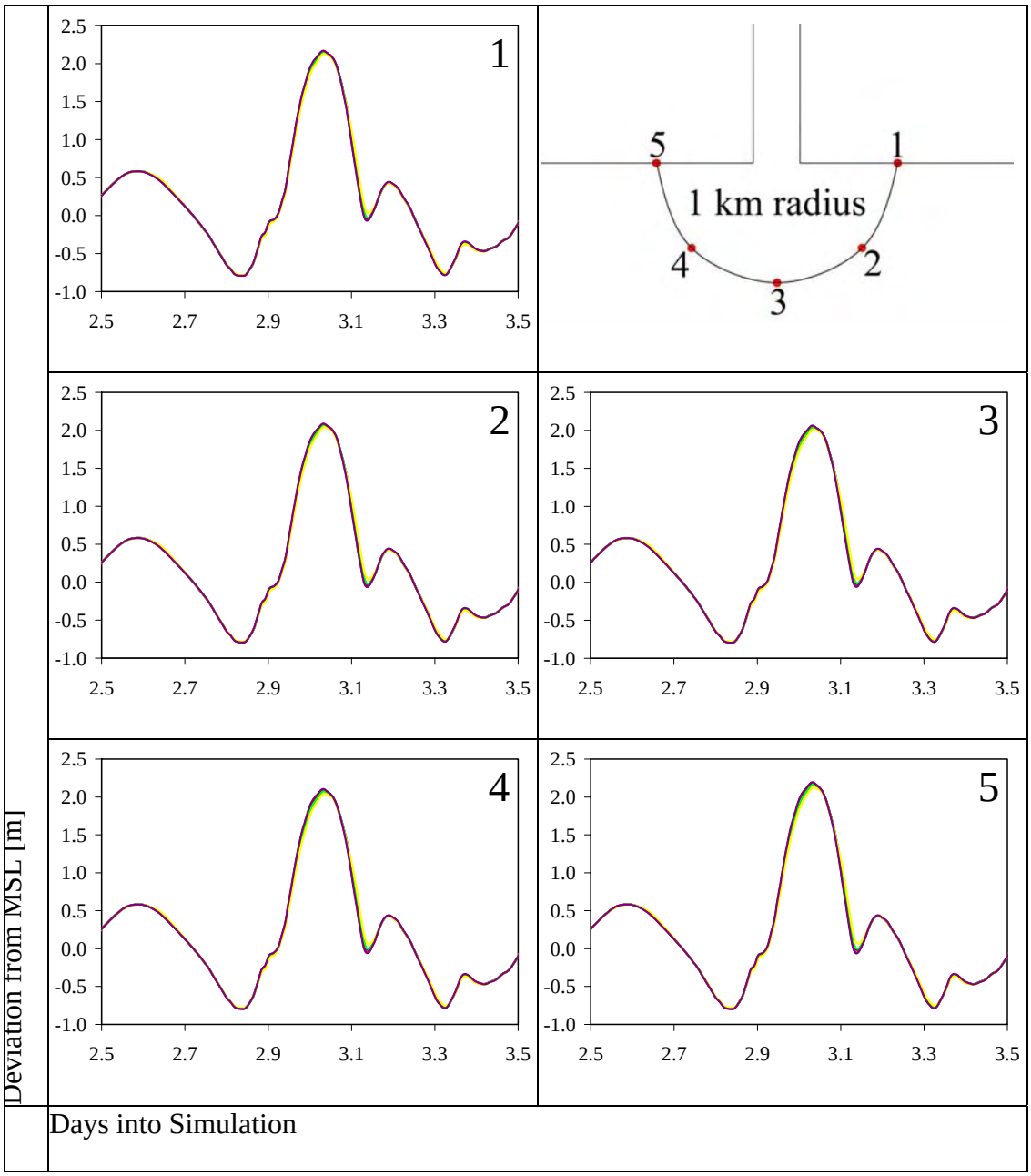

Figure 2A-1: Storm surge hydrographs for the west/northeast Florida shelf profile along the 1 km radius observation arc.

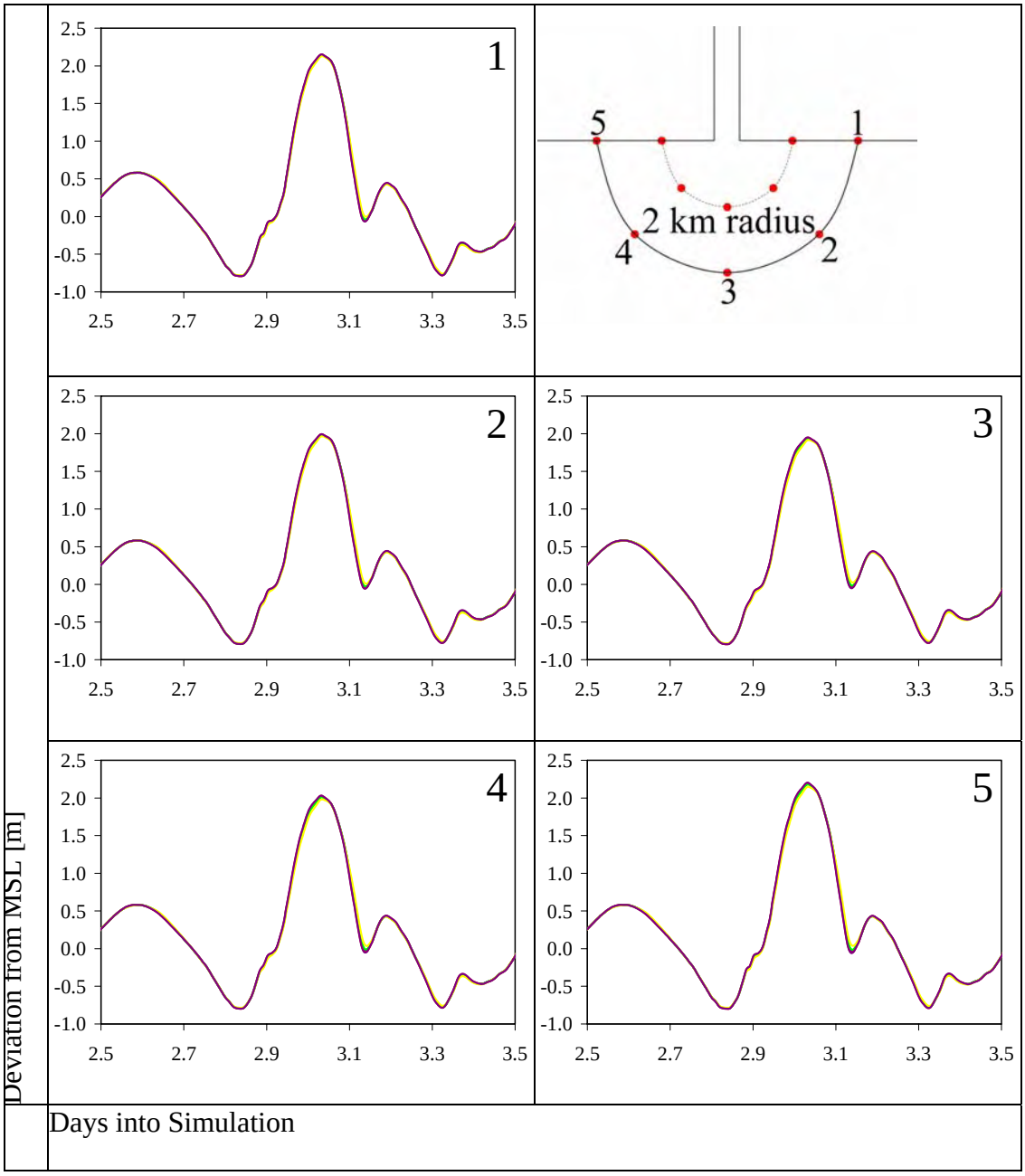

Figure 2A-2: Storm surge hydrographs for the west/northeast Florida shelf profile along the 2 km radius observation arc.

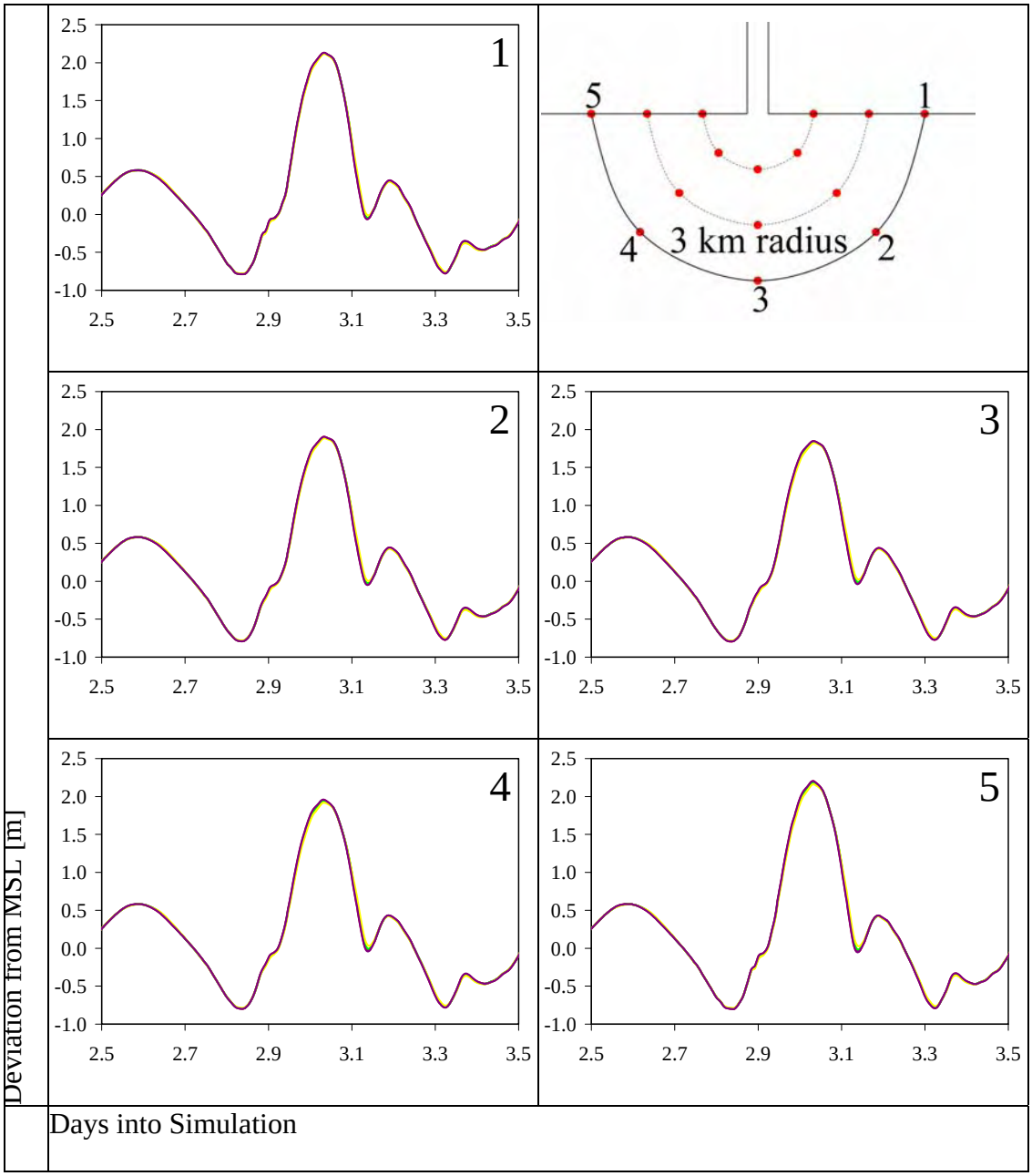

Figure 2A-3: Storm surge hydrographs for the west/northeast Florida shelf profile along the 3 km radius observation arc.

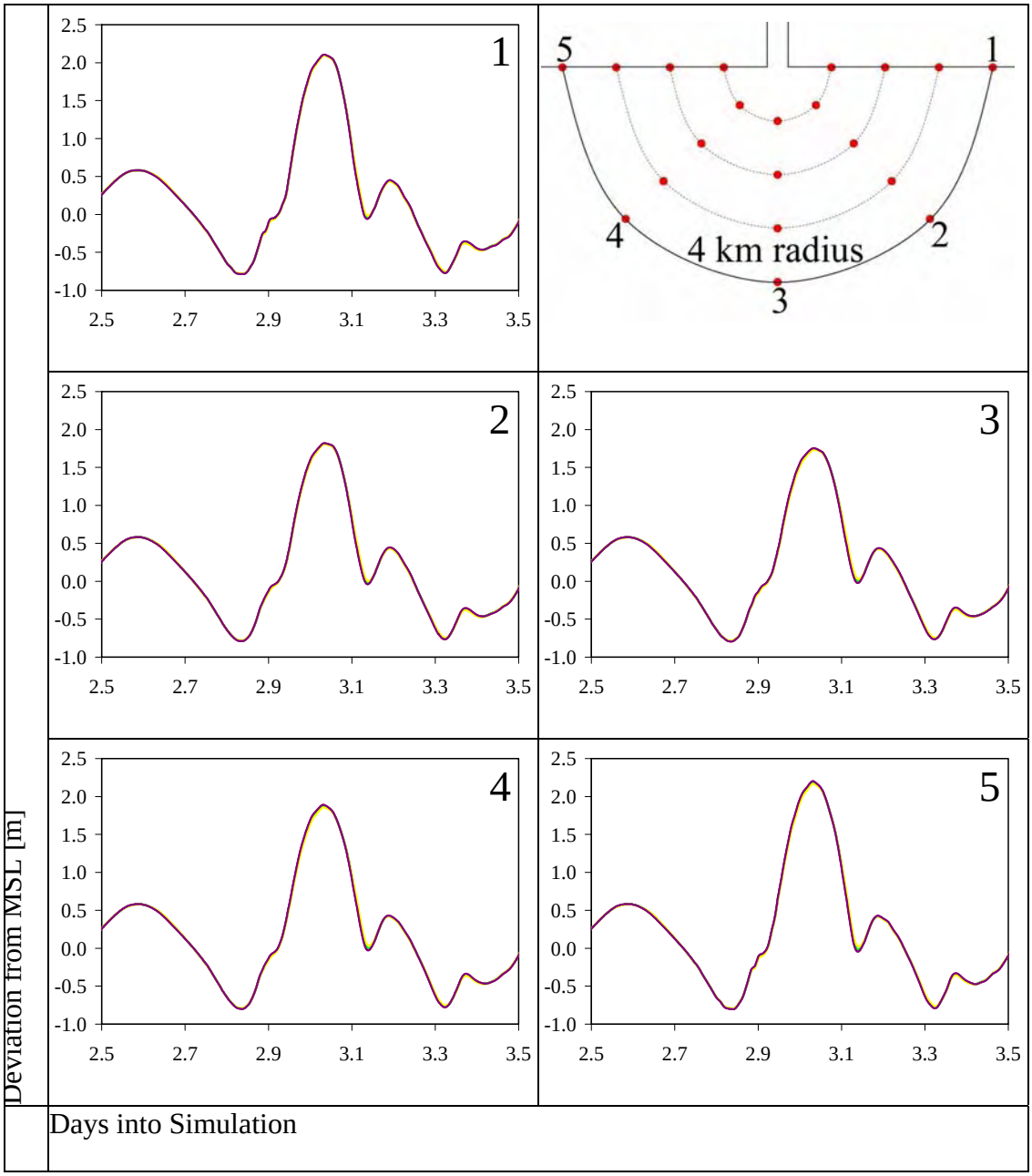

Figure 2A-4: Storm surge hydrographs for the west/northeast Florida shelf profile along the 4 km radius observation arc.

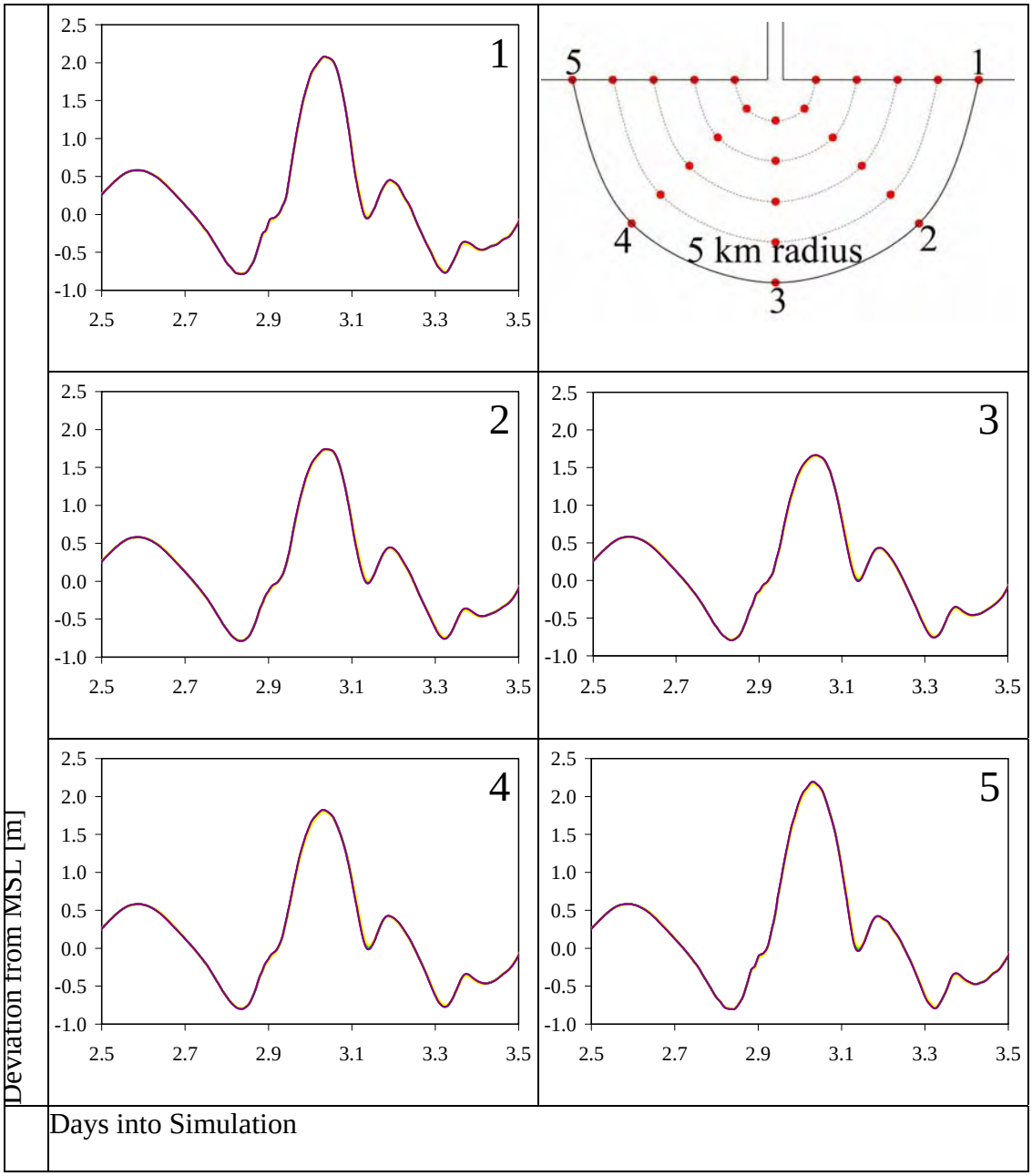

Figure A-5: Storm surge hydrographs for the west/northeast Florida shelf profile along the 5 km radius observation arc.

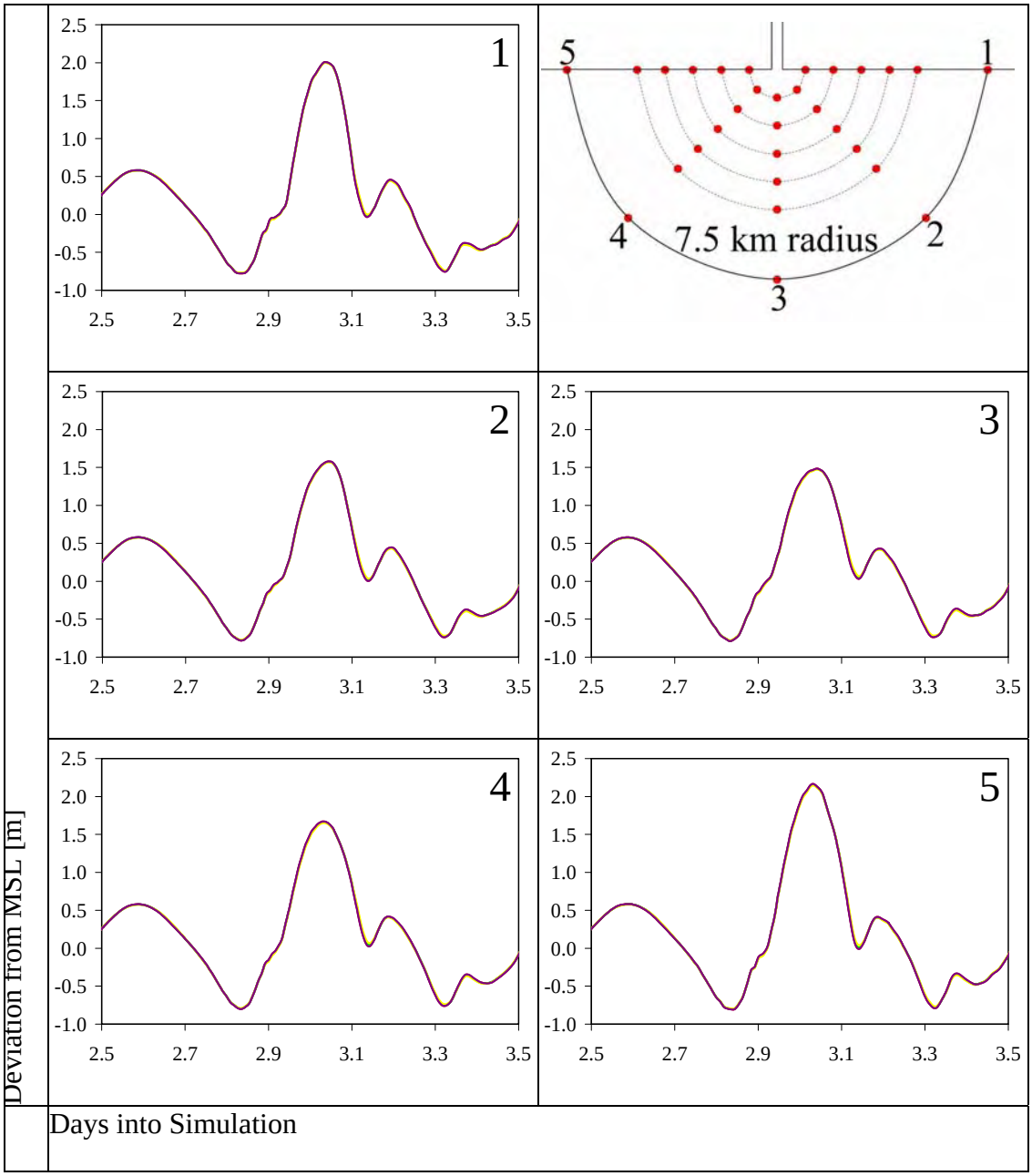

Figure A-6: Storm surge hydrographs for the west/northeast Florida shelf profile along the 7.5 km radius observation arc.

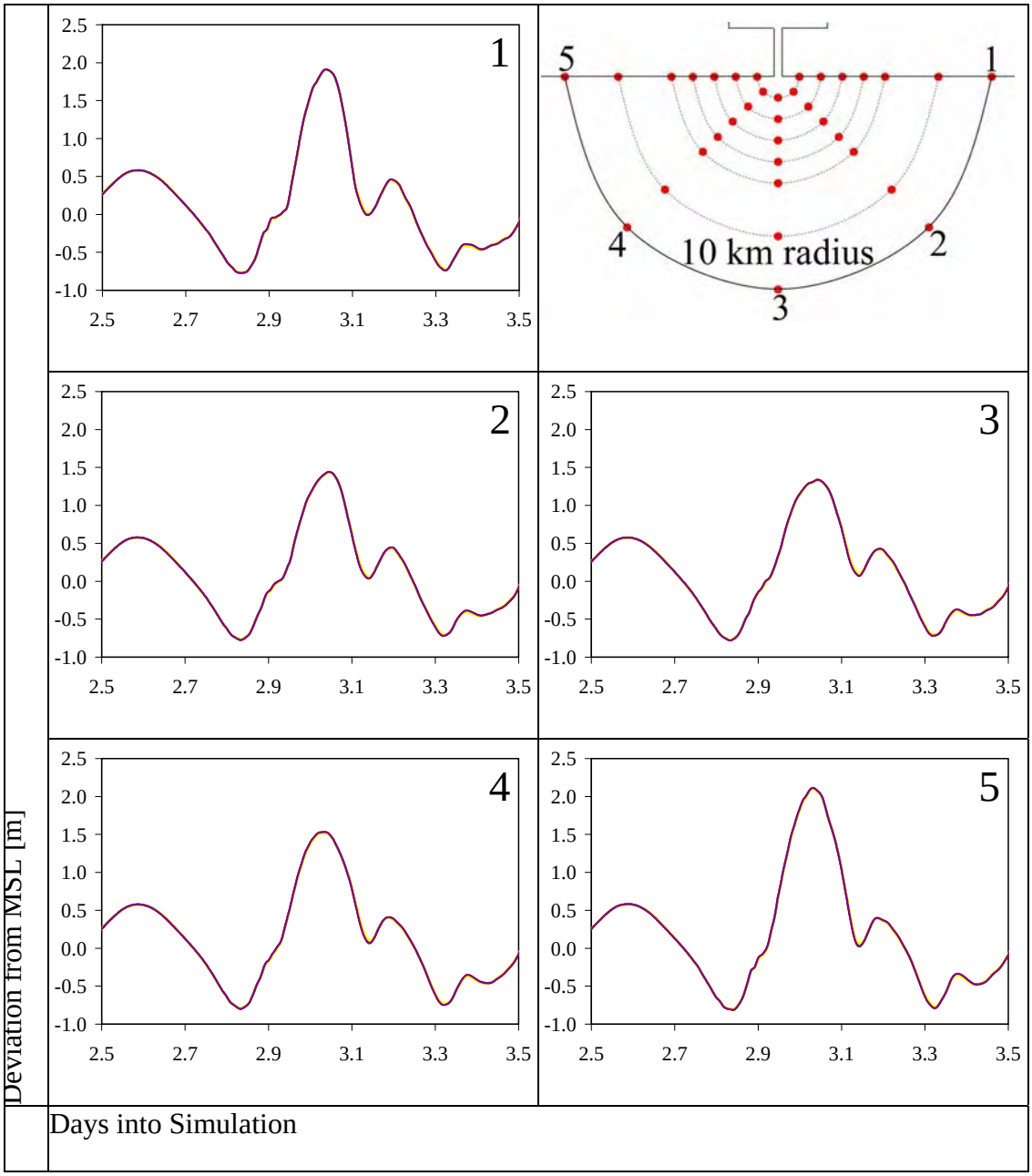

Figure A-7: Storm surge hydrographs for the west/northeast Florida shelf profile along the 10 km radius observation arc.

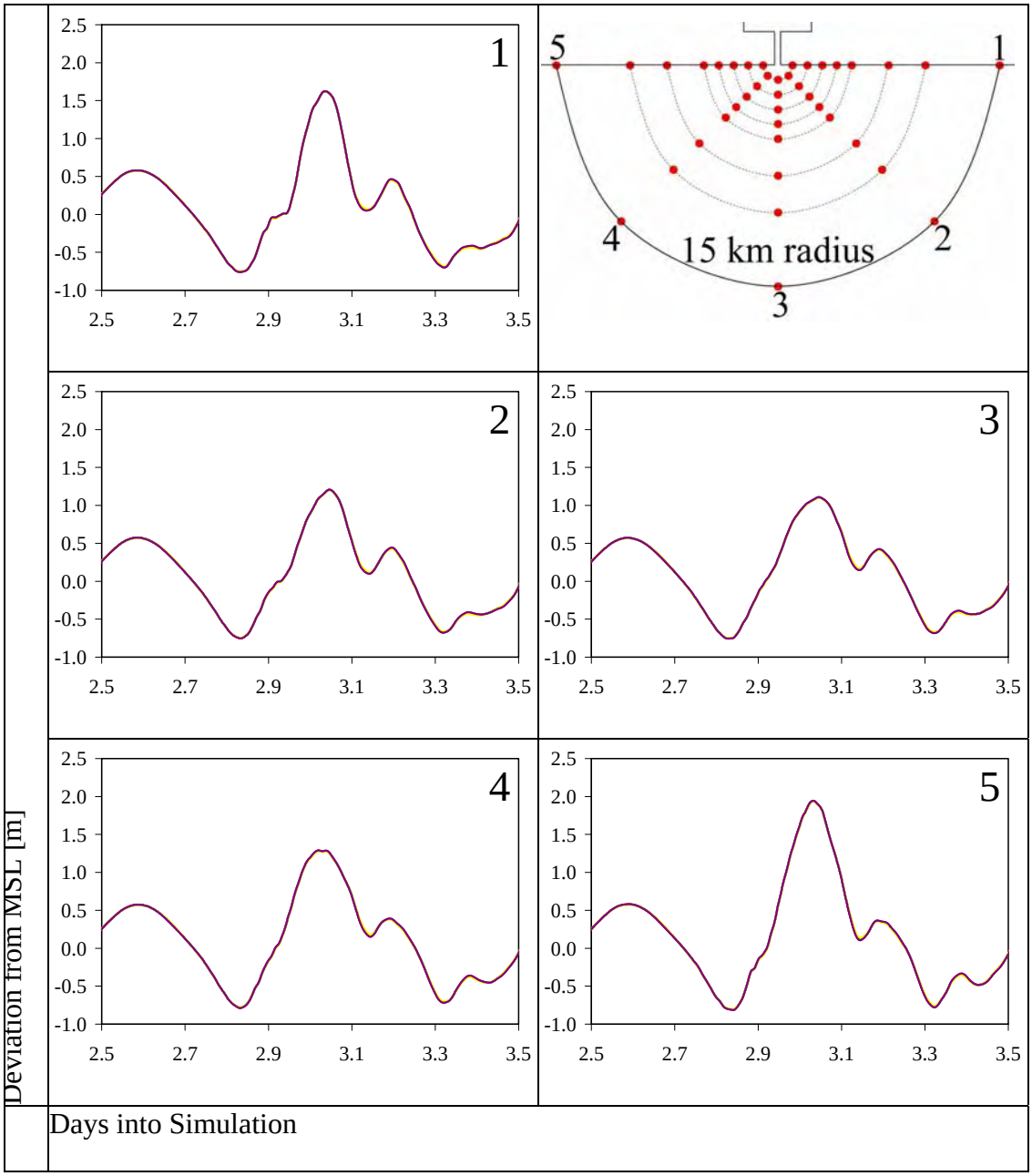

Figure A-8: Storm surge hydrographs for the west/northeast Florida shelf profile along the 15 km radius observation arc.

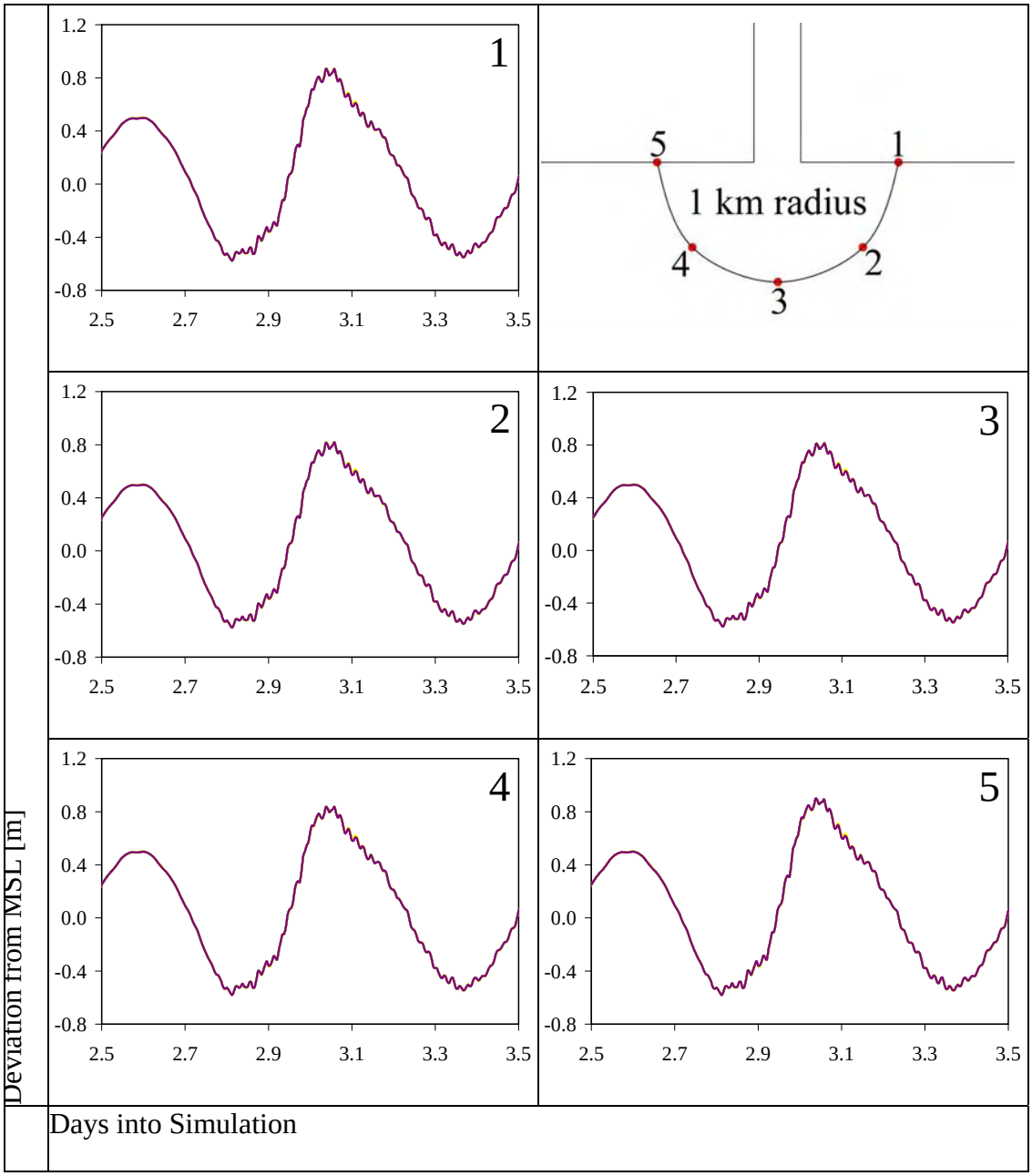

Figure A-9: Storm surge hydrographs for the southeastern Florida shelf profile along the 1 km radius observation arc.

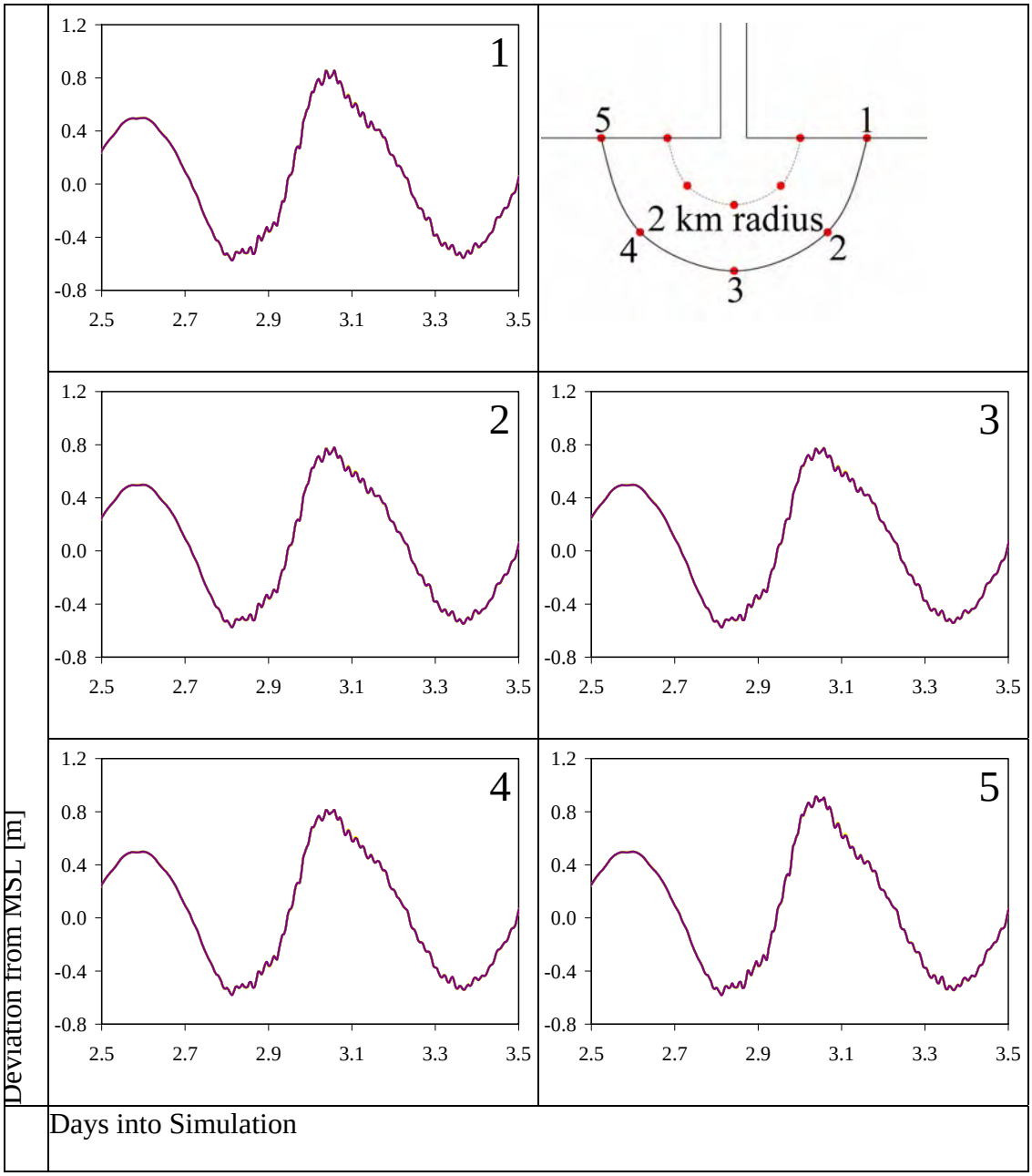

Figure A-10: Storm surge hydrographs for the southeastern Florida shelf profile along the 2 km radius observation arc.

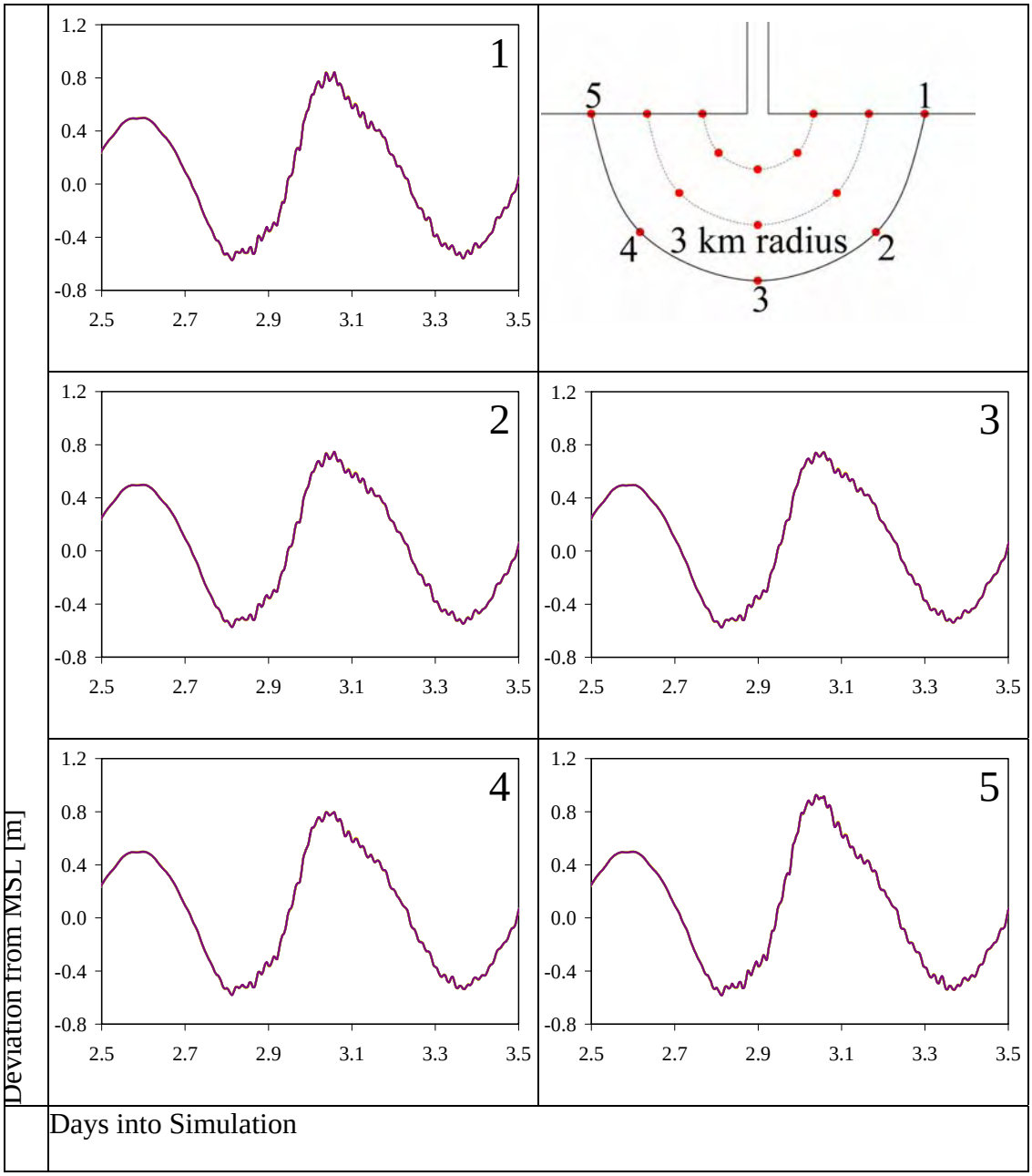

Figure A-11: Storm surge hydrographs for the southeastern Florida shelf profile along the 3 km radius observation arc.

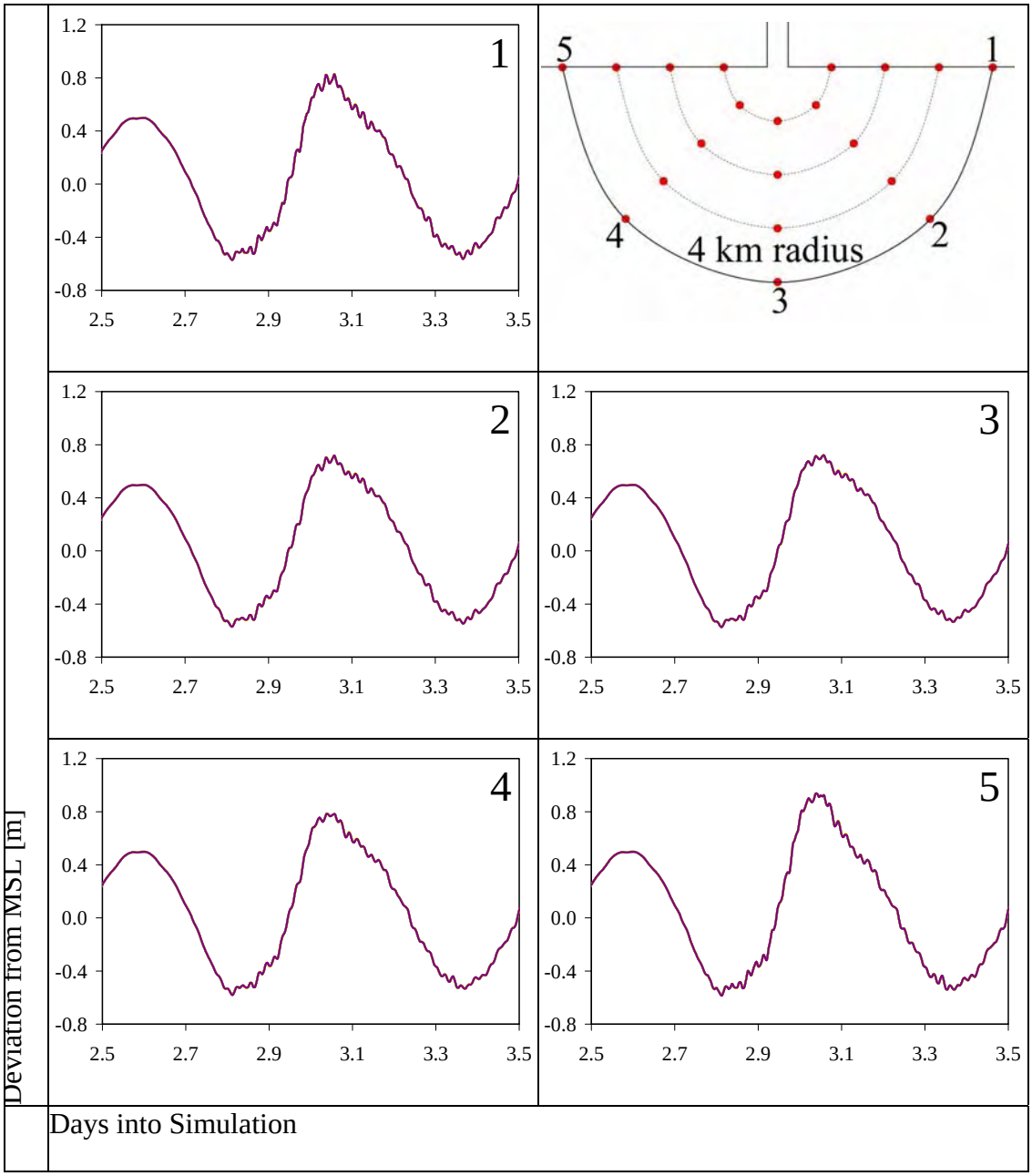

Figure A-12: Storm surge hydrographs for the southeastern Florida shelf profile along the 4 km radius observation arc.

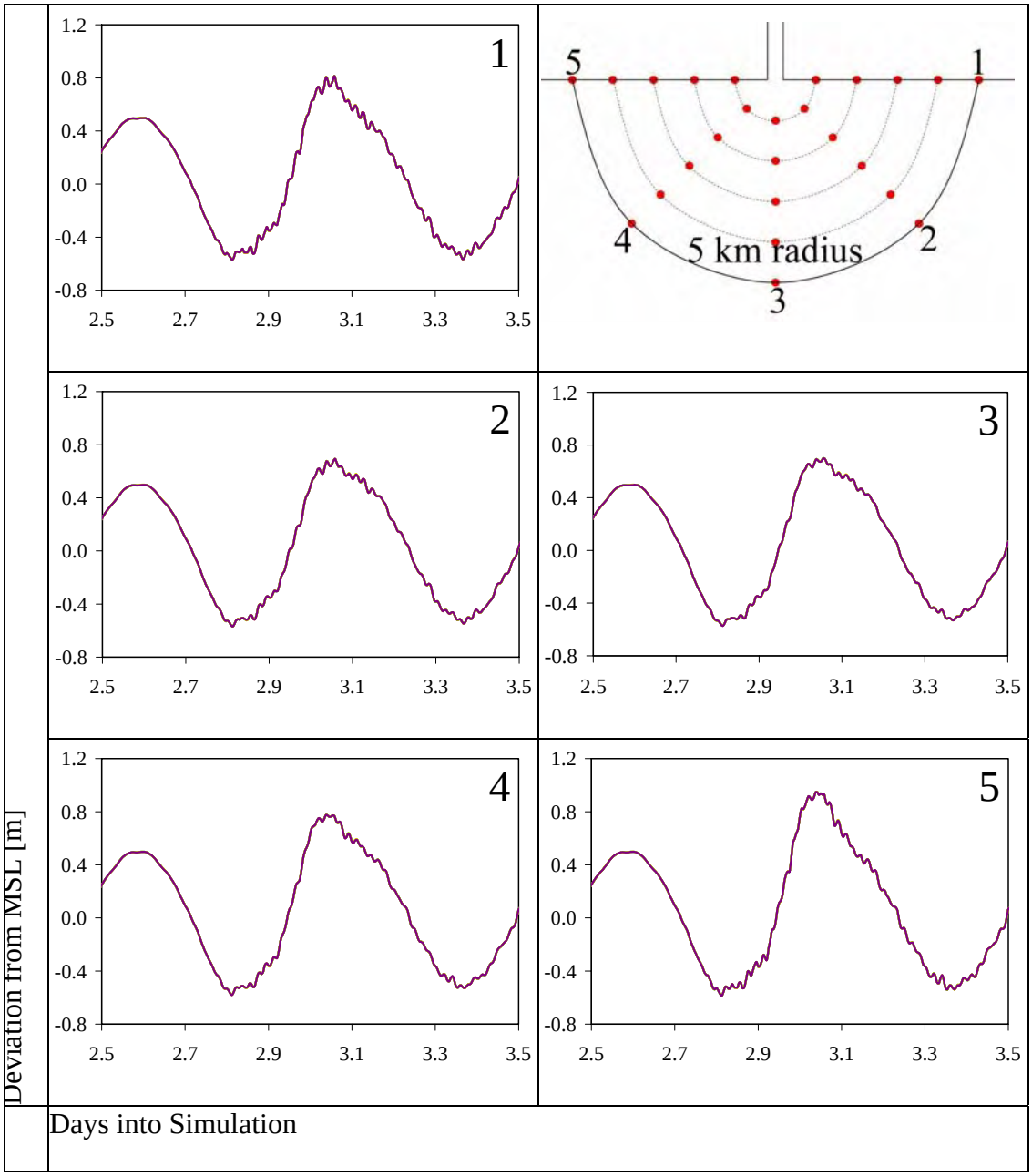

Figure A-13: Storm surge hydrographs for the southeastern Florida shelf profile along the 5 km radius observation arc.

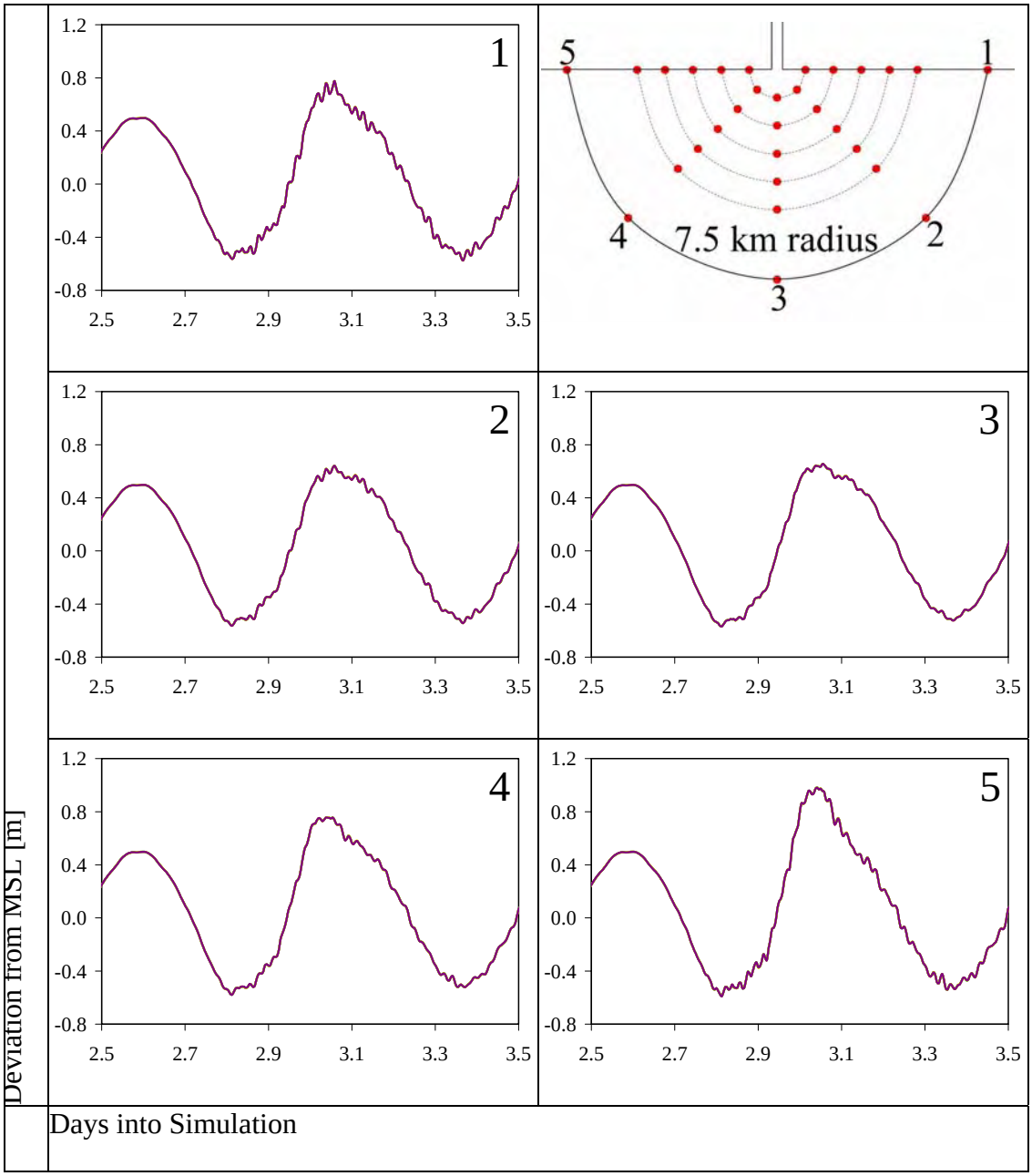

Figure A-14: Storm surge hydrographs for the southeastern Florida shelf profile along the 7.5 km radius observation arc.

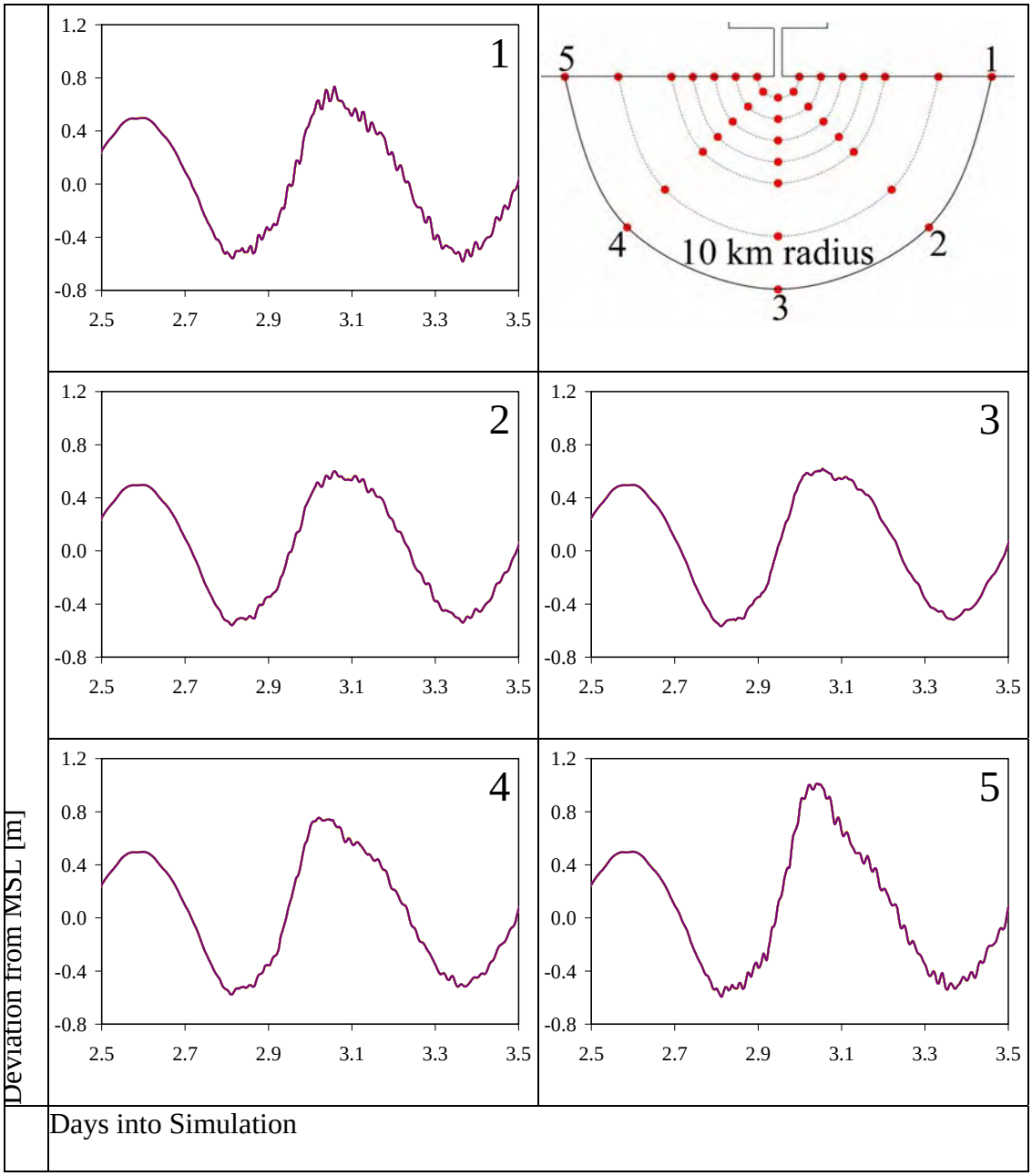

Figure A-15: Storm surge hydrographs for the southeastern Florida shelf profile along the 10 km radius observation arc.

REFERENCES

Blain, C.A., Westerink, J.J., Luettich, R.A., and Scheffner, N.W. (1994). ADCIRC: An Advanced Three-Dimensional Circulation Model for Shelves, Coasts, and Estuaries Report No. 4. Hurricane Storm Surge Modeling using Large Domains. Technical Report DRP-92-6, August 1994, U.S. Army Engineer Waterways Experiment Station, Vicksburg, Mississippi

Carr de Betts, Erica Eva (1999). An Examination of Flood Deltas at Florida's Tidal Inlets. Master's Thesis, Coastal and Oceanographic Engineering Department, University of Florida, Gainesville, Florida

Cox, A.T., Greenwood, J.A., Cardone, V.J., and Swail, V.R. (1995). An Interactive Objective Kinematic Analysis System. *Proceedings of 4th International Workshop on Wave Hindcasting and Forecasting*, Banff, Alberta, Canada.

Cox, A.T. and Cardone, V.J. (2000). Operational Systems for the Prediction of Tropical Cyclone Generated Winds and Waves. *Proceedings of 6th International Workshop on Wave Hindcasting and Forecasting*. Monterey, California.

Cox, A.T. and Cardone, V.J. (2002). 20 Years of Operational Forecasting at Oceanweather, *Proceedings of 7th International Workshop on Wave Hindcasting and Forecasting*. Banff, Alberta, Canada.

DeBusk, W.F., Poyer, I., and Herzfeld, I. (2002). Sediment Quality in the Pensacola Bay System. NWFWMD Technical File Report 02-03, 74 pages.

Dietsche, D. (2004). Storm Tide Simulations for Hurricane Hugo (1989): On the Significance of Including Inland Flooding Areas. Master's Thesis, Department of Civil and Environmental Engineering, University of Central Florida, Orlando, Florida

Douglass, S.L., Hughes, S.A., Rogers, S., and Chen, Q. (2004). The Impact of Hurricane Ivan on the Coastal Roads of Florida and Alabama: A Preliminary Report. Coastal Transportation Engineering Research & Education Center, University of South Alabama

Edge, B.L., Vignet, S.N., and Fisher, J.S. (1999). Determination of bridge scour velocity in an estuary. In E.V. Richardson and P.F. Lagasse (eds.): Stream Stability and Scour at Highway Bridges, Compendium of Papers ASCE Water Resources Engineering Conferences 1991-1998, ASCE, Reston, Virginia, pp. 738-747

Garrett, J.R. (1977). Review of the drag coefficients over oceans and continents. *Monthly Weather Review*: Vol. 105, pp. 915-929

Hagen, S.C. and Parrish, D.M. (2004). Unstructured mesh generation for the western North Atlantic tidal model domain. *Engineering with Computers*: Vol. 20, pp. 136-146

Hagen, S.C., Zundel, A.K., and Kojima, S. (2006). Automatic, unstructured mesh generation for tidal calculations in a large domain. *International Journal for Computational Fluid Dynamics*, in review

Head, C.M. and Marcus, R.B. (1987). The Face of Florida. Second Edition, Kendall/Hunt Publishing, Dubuque, Iowa

Hench, J.L., Blanton, B.O., and Luettich, R.A. (2002). Lateral dynamic analysis and classification of barotropic tidal inlets. *Continental Shelf Research*: Vol. 22, pp. 2615-2631

Jarrett, J.T. (1976). Tidal Prism-Inlet Area Relationships. General Investigation of Tidal Inlets Report 3, U.S. Army Engineer Waterways Experiment Station, Vicksburg, Mississippi

Kojima, S. (2005). Optimization of an Unstructured Finite Element Mesh for Tide and Storm Surge Modeling Applications in the Western North Atlantic Ocean. Master's Thesis, Department of Civil and Environmental Engineering, University of Central Florida, Orlando, Florida

Kolar, R.L., Gray, W.G., Westerink, J.J., and Luettich, R.A. (1994). Shallow water modeling in spherical coordinates: equation formulation, numerical implementation, and application. *Journal of Hydraulic Research*: Vol. 32, No. 1, pp. 3-24

Luettich, R.A., Westerink, J.J., and Scheffner, N.W. (1992). ADCIRC: An Advanced Three-Dimensional Circulation Model for Shelves, Coasts, and Estuaries Report No. 1. Theory and Methodology of ADCIRC-2DDI and ADCIRC-3DL, Technical Report DRP-92-6, November 1992, U.S. Army Engineer Waterways Experiment Station, Vicksburg, Mississippi

Mendenhall, W. and Sincich, T. (1995). Statistics for Engineering and the Sciences. Fourth Edition, Prentice Hall, New Jersey.

Murray, R.R. (2003). A Sensitivity Analysis for a Tidally-Influenced River System. Master's Thesis, Department of Civil and Environmental Engineering, University of Central Florida, Orlando, Florida

Parrish, D.M. (2001). Development of a Tidal Constituent Database for the St. Johns River Water Management District. Master's Thesis, Department of Civil and Environmental Engineering, University of Central Florida, Orlando, Florida

Powell, M.D., Houston, S.H., Amat, L.R., and Morisseau-Leroy, N. (1998). The HRD real-time hurricane wind analysis system. *Journal of Wind Engineering and Industrial Aerodynamics*: Vols. 77 & 78, pp. 53-64

Reid, R.O. (1990). Tides and Storm Surges. In J. Herbich (ed), Handbook of Coastal and Ocean Engineering. Houston, Texas: Gulf Publishing Company, pp. 533-590

Thompson, E.F. and Cardone, V.J. (1996). Practical modeling of hurricane surface wind fields. *ASCE Journal of Waterway, Port, Coastal, and Ocean Engineering*: Vol. 122, No. 4, pp. 195-205

Weaver, R.J. and Slinn, D.N. (2004). Effect of wave forces on storm surge. *Coastal Engineering*, in review

Westerink, J.J., Blain, C.A., Luettich, R.A., and Scheffner, N.W. (1994). ADCIRC: An Advanced Three-Dimensional Circulation Model for Shelves, Coasts, and Estuaries Report No. 2. User's Manual for ADCIRC-2DDI, Technical Report

DRP-92-6, January 1994, U.S. Army Engineer Waterways Experiment Station, Vicksburg, Mississippi

Zevenbergen, L.W., Richardson, E.V., and Edge, B.L. (1999). Computer models for tidal hydraulic analysis at highway structures. In E.V. Richardson and P.F. Lagasse (eds.): Stream Stability and Scour at Highway Bridges, Compendium of Papers ASCE Water Resources Engineering Conferences 1991-1998, ASCE, Reston, Virginia, pp. 807-814

Zundel, A.K. (2005). Users Manual for the Surface-water Modeling System, Version 9.0. Environmental Modeling Research Laboratory, Brigham Young University, Provo, Utah